DEVELOPMENT OF LIGHT ABSORPTIVE POLYMERIC FORM STABLE COMPOSITE PHASE CHANGE MATERIAL FOR THERMAL STORAGE

By

KEE SHIN YIING

A PhD thesis submitted to the Department of Petrochemical Engineering,
Faculty of Engineering and Green Technology,
Universiti Tunku Abdul Rahman,
in partial fulfillment of the requirements for the degree of
Doctor of Philosophy in Engineering
September 2018

ABSTRACT

DEVELOPMENT OF LIGHT ABSORPTIVE POLYMERIC FORM STABLE COMPOSITE PHASE CHANGE MATERIAL FOR THERMAL STORAGE

Kee Shin Yiing

Thermal energy storage (TES) are utilized when there is a mismatch between thermal energy supply and energy demand. Among all TES, phase change material (PCM) is popular because it has a high thermal storage density with a small temperature variation during phase change process. However, the practical applications of PCM as TES face two major issues: volume change during phase change process and lack of study on light absorption of PCM which can convert light energy into thermal energy. Therefore, the development of a new light absorptive polymeric form stable composite phase change material is proposed to improve is thermal stability and light absorption ability over phase change process. In this study, light absorptive polymeric form stable composite phase change material was prepared using solution blending and dip coating method. Myristic acid (MA) was used as PCM to store latent heat; Polymer coating was used to contain the PCM; reduced graphene oxide (RGO) was incorporated into the polymer coating as light absorption materials. This study was carried out in three phases. First phase is to apply polyacrylic (PA) and silicone conformal

coatings on composite PCM (MA/PMMA) with different weight percentage of MA to determine which coating is suitable to be used as polymer coating. Leakage test result showed that PA coating performed better in preventing leakage. However, adding PA coating and PMMA supporting material on PCM reduced latent heat significantly as the latent heat for coated PCM (MA/PMMA) in 60:40 wt% had low latent heat which was 91.42±7.22 J/g. Second phase is continued by maximizing the latent heat of PCM by directly applying different combination of PA and nitrile butadiene rubber (NBR) on MA pellet without PMMA supporting material. NBR was used in this phase because it was elastic to withstand the expansion during phase change process. The result showed that PANBR/MA pellet with 1-layer NBR (inner layer) and 1-layer PA (outer layer) was thermally stable and the melting latent heat was increased from 91.42±7.22 J/g to 131.84±5.76 J/g. Third phase is to improve light absorption of PANBR/MA pellet by adding RGO. RGO-PANBR/MA pellet with 1.5 wt% RGO loading had the highest amount of stored heat energy which was 48.91% higher than pellet without RGO. The average solar energy conversion of 1.5 wt% RGO-PANBR/MA pellet was about 21%. The melting point and latent heat of 1.5 wt% RGO-PANBR/MA pellet were 54.79±0.07 ºC and 119.91±6.67 J/g, respectively. All the above results showed that 1.5 wt% RGO-PANBR/MA pellet has potential to be used as light absorption thermal energy storage.

PUBLICATIONS

Based on the work of this thesis, a few papers have been published or submitted as shown in table below:

No	Category	Title	Publisher	Status
1	Journal (Impact factor in 2017 = 2.935)	Effect of preparation methods on the tensile, morphology and solar energy conversion efficiency of RGO/PMMA nanocomposite	Polymers, 9(6), p. 230, 2017.	Published (Appendix A)
2	Journal (Impact factor in 2017 = 2.467)	Thermal performance study of composite phase change material with polyacrylic and conformal coating	Materials, 10(8), p.873, 2017	Published (Appendix B)
3	Journal (Impact factor in 2017 = 3.771)	Review of solar water heaters incorporating solid-liquid organic phase change materials as thermal storage.	Applied Thermal Engineering , 131, pp.455–471	Published (Appendix C)
4	Conference Proceeding of International Symposium Green and Sustainable Technology (ISGST2017) (Scopus Index)	Thermal performance study of form-stable composite phase change material with polyacrylic	AIP Conference Proceedings 1828, 020008 (2017)	Published (Appendix D)

5	Conference Proceeding of 3rd Putrajaya International Built Environment, Technology and Engineering	Development of form stable composite phase change material with polymer coating for thermal energy storage	ISBN 978-967-2072-10-2	Published (Appendix E)
6	Conference Proceeding of 2nd International Symposium on Green Technology (Scopus Index)	Development of form stable Poly(methyl methacrylate) (PMMA) coated thermal phase change material for solar water heater applications	IOP Conference Series: Earth and Environmental Science, 140(1), p.012008. (2018)	Published (Appendix F)
7	Journal (Impact factor in 2017 = 2.35)	Performance study of form stable myristic acid/polymethyl methacrylate phase change material coated with nitrile rubber/polyacrylic layered coats	Coatings	Submitted
8	Journal (Impact factor in 2017 = 2.687)	Light absorptive polymeric form stable composite phase change material for thermal storage	Materials letters	Submitted

ACKNOWLEDGEMENTS

I would like to extend my gratitude to my supervisor Dr. Yamuna Munusamy and my co-supervisor Prof. Ir. Dr. Ong Kok Seng for their direction, assistance, and guidance. In particular, Dr. Yamuna Munusamy's numerous recommendations and suggestions have been invaluable for the project.

In addition, I also take this opportunity to express my sincere thanks to Prof. Hendrik Simon Cornelis Metselaar and Dr. Chee Swee Yong for contributing suggestions, materials and analysis tools to complete this project. I would also like to thank final year project student Yu Gen Qian and Shimalaa for assisting me in experiment. Special thanks must also go to all the UTAR lab officers from Faculty of Engineering and Green Technology (FEGT), Faculty of Science (FSC) and Lee Kong Chian Faculty of Engineering & Science (LKC FES) whom had continuously catered to my experiment needs and assisted me on sample analyses. At the same time, I am greatly appreciated the Ministry of Higher Education Malaysia [FRGS/1/2014/TK04/UTAR/02/1] and Malaysia MyPhd scholarship for providing financial support to carry out this research

Last but not least, I offer my deepest regards and blessings to my family members, friends and lab mates who supported me in any respect during the completion of the project.

APPROVAL SHEET

This dissertation/thesis entitled "**DEVELOPMENT OF LIGHT ABSORPTIVE POLYMERIC FORM STABLE COMPOSITE PHASE CHANGE MATERIAL FOR THERMAL STORAGE**" was prepared by KEE SHIN YIING and submitted as partial fulfillment of the requirements for the degree of Doctor of Philosophy in Engineering at Universiti Tunku Abdul Rahman.

Approved by:

_____

(Dr. YAMUNA MUNUSAMY) Date:……..
Associate Professor/Supervisor
Department of PetroChemical Engineering
Faculty of Engineering and Green Technology
Universiti Tunku Abdul Rahman

_____

(Prof. Ir. Dr. ONG KOK SENG) Date:……..
Professor/Co-supervisor
Department of Industrial Engineering
Faculty of Engineering and Green Technology
Universiti Tunku Abdul Rahman

FACULTY OF ENGINEERING AND GREEN TECHNOLOGY

UNIVERSITI TUNKU ABDUL RAHMAN

Date: _____

SUBMISSION OF THESIS

It is hereby certified that **KEE SHIN YIING** (ID No: **14AGD07934**) has completed this thesis entitled "DEVELOPMENT OF LIGHT ABSORPTIVE POLYMERIC FORM STABLE COMPOSITE PHASE CHANGE MATERIAL FOR THERMAL STORAGE" under the supervision of Dr. YAMUNA MUNUSAMY (Supervisor) from the Department of Petrochemical Engineering, Faculty of Engineering and Green Technology, and Prof. Ir. Dr. ONG KOK SENG (Co-Supervisor) from the Department of Industrial Engineering, Faculty of Engineering and Green Technology.

I understand that University will upload softcopy of my thesis in pdf format into UTAR Institutional Repository, which may be made accessible to UTAR community and public.

Yours truly,

_____

(KEE SHIN YIING)

DECLARATION

I KEE SHIN YIING hereby declare that the dissertation/thesis is based on my original work except for quotations and citations which have been duly acknowledged. I also declare that it has not been previously or concurrently submitted for any other degree at UTAR or other institutions.

_____

(KEE SHIN YIING)

Date_____

TABLE OF CONTENTS

		Page
ABSTRACT		**ii**
PUBLICATIONS		**iv**
ACKNOWLEDGEMENTS		**vi**
APPROVAL SHEET		**vii**
DECLARATION		**ix**
LIST OF TABLES		**xvi**
LIST OF FIGURES		**xviii**
LIST OF SYMBOLS / ABBREVIATIONS		**xxiii**
CHAPTER		
1.0	**INTRODUCTION**	**1**
1.1	Background of Study	1
1.2	Problem statement	3
1.3	Aims and Objectives	5
1.4	Research Methodology	6
1.5	Outline of Thesis	10
2.0	**LITERATURE REVIEW**	**14**
2.1	Thermal Energy Storage (TES)	14
2.2	Phase Change Material	17
2.3	Composite PCM as TES	22

2.4 Recent Development of Composite PCM to Improve Thermal Stability 23
2.4.1 Adsorption by layered and porous structure 24
2.4.2 Blending with polymer matrix 31
2.4.3 Encapsulation 35
2.4.3.1 Chemical methods 36
2.4.3.2 Physical methods 40
2.4.4 Form stable material 44
2.5 Recent development of composite PCM to improve light absorption 46
2.5.1 Light absorption material 52
2.5.1.1 Overview of graphene and graphene/polymer 53
2.5.1.2 Overview and synthesis of RGO 54
2.6 Summary 57

3.0 MATERIALS AND METHODOLOGY 58
3.1 Materials and Chemicals 58
3.2 Methodology for preparation of FSCPCM to improve thermal stability 60
3.2.1 Form stable composite PCM (MA/PMMA) in powder form 60
3.2.1.1 Preparation method 60
3.2.1.2 Immersion and filtration coating method 62
3.2.2 Form stable PCM (MA) in pellet form 62
3.2.2.1 Preparation method 63

3.2.2.2 Dip-coating method 63
3.3 Preparation of FSCPCM to improve light absorption 64
3.3.1 Synthesis of RGO 64
3.3.2 Preparation of RGO blended PA coating solution 66
3.4 Chemical Properties 67
3.4.1 Fourier transform infrared spectroscopy (FTIR) 67
3.4.2 X-ray diffraction (XRD) 68
3.4.3 Raman spectroscopy 68
3.4.4 X-ray Photoelectron spectroscopy (XPS) 69
3.5 Tensile 69
3.6 Morphology analysis 70
3.6.1 Metallurgical analysis microscope 70
3.6.2 Field Emission Scanning electron microscopy (FESEM) 71
3.6.3 Transmission electron microscopy (TEM) 71
3.6.4 Atomic Force Microscope (AFM) 71
3.7 Thermal properties 72
3.7.1 Differential Scanning Calorimetry (DSC) 72
3.8 Thermal stability analysis 73
3.8.1 Leakage analysis 73
3.9 Durability analyses 74
3.9.1 Thermal cycling 74
3.9.2 Weathering 75
3.10 Light absorption measurement 76

3.10.1 UV-Vis absorption analysis 76

3.10.2 Solar energy conversion efficiency 77

3.10.2.1 Specific heat capacity measurement 77

3.10.2.2 Outdoor solar energy conversion efficiency measurement 83

3.11 Summary 89

4.0 RESULTS AND DISCUSSION FOR FORM STABLE COMPOSITE PCM WITH SUPPORTING MATERIAL AND COATING TO PREVENT LEAKAGE 90

4.1 Introduction 90

4.2 Leakage Test 93

4.3 Tensile Properties 96

4.4 Chemical Properties: Fourier Transform Infrared Spectroscopy (FTIR) 100

4.5 Morphology Analysis: Field Emission Scanning Electron Microscope (FESEM) 104

4.6 Thermal Properties: Differential Scanning Calorimetry (DSC) 105

4.7 Durability: Thermal cycling 110

4.8 Summary 113

5.0 RESULT AND DISCUSSION FOR FORM STABLE COMPOSITE PCM WITH ENHANCED COATINGS COMBINATION TO MAXIMIZE LATENT HEAT 116

5.1 Introduction 116

5.2 Leakage Analysis 119

5.3 Mechanical Properties of Film: Tensile 122

5.4 Chemical Properties: Fourier Transform Infrared Spectroscopy (FTIR) 125

5.5 Morphology Analysis: Microscope 128

5.6 Thermal Properties: Differential Scanning Calorimetry (DSC) 131

5.7 Durability: Thermal cycling 134

5.8 Summary 135

6.0 RESULT AND DISCUSSION FOR FORM STABLE COMPOSITE PCM WITH ENHANCED COATINGS BLENDED WITH RGO TO IMPROVE LIGHT ABSORPTION 138

6.1 Introduction 138

6.2 Characterization of RGO 141

6.2.1 Fourier Transform Infrared Spectroscopy (FTIR) 141

6.2.2 X-Ray Diffraction (XRD) 143

6.2.3 X-ray Photoelectron Spectroscopy (XPS) 144

6.2.4 Raman Spectroscopy 145

6.2.5 Morphology Analysis: Field Emission Scanning Electron Microscopy (FESEM) 146

6.2.6 Transmission Electron Microscopy (TEM) 149

6.2.7 UV-Visible Absorption Analysis 150

6.3 Dispersion Analysis of RGO in PA film 151

6.3.1 X-ray Powder Diffraction (XRD) 152

6.3.2 Field Emission Scanning Microscopy (FESEM) 153

6.3.3 Atomic Force Microscope (AFM) 154

6.4 Characterization and Performance Analysis of Light Absorptive Polymeric Form Stable Composite PCM 155

6.4.1 Solar Energy Conversion Efficiency 155

6.4.2 Chemical Properties: Fourier Transform Infrared Spectroscopy (FTIR) 159

6.4.3 Thermal Properties: Differential Scanning Calorimetry (DSC) 161

6.4.4 Durability 164

6.4.4.1 Durability: Thermal cycling 164

6.4.4.2 Durability: Weathering 166

6.5 Summary 168

7.0 CONCLUSION & FUTURE WORK 171

7.1 Conclusions 171

7.2 Future Work 174

APPENDIX A 189

APPENDIX B 190

APPENDIX C 191

APPENDIX D 192

APPENDIX E 193

APPENDIX F 194

LIST OF TABLES

Table		Page
2.1	Criteria of Ideal PCM as TES Material	16
2.2	Comparison of Different Categories of PCMs (Zhou et al., 2012; Cabeza et al., 2011)	19
2.3	Melting Point, Thermal Conductivity and Latent Heat: Fatty Acids (Sharma et al., 2004)	21
2.4	Examples of FSCPCM prepared by adsorption into layered and porous structure and some of their thermal properties	25
2.5	Examples of FSCPCM prepared by blending with polymer matrix and some of their thermal properties	32
2.6	Examples of FSCPCM prepared by encapsulation and some of their thermal properties	37
2.7	Examples of FSCPCM prepared by coating method and some of their thermal properties	41
2.8	Examples of FSCPCM with light absorption and some of their thermal properties	48
3.1	List of Chemicals Used	58
3.2	Calculation of the Specific Heat Capacity	81
3.3	Calculation of the Solar Energy and Heat Energy	88
4.1	Leakage Area for Composite PCMs (MA/PMMA) with and those without Coatings	93
4.2	Thermal Properties of Composite PCMs (MA/PMMA) at Different Weight Percentage of MA	106
4.3	Thermal Properties of Composite PCMs (MA/PMMA) in Different Weight Percentage of MA	108

Table		Page
4.4	DSC Results of Melting and Freezing Point before and after 1000 Thermal Cycling.	111
4.5	DSC Results of Melting and Freezing Latent Heat before and after 1000 Thermal Cycling.	112
4.6	Summary of the Outcome of the Characterization Tests	114
5.1	Leakage Area for MA pellet with Different Polymer Coating Combination after 10 Hours Heating	119
5.2	Tensile Properties of Polymer Coating Films	124
5.3	Thermal Properties of Dip Coated MA Pellet with Different Polymer Coating Combination	132
5.4	DSC Results of PANBR/MA Pellet before and after 1000 Thermal Cycling	135
5.5	Summary of the Outcome of the Characterization Tests	136
6.1	Thermal Properties of RGO-PARB/MA Pellets in Various RGO Loadings	162
6.2	Comparison Survey of Thermal Performance for Light Absorptive PCM	163
6.3	DSC Results of RGO-PANBR/MA Pellet before and after 1000 Thermal Cycling	165
6.4	Summary of the Outcome of the Characterization Tests	169

LIST OF FIGURES

Figures		Page
1.1	Concept of Light Absorptive Polymeric Form Stable Composite Phase Change Material	3
1.2	Flow Chart of the Research Methodology	7
1.3	Schematic of Light absorptive polymeric FSCPCM	10
2.1	Classification of Solid-liquid PCMs (Kee et al., 2018)	18
2.2	Structure of Core-Shell of Encapsulated PCM	35
2.3	Chemical Structure of RGO	55
2.4	Chemical Structure of Graphene Oxide (GO)	56
3.1	Solution Blending Setup for Preparation of Composite PCM (MA/PMMA) in Powder Form	61
3.2	Immersion and Filtration Method	62
3.4	Dip Coating Method	64
3.5	Experiment Setup for Reduction of GO to RGO under Reflux	66
3.6	Specimen for Tensile Test	70
3.7	Leakage Test Layout	74
3.8	In house Thermal Cycling Test System	75
3.9	Experiment Setup for Weathering	76
3.10	Specific Heat Capacity Measured by Using DSC	78
3.11	Linear Interpolation of Cs at Any Temperature T	82
3.12	Solar Energy Conversion System	83

Figures **Page**

3.13	The Outdoor Experiment Setup for Solar Energy Conversion Efficiency Measurement	84
3.14	Energy Transfer of a Sample	85
3.15	Numerical Integration of Solar Irradiance with Respect to Time	87
4.1	Work Flow of Phase 1 Experiment	92
4.2	Leakage Image of MA After Heating in Oven.	95
4.3	Leakage Comparison for Composite PCM (MA/PMMA, 60/40 wt %): (a) Without Coating (b) With Conformal Coating (c) With PA Coating	95
4.4	Stress Strain Curve for PA and Conformal Coating	97
4.5	E-Modulus of PA and Conformal Coating Film	97
4.6	Tensile of PA and Conformal Coating Film	98
4.7	Elongation at Break of PA and Conformal	99
4.8	FTIR Spectra for the Pure PMMA, Pure MA and Composite PCM (MA/PMMA, 60/40 wt %)	101
4.9	FTIR Spectra for Composite PCM (MA/PMMA, 60/40 wt %), Pure Silicone Conformal Coating Film and Composite PCM (MA/PMMA, 60/40 wt %) with Conformal Coating	102
4.10	FTIR Spectra for the Composite PCM (MA/PMMA, 60/40 wt %), Pure PA Film and Composite PCM (MA/PMMA, 60/40 wt %) with PA Coating	103
4.11	FESEM Photograph of Composite PCM (MA/PMMA, 60/40 wt %)	104
4.12	FESEM Photograph of Composite PCM (MA/PMMA, 60/40 wt %): (a) with Conformal Coating and (b) with PA Coating	105
4.13	DSC Curves of Composite PCM (MA/PMMA) at Different Weight Percentage of MA	107

Figures **Page**

4.14	DSC Curves of Composite PCMs (MA/PMMA) with Conformal Coating in Different Weight Percentage of MA	109
4.15	DSC Curves of Composite PCMs (MA/PMMA) with PA Coating in Different Weight Percentage of MA	110
4.16	DSC Curves of Composite PCMs (MA/PMMA, 80/20 wt%) without Coating before and after 1000 Thermal Cycling	112
4.17	DSC Curves of Composite PCMs (MA/PMMA, 80/20 wt%): (a) with Conformal Coating and (b) with PA Coating before and after 1000 Thermal Cycling	113
5.1	Work flow of Phase 2 Experiment	118
5.2	Changes of Leakage Area for Samples Over 10 Hours	120
5.3	Leakage Comparison for (a) MA Pellet, (b) PA/MA Pellet, (c) NBR/MA, (d) 2PA/MA, (e) 2NBR/MA (f) PARB/MA after Heating in Oven at 65°C for 10 Hours	121
5.4	Leakage Comparison for (a) 2NBR/MA Pellet and (b) PANBR/MA Pellet after Heating in Oven at 65°C for 24 Hours	122
5.5	Stress Strain Curve for PA, NBR and PA+NBR	123
5.6	FTIR Spectra for the NBR Film, PA Film and MA Pellet	126
5.7	FTIR Spectra for PA Film, PA/MA Pellet, 2PA/MA Pellet and PANBR/MA Pellet	127
5.8	FTIR Spectra for NBR Film, NBR/MA Pellet and 2NBR/MA Pellet	128
5.9	Optical Micrograph of the Cross Section of PA/MA Pellet	129

Figures **Page**

5.10	Optical Micrograph of the Cross Section of NBR/MA Pellet	129
5.11	Optical Micrograph of the Cross Section of PANBR/MA Pellet	130
5.12	DSC Curves of Dip Coated MA Pellet with Different Polymer Coating Combination	133
5.13	DSC Curves of PANBR/MA Pellet before and after 1000 Thermal Cycling	134
6.1	Work Flow of Phase 3 Experiment	140
6.2	FTIR Spectra of GNF, GO and RGO	142
6.3	XRD Diffractogram of GNF, GO and RGO	144
6.4	The C1s XPS Spectrum of (a) GO; (b) RGO	145
6.5	Raman Spectra of GO and RGO	146
6.6	FESEM Image of GNF	147
6.7	FESEM Image of GO	148
6.8	FESEM Image of RGO	148
6.9	Cross Section TEM Image of RGO	149
6.10	UV-Visible Spectrum of RGO Disperse in Water	151
6.11	XRD Diffractogram of RGO and PA at Various RGO Loading	153
6.12	Temperature of RGO-PANBR/MA Pellets with Various Loading after Exposing to Sunlight for 8000 seconds	156
6.13	Total Stored Heat Energy in RGO-PANBR/MA Pellets with Various Loading	157
6.14	Solar Energy Conversion Efficiency of RGO-PANBR/MA Pellets with Various Loading	159
6.15	FTIR Spectra of RGO, PANBR/MA Pellet and 1.5 wt% RGO-PANBR/MA Pellet	160

6.16	DSC Curves of PANBR/MA Pellet with Different RGO Loadings	163
6.17	DSC Curves of RGO-PANBR/MA Pellet before and after 1000 Thermal Cycling	165
6.18	FTIR spectra of 1.5 wt% RGO-PANBR before and after weathering test	168

LIST OF SYMBOLS / ABBREVIATIONS

Symbols / Abbreviations	Description
General	
Max	Maximum
Endo	Endothermic
Exo	Exothermic
N/A	Non-available
UV	Ultraviolet
UV-VIS	Ultraviolet-visible
Material Names and Chemical Structures	
AA	Acrylic acid
BA	Butyl acrylate
C	Carbon atom
C=C	Carbon double bond carbon
C=O	Carbonyl group
C≡N	Nitrile group
C-H	Carbon-hydrogen bond
CH_3	Methyl group
CU_2O-CU	Copper (I) oxide –copper
EVA	Ethylene-vinyl acetate
FSCPCM	Form stable composite phase change material
GNF	Graphite nanofiber
GO	Graphene oxide
H	Hydrogen atom
HDPE	High-density polyethylene

Symbols / Abbreviations	Description
KBr	Potassium bromide
LDPE	Low-density polyethylene
MA	Myristic acid
MMA	Methyl methacrylate
MPEG	Methoxypolyethylene glycol
MWCNTs	Multi walled carbon nanotubes
NBR	Nitrile butadiene rubber
O	Oxygen atom
-O-CH_3	Methoxy group bond
O-H	Hydroxyl group
PA	Polyacrylic coating
PCM	Phase change material
PEG	Polyethylene glycol
PEO	Poly(ethylene oxide)
PMMA	poly(methyl methacrylate)
RGO	Reduced graphene oxide
Si	Silicone
Si-C	Silicone-carbon bond
Si-CH_3	Silicone-methyl
Si-O	Silicone-oxygen bond
SiO_2	Silicone dioxide/ silica
SMA	Styrene maleic anhydride copolymer
TES	Thermal energy storage
Ti_4O_7	Titanium black

Chemical Analysis

ATR	Attenuated Total Reflectance

Symbols / Abbreviations	Description
DSC	Differential scanning calorimetry
FESEM	Field emission scanning electron microscope
FTIR	Fourier-transform infrared spectroscopy
TEM	Transmission electron microscope
TGA	Thermogravimetric analysis
XPS	X-ray photoelectron spectroscopy

Measurement Units

%	Percentage
°	degree
°C	Degree Celcius
µL	microlitre
Å	Angstrom, 10^{-10} m
eV	electronvolt
g	gram
J/g	Joule per gram
KJ/Kg	Kilojoules per kilogram
kV	kilovolts
min	minutes
ml	milliliter
mm	Millimetre
MPa	Millipascal
N	Newton
nm	nanometre
s	Seconds
W	Watts
W/mK	Watts per meter Kelvin

Symbols / Abbreviations	Description
wt%	Weight percentage

Symbols

A	Top surface area of the sample (m^2)
c_c	Specific heat capacity of the crucible ($jg^{-1}k^{-1}$)
c_s	Specific heat capacity of the sample ($jg^{-1}k^{-1}$)
E_{heat}	Heat energy absorbed by the sample which increase the temperature (j)
E_{loss}	Energy loss (j)
E_{solar}	Solar energy from the sun (j)
I_{solar}	Solar irradiance measured by using the pyranometer (wm^{-2})
M_{AW}	Mass pellet after weathering
M_{BW}	Mass pellet before weathering
m_c	Mass of the crucible (g)
M_{loss}	Mass loss percentage (%)
m_s	Mass of the sample (g)
$Q_{L(R)}$	Heat energy loss from the empty crucible (J)
$Q_{L(S)}$	Heat energy loss from the crucible with the sample (j)
$Q_{S(R)}$	Heat energy supplied to the empty crucible (J)
$Q_{S(S)}$	Heat energy supplied to the crucible with the sample (J)
T_{AC}	Thickness of pellet after coating
T_{BC}	Thickness of pellet before coating
T_{film}	Thickness of one side coating film
T_s	Temperature of the sample (°c)
ΔT	Change in temperature (k)

Symbols / Abbreviations	Description
ΔT	The period of time for the change in temperature δt (s)
η	Solar energy conversion efficiency of the sample (%)

CHAPTER 1

INTRODUCTION

1.1 Background of Study

In the face of depleting energy resources and the need to curb greenhouse gas emissions, solar energy has again raised to the forefront of renewable and sustainable energy studies. Thermal energy storage (TES) has become an important part of renewable energy technology systems because it is able to absorb and store heat during high solar gain and release the stored heat energy during low solar gain for heating and cooling applications (Sarbu and Sebarchievici, 2016). Therefore, development of TES would reduce the fossil fuel usage for generating heat and indirectly reduce the emission of harmful greenhouse gases.

There are three main types of TES which is sensible heat, latent heat and chemical heat storage (Tian and Zhao, 2013). Among all, latent heat storage material, also known as phase change material (PCM) is one of the most popular TES storage types because it has high storage density and able to store large amount of heat at a nearly constant temperature (Agyenim et al., 2010).

PCMs are generally divided into organic PCMs, inorganic PCMs and eutectic PCMs (Tyagi and Buddhi, 2007; Iten et al., 2016). In this study, the organic PCM -myristic acid (MA) is used as TES because it has suitable phase

change temperature, high latent heat, good thermal properties and thermal reliability (Sarı et al., 2008a). However, fatty acid is acidic and it can cause the corrosion of container. Therefore, many studies were carried out to develop form stable composite fatty acids using three different methods: (i) adsorption; (ii) polymer blending and (iii) encapsulation. There are many advantages of using form stable composite fatty acid PCMs, including the enhancement of thermal stability and the increase of specific heat transfer area (Yuan et al., 2014).

Recent researches also study on enhancement of light absorption of PCM by adding light absorption materials. Light absorption materials serve as a photon antenna to capture sunlight and convert light to heat energy due to its strong absorbance and excellent light-thermal conversion capability (Wang et al., 2012d). Therefore, PCM with light absorption material is able to convert light to heat energy and thus improve the efficiency of TES system.

In this research, a new light absorptive polymeric form stable composite phase change material (FSCPCM) is developed with improved thermal stability and light absorption ability during phase change process. The concept of light absorptive polymeric FSCPCM is shown in Figure 1.1. PCM is encapsulated by light absorptive polymer coating to absorb sunlight and store heat energy in latent heat form. It is expected to improve light harvesting and solar energy conversion efficiency of the PCM. Besides, a new in-house design setup was developed to quantitatively measure stored heat energy and solar energy conversion efficiency at outdoor environment.

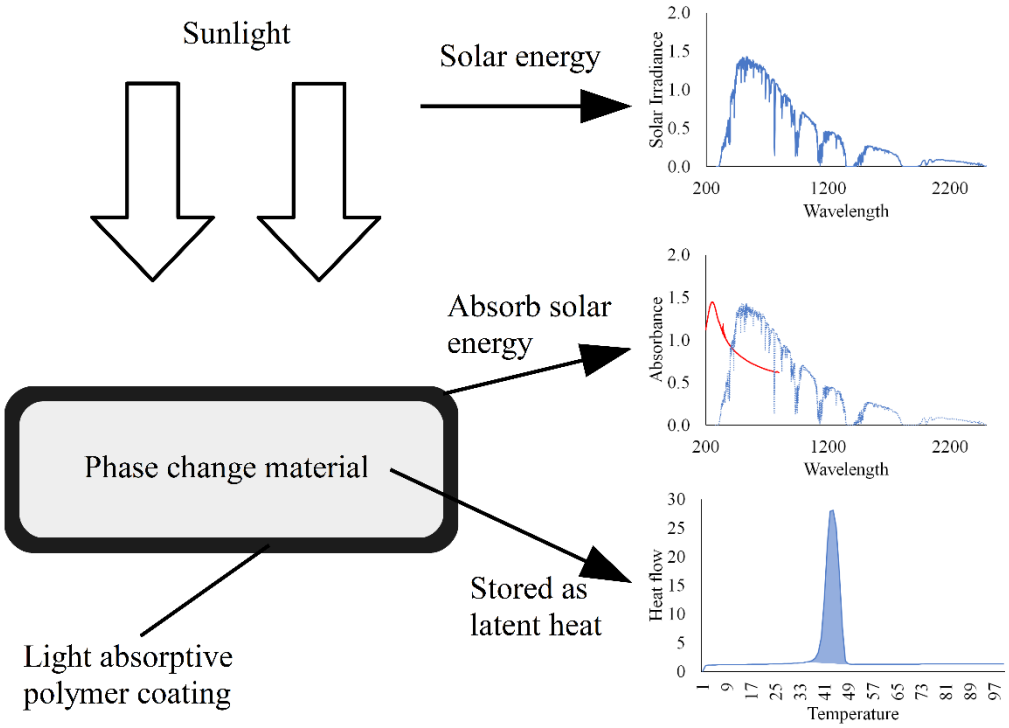

Figure 1.1: Concept of Light Absorptive Polymeric Form Stable Composite Phase Change Material

1.2 Problem statement

Malaysia climate is very suitable for the application of TES system because the average daily solar radiation is 4000 – 5000 Wh/m^2, with the average daily sunshine duration about 6 hours (Irwan et al., 2013; Markos and Sentian, 2016). However, the practical application of PCM as TES has two major issue which is large volume change during phase change process and the lack of study on light absorption of composite PCM which can convert light energy into heat energy.

Solid-liquid PCMs undergo phase change from solid to liquid during melting or vice versa. The large volume change and pressure build up during melting and cooling are associated with the containment problem and hence limits its practical application. Furthermore, PCMs such as fatty acid which is weak acid will cause the corrosion of the container (Ferrer et al., 2015). Therefore, FSCPCM is develop to maintain its shape and minimize the volume change, although it is heated above its melting point (Sarı, 2004). Coating is one of the methods to produce FSCPCM. Few studies showed that coating applied on composite PCM with supporting material has improved thermal stability and minimized the volume change during phase change process (Ramakrishnan et al., 2015; Kheradmand et al., 2015; Kong et al., 2016). However, adding both supporting material and coating reduced PCM mass percentage which contribute to the latent heat. An efficient TES require high latent heat PCM.

Despite PCMs have the ability to improve the utilization of heat energy efficiency, but majority of PCMs have low solar energy conversion ability which limits its practical application (Yang et al., 2017). To address this problem, light absorption material is added on PCM to improve the light harvesting effectiveness of solar irradiation and solar energy conversion, storage and utilization. Previous studies showed that light absorption materials such as dye and nano materials with good optical absorption properties able to absorb light efficiently and convert it to heat energy for storing (Tang et al., 2017b). The stored energy will be released during phase change process.

Since the development of PCM with light absorption properties is a new field of interest, this study focuses on exploring new materials which can absorb wider range of wavelength to promote solar energy conversion and energy storage. Thin sheet reduced graphene oxide (RGO) is chosen to be used because it has never been used as light absorptive material in FSCPCM before. Carbon and carbon-based material are worth to be explored because of their unique optical, electrical, and mechanical properties (Dai et al., 2012; Chen et al., 2012). Recent studies showed that graphene provide good optical properties as it absorbs a 2.3% fraction of incident white light (Bablich et al., 2016). New in-house design setup is introduced for measuring solar conversion efficiency to heat energy by composite PCM with light absorption material.

1.3 Aims and Objectives

The aim of this research is to develop new light absorptive polymeric FSCPCM with high thermal stability, latent heat and solar energy conversion efficiency. Specific objectives are listed below:

I. To produce FSCPCM using new coating material.

II. To enhance latent heat of FSCPCM by directly applying coating film on PCM.

III. To characterize the light to heat conversion properties of RGO-FSCPCM.

1.4 Research Methodology

This research aims to develop light absorptive polymeric FSCPCM for TES using dip coating method. The research methodology for producing this light absorptive polymeric FSCPCM is shown in Figure 1.2.

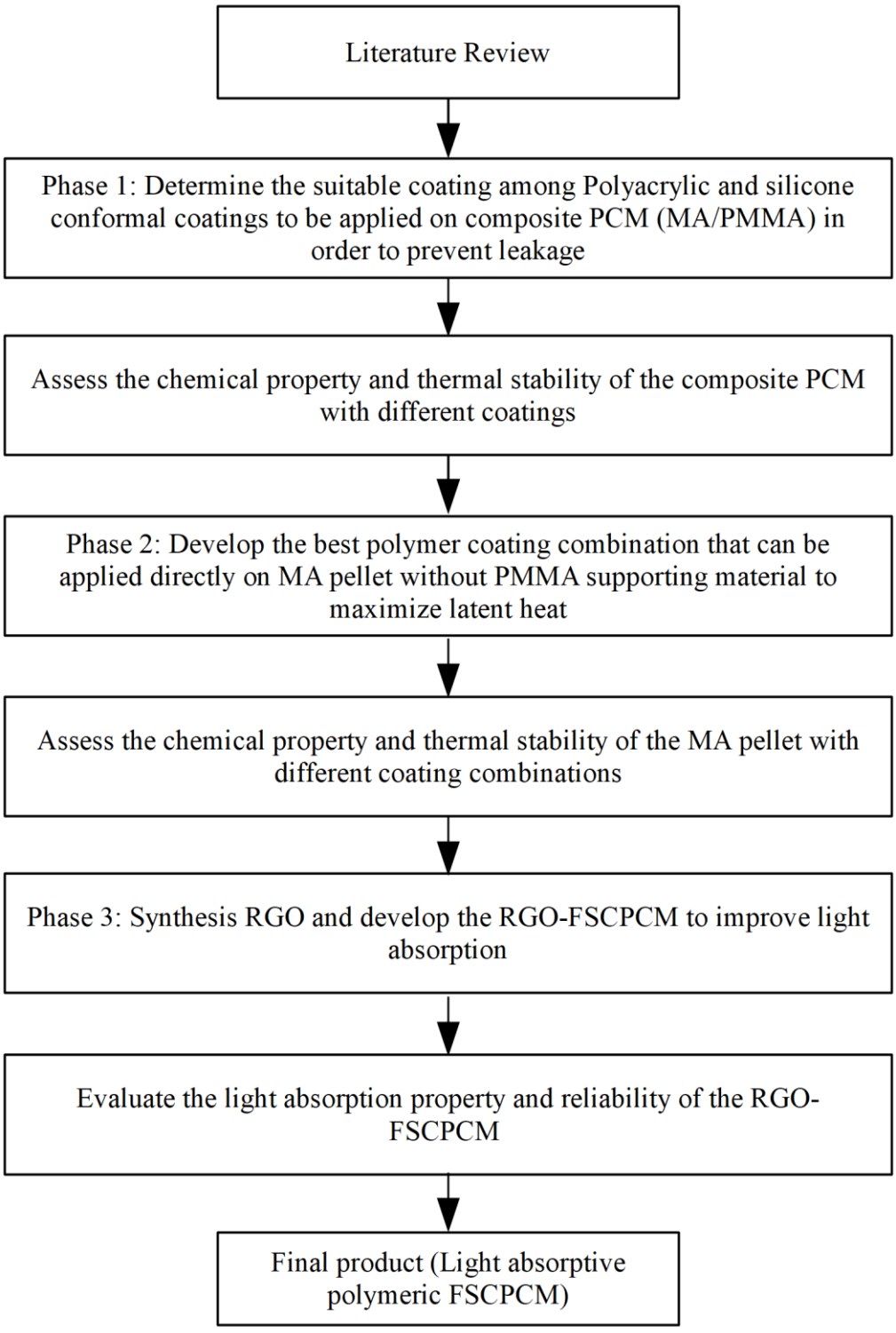

Figure 1.2: Flow Chart of the Research Methodology

Step 1: Literature Review

All the topics related to the FSCPCM and light absorption materials were reviewed. The relevant topics includes: categories of FSCPCM, preparation methods, potential coatings and light absorption materials.

Step 2: Phase 1 - Determine the Suitable Coating among Polyacrylic and Silicone Conformal Coatings to be Applied on Composite PCM (MA/PMMA) in order to Prevent Leakage

Prepare and characterize two types of coatings - polyacrylic coating (PA) and silicone conformal coating - on composite PCM (MA/PMMA) with different weight percentage of MA to prevent leakage. The chemical property and thermal stability of the composite PCM (MA/PMMA) with these two coatings are accessed and compared. The results are used to determine which polymer coating is the best in preventing leakage and continue to be used in phase 2.

Step 3: Phase 2 - Develop the Best Polymer Coating Combination that can be Applied Directly on MA Pellet without PMMA Supporting Material to Maximize Latent Heat

The polymer coating identified in phase 1 which has better performance in preventing leakage is then combined with nitrile butadiene rubber (NBR) in

different layer combinations to enhance its elasticity properties. Different polymer coating layer combinations are directly applied on MA pellet without PMMA supporting material to maximize the latent heat of PCM. The chemical properties and thermal stability of the MA pellet with different coating layer combinations are accessed. The best polymer coating layer combination which can prevent leakage is continue to be used in phase 3 to produce RGO-FSCPCM without leakage.

Step 4: Phase 3 - Synthesis RGO and Develop the RGO-FSCPCM to Improve Light Absorption

RGO is synthesised according to the established method. After that, the RGO was blended with outer layer of polymer coating in different loading to determine the optimum loading for light absorption. The light absorption property and reliability RGO-FSCPCM are evaluated. Besides, solar energy conversion efficiency and total amount of stored heat for RGO-FSCPCMs are determined in this phase as well.

Step 5: Final Product (Light Absorptive Polymeric FSCPCM)

Lastly, the light absorptive polymeric FSCPCM (RGO-FSCPCM), as shown in Figure 1.3, which is able to absorb sunlight and thermally stable during the phase change process is developed. The light absorptive polymeric FSCPCM

consists of two main parts: PCM as the core and polymeric coating as the shell. The PCM is used to store heat energy as latent heat while the polymeric coating is used to contain the PCM and prevent leakage of the PCM material after the phase change process. Besides, RGO is also blended into the outer layer of polymeric coating to absorb solar energy and convert the solar energy into heat energy.

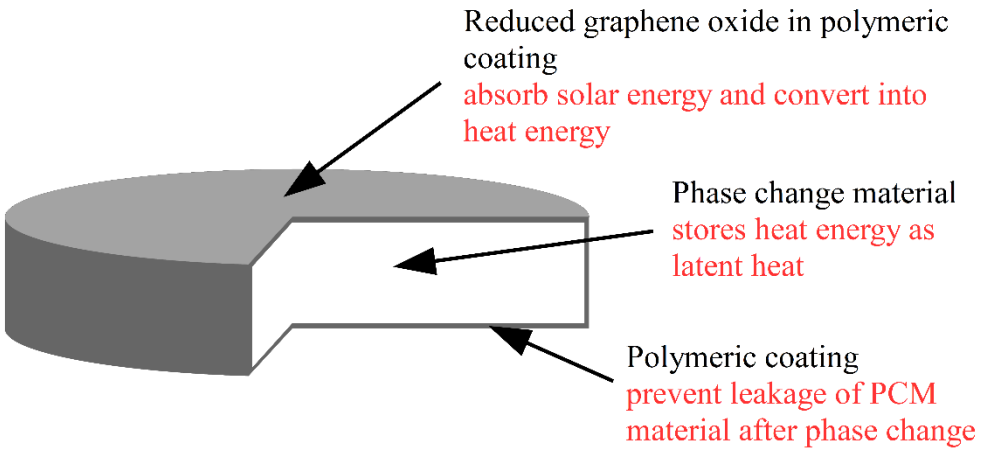

Figure 1.3: Schematic of Light absorptive polymeric FSCPCM

1.5 Outline of Thesis

The structure of the thesis is outlined in the following manner:

Chapter 2 is a comprehensive literature review on the topic. The reviews of several subjects related to the topic are included in the chapter, including the types of TES, criteria of PCMs as good TES and classification of PCMs. Besides,

review of recent development of composite PCM as TES to improve thermal stability and light absorption are also included. The examples, thermal performance, preparation method and significant finding in the recent development of composite PCM are summarized. Furthermore, the polymeric coating materials and light absorption materials used in this study are reviewed as well.

In chapter 3, the main experimental materials and techniques used in this study, including the synthesis of RGO and the development of light absorptive polymeric FSCPCM are presented. The instruments used for characterization tests such as chemical properties, mechanical properties, morphology analyses, thermal stability and reliability analyses are also listed down in this chapter. Experimental setup for solar energy conversion system is presented as well.

In Chapter 4, result and discussion for phase 1 of the research study are presented. PA and silicone conformal coating are applied on composite PCM (MA/PMMA) to prevent leakage. This chapter also contains characterization and performance analysis tests of the composite PCM with coating, such as leakage analysis, tensile test, Fourier-transform infrared spectroscopy (FTIR), field emission scanning electron microscopy (FESEM), differential scanning calorimetry (DSC) and thermal cycling test. The coating material suitable for the next phase is identified from the results.

Chapter 5 comprises the result and discussion for phase 2 of research study. MA pellet is dip coated with different polymer coating combination to determine the best polymer coating combination for MA pellet without PMMA supporting material to maximize latent heat. This chapter also contains the characterization and performance analysis tests of MA pellet with coating such as leakage analysis, tensile test, FTIR, FESEM, DSC and thermal cycling test. Lastly, the polymer coating combination that provide the best thermal stability for MA pellet is identified from the results. The product in this phase is known as FSCPCM because it is thermally stable and leakage free during its phase change process.

In Chapter 6, the result and discussion for phase 3 of the research study are presented. RGO is introduced into FSCPCM to improve the light absorption. This chapter contains characterization analysis of RGO such as FTIR, X-ray photoelectron spectroscopy (XPS), Raman spectroscopy, X-Ray Diffractometer (XRD), FESEM, transmission electron microscope (TEM) and UV-Visible absorption analysis. Dispersion of RGO in PA also studied using XRD, FESEM and atomic force microscope (AFM). Besides, characterization and performance analysis of dip coated MA pellet with RGO such as solar energy conversion efficiency, DSC, FTIR, thermal cycling test and weathering test results are performed and discussed as well. The optimum RGO loading that results in the highest solar energy conversion efficiency was identified from the results. The product in this phase is known as light absorptive polymeric FSCPCM because

it is thermally stable, able to absorb sunlight and leakage free during phase change process.

Chapter 7 is the conclusion of the research study where all the results and discussions of the research as well as the potential future work that can be done are summarized and presented.

CHAPTER 2

LITERATURE REVIEW

In this chapter, literature reviews on several topics related to the title of this research are presented. Types of TES and criteria of PCMs as good TES are described in the first section, followed by the classification of PCMs. Recent development of composite PCM as TES to improve thermal stability and light absorption are introduced next. Polymer coatings such as conformal coating, PA coating and NBR used in this study is reviewed. Besides, properties and preparation of RGO used as light absorption material are discussed. Lastly, summary of the literature review is made.

2.1 Thermal Energy Storage (TES)

Environmental issue, energy shortage, high cost of energy and new power plant are among the major issues faced by human beings nowadays (Agyenim et al., 2010). Therefore, TES is developed to store excess heat energy and bridge the gap between energy generation and consumption (Sarbu and Sebarchievici, 2018). TES is a technology that allow the heat transfer and storage by heating or cooling a storage medium so that the stored heat energy can be used at a later time for heating and cooling applications such as in heat pump (Maaraoui et al., 2012), solar water heater (Mahfuz et al., 2014), and thermo-regulating textile composite (Siddiqui and Sun, 2015). Hence, it can reduce the fossil fuel usage

for generating heat and indirectly reduce emission of harmful greenhouse gases to environment.

There are three main types of TES which are sensible heat, latent heat and chemical heat storage (Tian and Zhao, 2013). Sensible heat storage media store heat based on the temperature change in the material. Examples of sensible heat storage media are water, soil and stone. Whereas latent heat storage media store heat through phase change process of the material at a certain temperature of phase change. Therefore, latent heat storage material is also known as phase change materials (PCMs). Examples of PCMs are paraffin and fatty acid. Chemical heat storage media store heat energy through sorption or thermo-chemical reactions of material. Examples of chemical heat storage media are solid silica gel and metal hydrides (Hastings and Wall, 2007).

Among all, PCM is one of the most popular TES storage types because it has high storage density and able to store large amounts of heat with only a small temperature change. Hence, a relatively smaller volume of the PCM is sufficient to store the required amount of heat energy. Besides, it has near isothermal behaviour during the charging and discharging processes (Sharma et al., 2004). An ideal PCMs used as TES should meet a number of criteria related to the desirable thermal, physical, kinetic and chemical properties as summarized in Table 2.1 (Sharma et al., 2009; Pielichowska and Pielichowski, 2014).

Table 2.1: Criteria of Ideal PCM as TES Material

No	Properties	Criteria
1	Thermal	• Suitable phase change temperature. • High latent heat so that high storage density can be achieved. • Good thermal conductivity to assist in the charging and discharging of the stored energy.
2	Physical	• Small volume change during phase change. • Low vapor pressure at operating temperatures. • Congruent melting of the PCM for a constant storage capacity of the material with each freezing/melting cycle.
3	Kinetic	• Little supercooling to assure that melting and solidification can proceed in a narrow temperature range. • High crystallization growth rate to meet demands of heat recovery from the storage system.
4	Chemical	• Long-term chemical stability. • No degradation after a large number of thermal cycling. • Chemical compatibility with materials of construction. • Non- toxic, non-corrosive, non-flammable and non-explosive for safety.
5	Economics	• Low cost. • Good recyclability and long lifetime. • Abundant and large-scale availability in market.

2.2 Phase Change Material

Latent heat storage (LHS) media or known as PCM absorbs or releases heat with the changes of physical state during phase change process. In general, there are four categories of PCMs: solid-solid, solid-liquid, solid-gas and liquid-gas PCMs (Ge et al., 2013). However, only solid-liquid PCMs are commonly used as TES in a wide range of applications because the other three types of PCMs have following limitations:

a) Solid-solid PCMs have small latent heat (Tatsidjodoung et al., 2013).
b) Solid-gas and liquid-gas PCMs have the large volume variations or high pressure with the presence of gas phase (Cárdenas and León, 2013).

For solid-liquid PCMs, LHS is achieved by solid to liquid phase change. During daytime, temperature of PCM rises as it absorbs heat. When the PCM reaches melting point, it absorbs a large amount of heat at an almost constant temperature. The PCM continues to absorb and store heat without significant rise in temperature until all the material has changed from solid to liquid (Cui et al., 2014). During the night or when heat is withdrawn from the system, the surrounding temperature of the liquid PCM falls. The PCM solidifies and releases the stored latent heat to the surrounding environment (Souayfane et al., 2016).

Solid-liquid PCMs are generally divided into organic PCMs, inorganic PCMs and eutectic PCMs (Tyagi and Buddhi, 2007; Kenisarin and Mahkamov, 2007; Sharma et al., 2015). Classification of the solid-liquid PCMs is illustrated in Figure 2.1 (Kee et al., 2018). They are available in different phase change temperature ranges. A comparison of these three categories of PCMs is shown in Table 2.2 (Zhou et al., 2012; Cabeza et al., 2011).

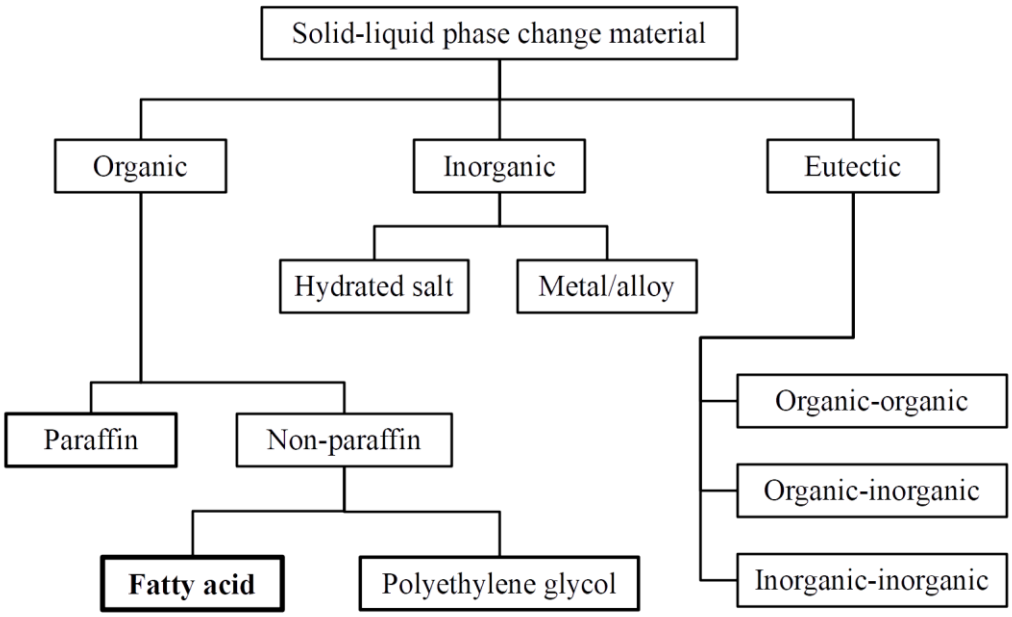

Figure 2.1: Classification of Solid-liquid PCMs (Kee et al., 2018)

Table 2.2: Comparison of Different Categories of PCMs (Zhou et al., 2012; Cabeza et al., 2011)

Classification	Examples	Advantages	Disadvantages
Organic PCMs	Paraffin, fatty acid, ester and polyethylene glycol	• Low supercooling • Chemically and thermally stable • Available in a large temperature range (from 20 °C up to 70 °C) • High latent heat • Good compatibility with other materials	• Low thermal conductivity (around 0.2W/mK) • Relatively large volume change • Flammable
Inorganic PCMs	Hydrated salt, molten salts, metals and alloys	• High latent heat • High thermal conductivity (around 0.5 W/mK) • Low volume change • Cheap	• Supercooling • Latent heat decreased over repeated thermal cycling.
Eutectics	Organic-organic, organic-inorganic and inorganic-inorganic	• Sharp melting temperature • High volumetric thermal storage density	• Lack of currently available data of thermo-physical properties

From Table 2.2, it is clearly seen that each particular group of PCM has its advantages and disadvantages. The organic PCMs are widely used as TES because they have suitable phase change temperature and high latent heat. There

are two main groups of organic PCMs: paraffin and non-paraffin. Paraffin wax or *n*-alkane is a family of long chain saturated hydrocarbons with the molecular formula C_nH_{2n+2}. The melting temperatures of paraffin waxes are in the range from 23 °C to 67 °C due to the variation in hydrocarbon chain length (Akgün et al., 2007). Paraffin waxes are non-poisonous, chemically stable and exhibit small volume change during phase change process (He et al., 2004). However, they have low thermal conductivity and moderately flammable (Su et al., 2015).

On the other hand, non-paraffin organic PCM consists of fatty acid, polyethylene glycol (PEG), alcohols and glycols. Among them, fatty acid and PEG are the two main large group of candidate materials used for TES. Fatty acid is weak acid with the chemical formula $CH_3(CH_2)_{2n}COOH$. The phase change temperature and latent heat of saturated fatty acids increases with the increase of the carbon chain length (Yuan et al., 2014). The long carbon chain tails of fatty acid cause it to exhibit the same characteristics as paraffin. However, fatty acids generally have higher latent heat than paraffin. Another one main sub groups of non-paraffin organic PCM is PEG. PEGs also known as macrogols, are liquid or solid polymers with the general formula of $H(OCH_2CH_2)n{\cdot}OH$. PEG is a good TES material because of its relatively large latent heat, congruent melting behaviour and non-corrosiveness (Alkan et al., 2012). However, PEG undergoes degradation after certain period of exposure to sunlight. Thermal degradation of PEG produces low molecular weight products, which causes a lowering of the melting point and the latent heat (Han et al., 1997).

Among all organic solid-liquid PCMs, fatty acid is chosen to be used as TES in this study because it has suitable phase change temperature for particular application in the tropical country likes Malaysia. Moreover, they also show reproducible melting and freezing behavior and freeze with no supercooling (Baetens et al., 2010). For example, stearic acid was reported to have stable properties after 1500 cycles (Sharma et al., 2002). However, fatty acids are mildly corrosive because they are weak acid.

A few fatty acids that are commonly used as PCMs are shown in Table 2.3 (Sharma et al., 2004). MA which has high latent heat was used as PCM in this study. This is because thermal storage capacity of the PCM is dependent on latent heat. Latent heat is the amount of thermal energy that a material absorbs or releases when it changes from solid to liquid or vice versa. The higher latent heat of PCMs lead to more efficient system in heating or cooling application (Koschenz and Lehmann, 2004; Socaciu et al., 2014).

Table 2.3: Melting Point, Thermal Conductivity and Latent Heat: Fatty Acids (Sharma et al., 2004)

Name	Meting Point (°C)	Thermal conductivity (W/mK)	Latent heat (kJ/kg)
Capric Acid	32	$0.153^{38.5C}$	152.7
Erucic Acid	33	n.a.*	n.a.*
Lauric Acid	42 - 44	n.a.*	178
Elaidic Acid	47	n.a.*	218

Pelargoinc Acid	48	n.a.*	n.a.*
Myristic Acid	49 - 51	n.a.*	205
Palmitic Acid	64	$0.1626^{8.4C}$	185.4
Stearic Acid	69	0.172^{70C}	202.5
Valporic Acid	120	n.a.*	n.a.*

n.a* Not available

2.3 Composite PCM as TES

In early years, researchers studied and discovered different types of PCM materials which are suitable to be used as TES. They characterized PCMs in the aspects of melting point, latent heat, thermal conductivity and other properties. However, none of each particular group of PCM is able to meet up all the requirements as an ideal TES material. Therefore, current research work is focused on the development of new composite PCMs and modification of existing PCM to overcome the limitations.

The issue of volume change of PCM during phase change process limit its future development as TES. To address these issues, current research work is focused on the development of new composite PCMs with improve thermal stability. Thermal stability of PCM can be improved by incorporating PCM into different supporting materials to produce form stable composite PCM which have small volume change and low vapor pressure during phase change process (Wang et al., 2011b). In addition, research on enhancement of light absorption

of PCM by adding photothermal energy conversion materials are gaining attention because they are able to convert light to heat energy and thus improve the efficiency of the TES system (Wang et al., 2014). The next section gives some examples of solid-liquid organic composite materials developed to improve different properties of PCM.

2.4 Recent Development of Composite PCM to Improve Thermal Stability

There are three common methods to produce form stable composite PCM (FSCPCM): (i) adsorption by layered and porous structure, (ii) blending with polymer matrix and (iii) encapsulation. FSCPCM is the composite PCM which can maintain its shape, although it is heated above its melting point (Yuan et al., 2014). During melting process, FSCPCM contain PCM in liquid phase to prevent it to interact with surroundings as PCM materials such as fatty acid is weak acid and corrosive. Moreover, FSCPCM also increase compatibility of PCM with other materials in the storage system and provide a suitable surface for heat transfer (Fang et al., 2010a). It also minimizes volume change during the phase transition (Kenisarin and Kenisarina, 2012)

In many researches works, thermal cycling test had been carried out as a benchmark to determine thermal and chemical reliability of FSCPCM with respect to the repeated melting and freezing cycles. FSCPCM is considered as thermally reliable if it has very little changes of phase change temperature and latent heat after repeated thermal cycling test. Whereas FSCPCM is durable if its chemical structure is not affected by repeated thermal cycling. The durability

could be confirmed if the shape and frequency value of all peaks in Fourier-transform infrared spectroscopy (FTIR) spectra are consistent before and after repeated thermal cycling test for the PCM (Mehrali et al., 2013).

2.4.1 Adsorption by layered and porous structure

FSCPCM can be prepared by adsorption PCM in the interlayer and pore structure of layered and porous matrix (Zhang et al., 2006; Sarı et al., 2009). The PCM is physically adsorbed into the matrix because both layered and porous materials have high surface area and large adsorption capacity (Li et al., 2011; Song et al., 2014a). During the melting process, the PCM is confined in the layered and porous structure and the movement of the PCM is restricted. The following Table 2.4 gives examples of FSCPCMs prepared by adsorption method and some of their thermal properties. For each reported work, the FSCPCM with optimum thermal stability had been taken into consideration and its thermal properties were compared with pure PCM.

Generally, the latent heat for FSCPCM prepared by adsorption method is lower than pure PCM. Therefore, layered and porous structure with high adsorption capability should be chosen to maximize adsorption ratio of PCM and hence producing FSCPCM with high latent heat.

Table 2.4: Examples of FSCPCM prepared by adsorption into layered and porous structure and some of their thermal properties

No	Materials and method	PCM Melting Point (°C), Latent Heat (J/g)	FSCPCM Melting Point (°C), Latent Heat (J/g)	Maximum adsorption ratio	Findings	Ref.
1	PCM: Lauric acid Porous material: Expanded Perlite Method: Vacuum impregnation method	44.15, 158.73	44.10, 93.40	60 wt%	Thermally and chemically reliable: After 1000 thermal cycling tests, the reduction of latent heat is 1.2% and no much changes of shape and frequency value of all FTIR peaks. FESEM image of lauric acid/expanded perlite are very similar after thermal cycling, indicating no degradation in the structure.	(Sarı et al., 2009)
2	PCM: Capric acid Porous material: Halloysite nanotube	29.62, 139.77	29.34, 75.52	60 wt%	Maintain its original shape perfectly without leakage after 50 thermal cycling. Nanotubes possess hollow nanotubular structure and large specific surface area.	(Mei et al., 2011)

	Method: Adsorption by capillary and surface tension force					
3	PCM: Capric-palmitic acid Porous material: Attapulgite Method: Vacuum	21.80, 138.20	21.70, 48.20	35 wt%	Thermally stable because attapulgite has large surface area for adsorption of capric-palmitic acid.	(Li et al., 2011)
4	PCM: PEG Porous material: diatomite Method: Vacuum impregnation method	33.32, 143.16	27.70, 87.09	50 wt%	Thermally reliable: After 1000 thermal cycling test, the reduction of latent heat of melting is 1.1%. PEG was impregnated and confined into the pores of diatomite because diatomite has high porosity and absorptive.	(Karaman et al., 2011)
5	PCM: PEG Porous material: activated carbon	N/A, N/A	45-65, 81-86	70 %	Thermal stability is assessed by TGA and no decomposition was found below 250 °C. It is thermally stable because activated carbon has extensive pore	(Feng et al., 2011)

	Method: Direct blending and impregnating				structures with high specific surface area and absorption capacity for PEG.	
6	PCM: PEG Porous material: Expanded graphite Method: Direct blending and impregnating	N/A, N/A	60-65, 150-160	90 wt%	Expanded graphite with macroporous structures can effectively stabilize the melted PEG through both the capillary force of the pores and the hydrogen bonding resulting from the surface functional groups.	(Wang et al., 2012a)
7	PCM: Composite paraffin Porous material: Calcined diatomite Method: Fusion adsorption method	29.94, 145.90	33.04, 89.5	61%	Thermally reliable: After 200 thermal cycling tests, the reduction in latent heat is less than 5%. Composite paraffin was impregnated and confined into the pores of calcine diatomite because diatomite has high porosity, high permeability and large specific surface area.	(Sun et al., 2013)

8	PCM: Stearic acid Layered material: Graphene oxide (GO) Method: Mixing and vacuum drying	74.00, 140.90	33.00, 55.70	50%	Stearic acid was confined well in the interlayer space of GO because strong interface interactions between stearic acid and GO was formed via their functional groups.	(Li et al., 2013)
9	PCM: Capric-auric-palmitic acid Porous structure: Carbon nanotube Method: Infiltration method	16.80, 140.50	17.20, 101.60	80 wt%	FESEM image indicated that fatty acid was effectively adsorbed into the porous structure of the carbon nanotubes as the pore volume is reduced significantly.	(Meng et al., 2013)
10	PCM: Paraffin Layered structure: GO sheet Method: Vacuum impregnation method	53.46, 131.92	53.57, 63.76	48.3 wt%	Thermally reliable: After 2500 thermal cycling tests, the reduction of latent heat is only 1.73%.	(Mehrali et al., 2013)

11	PCM: Lauric acid Porous material: Diatomite Method: Direct impregnation	44.40, 141.90	40.90, 57.20	60 wt%	The decomposition temperature of lauric acid in lauric acid /diatomite composite occurs from 157 to 203 °C, higher than that of pure lauric acid, indicating that the thermal stability of lauric acid increases after the lauric acid is impregnated into the porous diatomite.	(Fu et al., 2015)
12	PCM: PEG Porous material: mesoporous-calcium-silicate Method: Facile blending and impregnation method	58.95, 183.10	57.03, 122.10	70%	Thermally reliable: After 200 thermal cycling tests, no leakage of PEG was found. PEG was confined into the mesopores of calcium silicate because it has excellent thermal stability and high storage capacity.	(Qian et al., 2015)
13	PCM: Paraffin Porous material: kaolin	28.27, 150.90	23.88, 27.88	18%	Thermally stable: TGA results showed that no sign of degradation below 150 °C.	(Memon et al., 2015)

	Method: Vacuum impregnation					
14	PCM: Capric-palmitic-stearic acid Porous material: Nano-SiO_2 Method: Impregnation	18.45, 139.30	17.16, 99.43	75 wt%	Thermally reliable: After 500 thermal cycling tests, the reduction of latent heat is 5.17%. Low thermal conductivity and ultra-light weight	(Luo et al., 2017)
15	PCM: Palmitic-stearic acid Layered structure: Bentonite +expanded graphite Method: Impregnation	56.85, 89.47	56.85, 89.12	60%	Thermally reliable: After 50 thermal cycling tests, the reduction of latent heat is 14.6 %.	(Huang et al., 2017)

2.4.2 Blending with polymer matrix

FSCPCM can be prepared by blending of PCM with polymer matrix. For blending method, polymer matrix holds the PCM into a polymer network and restricts its movement during melting process (Sarı et al., 2009). Polymers such as poly(vinyl chloride), poly(vinyl alcohol), poly(methyl methacrylate) (PMMA), styrene maleic anhydride copolymer (SMA) and poly(ethylene oxide) (PEO) have been used to blend with PCM to produce form-stable composite PCM (Sari et al., 2006; Sari and Kaygusuz, 2006; Sari and Kaygusuz, 2007; Alkan and Sari, 2008; Sarı et al., 2008b; Pielichowska et al., 2008). Previous research showed that these form-stable composite PCMs can keep their shape stabilized even when the PCM state changes from solid to liquid over their phase change process. The following Table 2.5 gives examples of FSCPCMs and some of their thermal properties. For each reported work, the FSCPCM with optimum thermal stability had been taken into consideration and its thermal properties were compared with pure PCM. Generally, blending of polymeric matrix reduced the PCM mass percentage which contributes to latent heat. Therefore, latent heat for composite PCM is generally lower than pure PCM.

Table 2.5: Examples of FSCPCM prepared by blending with polymer matrix and some of their thermal properties

No	Materials and method	PCM Melting Point (°C), Latent Heat (J/g)	FSCPCM Melting Point (°C), Latent Heat (J/g)	Max encapsulation ratio	Findings	Ref.
1	PCM: Stearic acid Polymeric matrix: PMMA Method: Blending and solution casting	66.87, 242.15	67.31, 187.72	80 wt%	PMMA was compatible with the fatty acid. Composite PCM do not leak upon leakage test.	(Alkan and Sari, 2008)
2	PCM: Stearic acid Polymeric matrix: styrene maleic anhydride copolymer	66.87, 242.15	67.35, 202.23	85 wt%	Composite PCM also do not leak over melting point of stearic acid. FTIR analysis also showed that the interaction between ether oxygen of the styrene maleic and hydroxyl group of stearic acid, resulting good compatibility of both components.	(Sarı et al., 2008b)

	Method: Blending and solution casting					
3	PCM: Stearic acid Polymeric matrix: Acylic resin (Eudragit E) Method: Blending and solution casting	66.82, 258.98	65.41, 185.64	70 wt%	Composite PCM also do not leak over melting point of stearic acid.	(Kaygusuz et al., 2008)
4	PCM: Soft Fischer-Tropsch paraffin wax Polymeric matrix: High-density polyethylene (HDPE) Method: Blending and melt pressed	58.40, 172.20	57.10 & 124.10, 148.4	50%	Analysis showed that paraffin waxes were distribute evenly in the polymer matrices and no leakage was observed.	(Molefi et al., 2010)

5	PCM: PEG Polymeric matrix: Epoxy resin Method: Casting molding method	55.3, 186.7	54.2, 132.4	75 %	FESEM cross section photograph showed that PEG was well dispersed into epoxy network. Epoxy network restrict movement of PEG upon melting.	(Fang et al., 2010b)
6	PCM: PEG Polymeric matrix: Chitosan Method: Blending and solution casting	53.23, 208.57	57.18, 152.16	80 wt%	Microscope analysis showed that composite PCM do not leak upon melting because single-phase morphology was observed. The leakage of PEG will cause phase separation. FTIR result also confirmed that the interaction between PEG and chitosan is hydrogen bonding and hence PEG was hosted in PEG matrix.	(Şentürk et al., 2011)

2.4.3 Encapsulation

FSCPCM can be prepared by encapsulation method. Encapsulation is the process of coating individual particles or droplets with a film to produce capsule (Khadiran et al., 2015). Figure 2.2 shows the image of encapsulated FSCPCM which consisted of two main parts: PCM as core while polymer or inorganic material as shell. Shell layer serves as wall to contain PCM and keeps the melted PCM in solid state. Encapsulated FSCPCM can be achieved via two methods which are chemical and physical method.

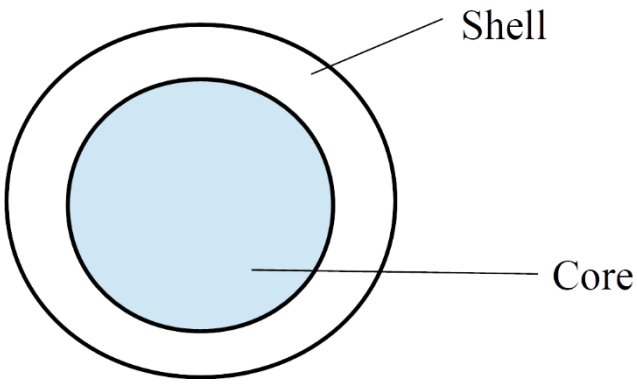

Figure 2.2: Structure of Core-Shell of Encapsulated PCM

2.4.3.1 Chemical methods

Chemical method is widely used to produce micro or nano-encapsulation of FSCPCM. In chemical method, the microcapsule wall is chemically formed through polymerization of monomer around microcapsule core. Examples of chemical formation are polymerization such as in situ polymerization, emulsion polymerization and suspension polymerization (Su et al., 2015). Similar to other FSCPCM, incorporation of polymeric or inorganic matrix reduced the PCM mass percentage which contributes to latent heat. Therefore, latent heat for encapsulated FSCPCM is generally lower than pure PCM. To overcome this problem, high encapsulation efficiency of polymeric or inorganic matrix should be achieved to maximize PCM mass percentage and hence producing composite PCM with high latent heat. Table 2.6 gives examples of FSCPCMs and some of their thermal properties. For each reported work, the FSCPCM with optimum thermal stability had been taken into consideration and its thermal properties were compared with pure PCM.

Table 2.6: Examples of FSCPCM prepared by encapsulation and some of their thermal properties

No	Materials and method	PCM Melting Point (°C), Latent Heat (J/g)	FSCPCM Melting Point (°C), Latent Heat (J/g)	Max encapsulation ratio	Findings	Ref.
1	PCM: Lauric-myristic acid Polymeric matrix: PMMA Method: self-polymerization	35.18, 162.27	N/A, 113.2	70 wt%	FESEM images showed that fatty acid eutectic was enwrapped by PMMA so that there was no leakage of melted fatty acid out of the composite during phase change process.	(Wang and Meng, 2010a)
2	PCM: Stearic acid Polymeric matrix: PMMA	59.90, 177.80	60.40, 92.10	51.8 wt%	Thermally and chemically reliable after 500 thermal cycling	(Wang et al., 2011a)

	Method: Dispersion polymerization					
3	PCM: Paraffin wax Polymeric matrix: Polyaniline Method: Microencapsulation using in situ polymerization	53-57, 131.92	53.8, 65.1	20%	Thermally reliable: After 1000 thermal cycling, no cracks were observed on the surface of the polyaniline coating and the reduction of latent heat is 7%.	(Silakhori et al., 2013)
4	PCM: *n*-eicosane Polymeric matrix: Polyurethane Method: Bulk polymerization	38.28, 251.70	37.99/57.43 , 141.20	25 %	TGA indicated that the composite PCM degraded at high temperatures.	(Chen et al., 2014)
5	PCM: Caprylic acid Polymeric matrix: Urea-formaldehyde resin	19.31, 158.44	13.90, 93.90	59 wt%	FESEM images showed that microcapsules have spherical structure and well encapsulated.	(Konuklu et al., 2014)

	Method: Microencapsulation (coacervation)					
6	PCM: Capric-stearic acid Polymeric matrix: Silica Method: emulsion polymerization	24.1, 161.35	21.4, 91.48	56.7 %	Thermally reliable: After 1100 thermal cycling, the reduction of latent heat is 2.6%.	(Song et al., 2014b)
7	PCM: Capric-stearic acid Polymeric matrix: PMMA Method: emulsion polymerization	26.04, 176.68	20.20, 116.25	65.8%	Morphological results showed that the encapsulate PCM had spherical structure. Thermogravimetric analysis (TGA) showed that encapsulate PCM had good thermal durable up to 80 °C. Thermally and chemically reliable after 5000 thermal cycling	(Sarı et al., 2015)

2.4.3.2 Physical methods

FSCPCM can be prepared by physical method where microcapsule wall is mechanically applied or condensed around microcapsule core (Jamekhorshid et al., 2014). For physical method, a thin film is formed to cover the surface of PCM. Hence, the film acts as a shell to hold PCM during phase change process (Xu et al., 2015). Examples of physical method are spray drying, solvent evaporation and coating (Jamekhorshid et al., 2014). The following Table 2.7 gives examples of FSCPCMs and some of their thermal properties. However, only paraffin wax was reviewed in this subsection as no study report on fatty acid and PEG yet. For each reported work, the FSCPCM with optimum thermal stability had been taken into consideration and its thermal properties were compared with pure PCM.

Table 2.7: Examples of FSCPCM prepared by coating method and some of their thermal properties

No	Materials and method	PCM Melting Point (°C), Latent Heat (J/g)	FSCPCM Melting Point (°C), Latent Heat (J/g)	Max encapsulation ratio	Findings	Ref.
1	PCM: *n*-octadecane (C18) Coating material: Titania Method: Aerosol	33.00, 233.00	28.70, 97.00	80%	The encapsulated FSCPCM had diameter of 0.1-0.5 µm and two structures of dense or hollow spheres.	(Fei et al., 2008)
2	Composite PCM: Praffin wax (Rubitherm RT27) Coating material: Low density polyethylene-ethylvinylacetate copolymer (LDPE-EVA)	29.41, 199.00	28.40, 98.14	49.32 wt%	Thermally reliable: After 3000 thermal cycling, no fracture was observed on surface of encapsulated FSCPCM under FESEM.	(Borreguero et al., 2011)

	Method: Spray drying					
3	Composite PCM: Paraffin (PX25) + cement paste Coating: hydrophobic fumed silica Method: mix and dry	24.13, 78.11	22.77, 13.44	N/A	Leakage was eliminated when hydrophobic fumed silica was used in a 2.3% mass fraction relative to paraffin.	(Li et al., 2014)
4	Composite PCM: Paraffin + silicone coated perlite Coating material: silicone Method: coating	24.50, 133.30	22.10, 60.90	N/A	Thermally reliable after 100 thermal cycling.	(Ramakrishnan et al., 2015)
5	Composite PCM: Paraffin (R5) + expanded vermiculite Coating material: Makote 3 (a waterproofing bituminous emulsion from MC-Bauchemie)	1.00-6.00, 180.00	N/A	N/A	Coating can minimize the leaking as only 0.5% leakage was found after thermal cycling	(Kheradmand et al., 2015)

	Method: soak and dry					
6	PCM: Paraffin + expanded perlite Coating material: Colloidal silica and organic acrylate Method: immerse and dry	25.80, 107.60	21.60, 56.30	N/A	Thermally reliable: After 1000 thermal cycling tests, the reduction of latent heat is 0.9 %	(Kong et al., 2016)

2.4.4 Form stable material

Among all preparation methods, coating method was chosen in this study to produce FSCPCM with improved thermal stability. This is because coating method is applicable to PCM in different shapes, either spherical, pellet or cylindrical. It also involves less complicated process (Fei et al., 2008; Xu et al., 2015). Moreover, there is no study on preparation of form stable composite fatty acid using coating method yet.

Three types of coatings were used in this study which is silicone conformal coating, PA coating and NBR. Silicone conformal coating (Dow corning 1-2620) is a commercial product from Dow Corning, United States. It is transparent low viscosity coating solution. It forms a firm, abrasion resistance surface after cure (Dow Corning, 2018). Besides, it also exhibits good barrier properties to moisture. Silicon conformal coating is used in electronic components such as printed circuit boards to minimize the degradation in electrical performance due to contamination (Montemayor and Midland, 2012).

PA coating is a terpolymer synthesized by Dr. Chee Swee Yong and her research team. This coating solution is the combination of methyl methacrylate (MMA) and butyl acrylate (BA) with acrylic acid (AA) as the tertiary co-monomer. MMA is the major segment of the copolymer as it has high mechanical strength, UV retention and transparency upon film processing

(Imperiyka et al., 2013). Rubbery BA (at room temperature) is copolymerized in a random arrangement with PMMA to improve chain flexibility. Short AA segment present within the P(MMA-co-BA) chain may show a good wetting property. Hence, PA coating may bond well to the surface of substance during coating. PA coating was used as polymeric solid state electrolytes for dye sensitized solar cell (Shanti et al., 2016).

Nitrile butadiene rubber (Synthomer X6311) is also commercial elastomer product from Synthomer, United Kingdom. It is an aqueous, colloidal dispersion of carboxylated butadiene-acrylonitrile copolymer with a medium acrylonitrile level. The dispersion contains an emulsifier system and is stabilized with an antioxidant (Synthomer, 2018). NBR is lightweight, resistance to corrosion and also having high tensile strength (Singh et al., 2012). It is widely used in paint, flexible multilayered coatings and rubber textile applications.

Literature review showed that these three coatings solution have never been used on PCM before. Besides, they also have common properties such as high tensile strength and able to dried off at room temperature to make them suitable to be used as new coating material on PCM.

2.5 Recent development of composite PCM to improve light absorption

Solar energy is one type of popular renewable energy in Malaysia because Malaysia receive a large amount of sunlight throughout the year. Therefore, conversion of solar energy to heat energy is important to improve solar energy utilization efficiency of TES.

In recent years, some studies focused on the enhancement of PCM's light absorption by adding light absorption materials such as dye and good optical absorption nano-materials. Light absorption materials serve as a photon antenna to capture sunlight and convert light to heat energy due to its strong absorbance and excellent light-thermal conversion capability (Wang et al., 2012d). The light to thermal conversion occurred due to the nonradiative decay process (vibrational relaxation, internal conversion, and intersystem crossing) of the light absorption materials under sunlight (Wang et al., 2012b). Therefore, composite PCM with light absorption materials can harvest sunlight efficiently and convert it to heat energy. Heat energy is effectively stored and released during phase change process of PCM.

The following Table 2.8 gives examples of solid-liquid organic PCMs with light absorption properties. Table 2.8 also shows that different light absorption materials have different light absorption wavelength. However, light absorption wavelength of materials can be controlled by changing its chemical structure.

Therefore, future work can be focused on modifying and exploring more materials which can absorb wider range of wavelength to promote solar energy conversion and energy storage.

Table 2.8: Examples of FSCPCM with light absorption and some of their thermal properties

No	Materials and method	Pure PCM/ Composite PCM Melting Point (°C), Latent Heat (J/g)	Composite PCM with light absorption Melting Point (°C), Latent Heat (J/g)	Optimum Loading	λ_{abs} (nm)	Findings	Ref.
1	PCM: PEG 6000 Light absorption material: 1,4-bis((2-hydroxyethyl) amino) anthracene-9,10-dione dye Method: condensation polymerization	65.90, 178.7	54.80, 78.70	N/A	500-650	PEG 6000-co-Dye exhibit higher temperature (70 °C) than pure PEG-6000 (55.1 °C) after 34 min exposure under solar light irradiation (0.30W).	(Wang et al., 2012d)

2	Composite PCM: methoxypolyethylene glycol (MPEG-750) + polyethylene polyamine Light absorption materials: yellow dye (dye Y) Method: replacement and Williamson reaction	30.80, 113.20	32.70, 103.70	Molar ratio of MPEG 750:polyethylene polyamine:dye Y 4:1:0.5	300-500	MPEG has no absorption in visible region. PCM with dye Y exhibit higher temperature (about 58 °C) than pure MPEG-750 (about 27 °C) after exposure for 2750 s in light irradiation from simulated light source.	(Wang et al., 2012c)
3	PCM: hexadecanol Light absorption material: dye-linked polyurethane Method: step condensation reaction and vacuum evaporation	42.10, 232.60	39.60 & 50.30, 229.50	36.2% dye-linked polyurethane	350-500	Hexadecanol/dye-linked polyurethane exhibit higher temperature (60 °C) than pure hexadecanol (32 °C) after exposure for 12000 s in irradiation under solar simulator (500W).	(Tang et al., 2016)

4	Composite PCM: PEG + silicon dioxide (SiO_2) Light absorption material: titanium black (Ti_4O_7) Method: doping Ti_4O_7 through acid-alkali catalytic sol-gel method	61.00, 145.20	59.80, 129.80	3% Ti_4O_7	N/A	Ti_4O_7 /PEG/SiO_2 exhibit higher temperature (67.9 °C) than pure composites without Ti_4O_7 (about 49 °C) after exposure for 6600 s under light radiation. This is because Ti_4O_7 has high thermal conductivity and broad range of UV-Vis light absorbance.	(Tang et al., 2017a)
5	Composite PCM: paraffin + multi walled carbon nanotubes (MWCNTs) Light absorption material: Copper (I) oxide –copper (Cu_2O-Cu) Method: organic precursor thermal decomposition method	52.40, 147.49	52.32, 136.11	6 wt.% Cu_2O-Cu	N/A	Cu_2O-Cu-MWCNT/paraffin exhibits higher temperature (about 88 °C) than MWCNT/paraffin (about 83°C) after exposure for 1500 s under simulation light radiation from four 60W lamps. This is due to the high light absorption ability of Cu_2O and Cu. Moreover, Cu_2O and Cu also reduce of interface thermal resistance between paraffin and MWCNTs.	(Xu et al., 2017)

						Therefore, it enhanced heat transfer process of composites.	
6	PCM: PEG Light absorption material: Graphene oxide aerogel Method: vacuum impregnation	64.15, 182.90	65.06, 177.70	N/A	N/A	Graphene oxide aerogel-PEG exhibits higher temperature (70.0 °C) than PEG (55.4 °C) after exposure for 20 min under simulation light from xenon lamps.	(Tang et al., 2017b)

2.5.1 Light absorption material

In this study, RGO is proposed to be used as light absorption material because RGO is efficient in light absorption because of its large optical absorptivity, tunable bandgap and band-position (Mukhopadhyay and Gupta, 2012; Sadasivuni et al., 2015). Graphene has very large charge mobilities, which are useful for charge collection and transportation. Optical absorption in graphene is dominated by intraband transitions at low photon energies (in the far-infrared spectral range) and by interband transitions at higher energies (from mid-infrared to ultraviolet) (Mak et al., 2012). The absorption of light by intraband transitions involves lattice vibration quanta or known as phonons. When a phonon has been exchanged with the lattice, the composite receive heat energy and temperature will raise up (Hummel, 2013).

Besides, previous studies showed that graphene oxide aerogel is a good light-driven heating unit that can effecctively capture photons and subsequenty convert light to heat energy (Tang et al., 2017b). Therefore, in this study, synthesised RGO in thin sheet structure is expected to have larger surface area and higher light absorption. Moreover, no study using RGO dispersed in polymer caoting as light absorption material on fatty acid yet.

2.5.1.1 Overview of graphene and graphene/polymer

Graphene is a two-dimensional single layer of sp^2 bonded carbon atoms densely packed in a honeycomb crystal lattice (Okhay et al., 2016). The carbon-carbon bond (sp^2) length in graphene is approximately 0.141nm (de Andres et al., 2008). Recently, graphene has attracted significant attention due to it has high carrier mobility, ballistic transport, large specific surface area, chemical inertness, high thermal conductivity, optical transmittance and excellent mechanical properties (Choi et al., 2010; Bramhaiah and John, 2012). Moreover, graphene is efficient in light absorption because of its large optical absorptivity, tunable bandgap and band-position (Mukhopadhyay and Gupta, 2012; Sadasivuni et al., 2015).

Nowadays, graphene system and graphene/polymer hybrid are popular to be used in energy applications such as solar cells, lithium ion batteries, supercapacitor, fuel cells and others (Cui et al., 2016). Graphene/polymer hybrid can be prepared by solution blending, melt blending and in situ polymerization method. In solution blending method, graphene and the polymer or prepolymer are dispersed in the same solvent system, and then followed by sonication and evaporation to produce uniform nanocomposite (Verdejo et al., 2011). While in melt intercalation method, graphene is mixed with the polymer matrix in molten state at high temperatures and strong shearing force (Das and Prusty, 2013). In the situ polymerization method,

graphene is first disperse within the liquid monomer, followed by adding initiator and the polymerization is initiated either by heat or radiation (Hu et al., 2010). In this study, RGO is blended with coating solution because solution blending is one of the most adopted method to produce uniform nanocomposites.

2.5.1.2 Overview and synthesis of RGO

Graphene is a single carbon layer of graphite. Graphene can be produced by few methods such as exfoliation and cleavage, chemical vapor deposition, chemical reduction and thermal decomposition methods. Among all, chemical reduction of GO is one of the conventional procedures to produce graphene in large quantities (Bhuyan et al., 2016). Besides, chemical reduction method is simple, reliable, low material and versatility in chemical functionalization (Tien et al., 2012). Chemical reduction of graphene is also known as reduced graphene oxide (RGO). RGO is graphene-like material but it still contains remaining oxygen functional group on the surface of carbon plane after the reduction process (Pei and Cheng, 2012). The chemical structure of RGO is shown in Figure 2.3.

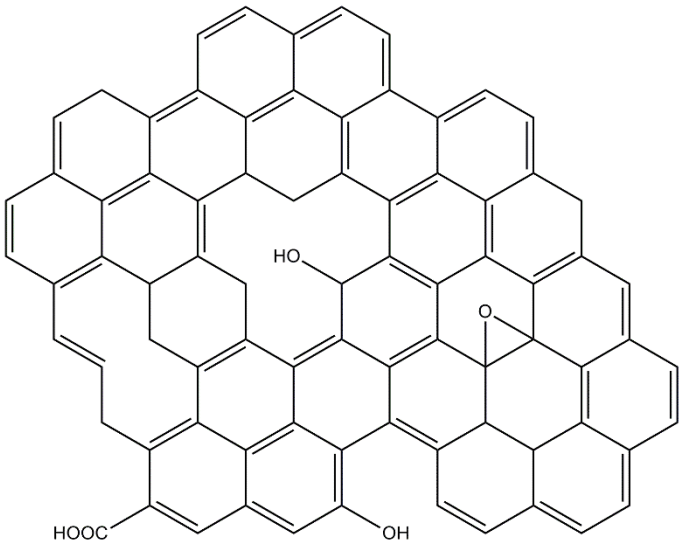

Figure 2.3: Chemical Structure of RGO

There are two main steps in producing RGO: (i) oxidation of graphite using oxidants, (ii) sonication and reduction of graphene oxide (GO) to RGO using reducing agent. Oxidants used for oxidizing graphite are concentrated sulfuric acid, nitric acid and potassium permanganate based on Brodie method (Brodie, 1860), Staudenmaier method (Staudenmaier, 1898) and Hummers method (Hummers and Offeman, 1958). Hummers method is safer and require lesser time for the reaction if compared to other two methods. After that, some modifications based on the Hummers method have been proposed. However, conventional Hummers method is chosen to be used in this study as it is one of the primary routes to prepare GO.

GO produced by the oxidation reaction is lighter in color than graphite due to loss of electronic conjugation. GO contains oxygen functional group such as

epoxide, hydroxyl, carbonyl and carboxyl groups as shown in Figure 2.4. Next, GO is reduced to RGO using reducing agent likes the addition of hydrogen gas occurs across the alkenes, coupled with the extrusion of nitrogen gas, large excess of $NaBH_4$ (Shin et al., 2009). Other reducing agents used include phenyl hydrazine (Pham et al., 2010), hydroxylamine (Zhou et al., 2011), glucose (Zhu et al., 2010), ascorbic acid (Zhang et al., 2010), hydrazine hydrate (Tripathi et al., 2013), hydroquinone (Wang et al., 2008a), alkaline solution (Fan et al., 2008), and pyrrole (Amarnath et al., 2011). Among all, hydrazine hydrate is chosen to be used as reducing agent in this study because it is the best reducing agents to produce a very thin graphene-like sheet with high specific surface area (Stankovich et al., 2007).

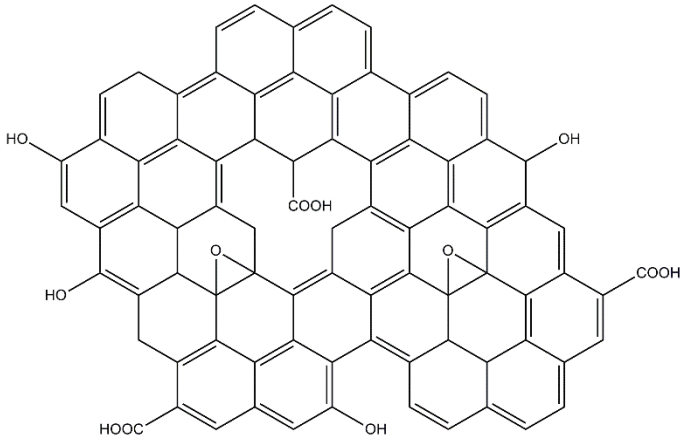

Figure 2.4: Chemical Structure of Graphene Oxide (GO)

2.6 Summary

In this chapter, criteria of PCMs as good TES has been reviewed. The categories of PCM used in TES such as paraffin wax, fatty acid and PEG were discussed. Besides, the development of composite PCM has also been reviewed. Recent development of composite PCM with improved thermal stability was discussed in term of materials, preparation method, encapsulation/ absorption efficiency, thermal performance and reliability. Coating materials that haven't been used on PCM - conformal coating, PA and NBR - has also been reviewed. Furthermore, recent development of composite PCM with improved light absorption was discussed also in term of light absorption materials, optimum loading, preparation method, thermal performance and light absorption wavelength. Light absorption material used in this study-RGO was also review in term of its advantages and synthesis method.

CHAPTER 3

MATERIALS AND METHODOLOGY

This chapter describes the main experimental materials and techniques used in this study, including synthesis of RGO and development of FSCPCM with improved light absorption. Instruments used for characterization tests are listed as well. Experimental setup for solar energy conversion system is presented in details.

3.1 Materials and Chemicals

All of the chemicals used were analytical grade and thus further purification was not needed. The chemical used for preparation of FSCPCM and RGO were listed in Table 3.1.

Table 3.1: List of Chemicals Used

Chemical	Purpose	Properties	Supplier
Polymethyl methacrylate (PMMA)	Supporting material for FSCPCM	Molecular weight ~ 120, 000	Sigma Aldrich
Myristic acid (MA)	PCM core for FSCPCM	purity ≥ 98%	R&M Chemicals
Chloroform	Solvent used to dissolve PMMA and MA prior	Purity~99%	R&M chemicals

	blending to form FSCPCM		
Silicone conformal Coating- Dow corning 1-2620	Coating material	-	Celtite Sdn Bhd
Polyacrylic coating (PA)	Coating material	Total solid content: 36.35%	Provided by Dr. Chee Swee Yong from faculty of Science, UTAR
Nitrile butadiene rubber (NBR)- Synthomer X6311	Coating material	Total solid content: 44.70%	Synthomer Sdn. Bhd
Graphite nanofiber (GNF)	Precursor to synthesis graphene oxide (GO)	-	Platinum Senawang Sdn. Bhd
Sulphuric acid	For oxidation of GNF to produce GO	95%	R&M chemicals
Hydrogen peroxide	For oxidation of GNF to produce GO	30%	R&M chemicals
Hydrochloric acid	For oxidation of GNF to produce GO	37%	R&M chemicals
Potassium Permanganate	For oxidation of GNF to produce GO	-	Bendosen Laboratory Chemicals
Sodium nitrate	For oxidation of GNF to produce GO	-	Bendosen Laboratory Chemicals
Hydrazine hydrate solution	For reduction of graphene oxide to produce RGO	78-82% iodometric	Sigma Aldrich

Triton X-100	Emulsifier for better dispersion of RGO during blending with PA coating solution	-	Sigma Aldrich

3.2 Methodology for preparation of FSCPCM to improve thermal stability

In this study, two different form of FSCPCMs were prepared. The preparation method and coating method are summarized in the following section.

3.2.1 Form stable composite PCM (MA/PMMA) in powder form

In phase 1 of the research study, form stable composite PCM (MA/PMMA) with different weight percentage of MA (20, 40, 60 and 80 wt%) were prepared. They were coated with two different types of coating solution which are PA coating solution and conformal coating solution in order to solve leakage problem.

3.2.1.1 Preparation method

Composite PCM (MA/PMMA) was prepared by solution blending method (Alkan and Sari, 2008). Solution of PMMA and MA in chloroform were prepared in separate beakers at concentration of 0.01g/mL and 0.05g/mL, respectively. After that, MA solution was poured into a separating funnel fixed on retort stand whereas

PMMA solution was poured into a Teflon folder container which placed on the hot plate. MA solution was added to PMMA solution dropwise using titration method as shown in Figure 3.1. The mixture solution was stirred during the titration process to ensure even mixing. The blend in the Teflon folded container was then dried at room temperature for 48 hours to remove chloroform. It is then followed by drying in Memmert universal oven UN110 at 40°C for 48 hours to complete the removal of solvent. Finally, the composite PCMs were obtained in powder form. Composite PCM (MA/PMMA) were prepared at different weight percentage of MA (20, 40, 60 and 80% w/w).

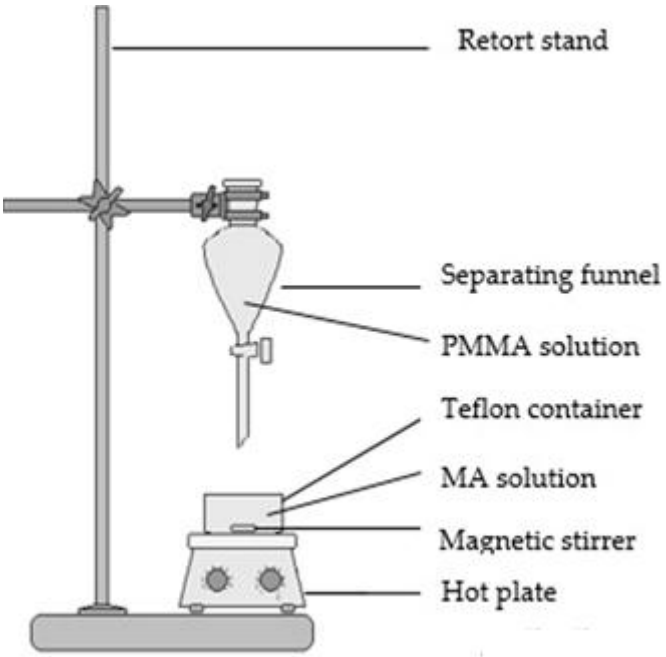

Figure 3.1: Solution Blending Setup for Preparation of Composite PCM (MA/PMMA) in Powder Form

3.2.1.2 Immersion and filtration coating method

Composite PCMs (MA/PMMA) with different MA weight percentage were immersed into coating solution for 10 minutes. It is followed by sonication in Elmasonic S 180 (H) ultrasonic water bath for five minutes to eliminate bubbles. After that, the composite PCMs (MA/PMMA) were filtered and taken out to dry on Teflon sheet at room temperature for 48 hours. The coating process is completed when the coating material changed into solid. The immersion and filtration method are shown in Figure 3.2.

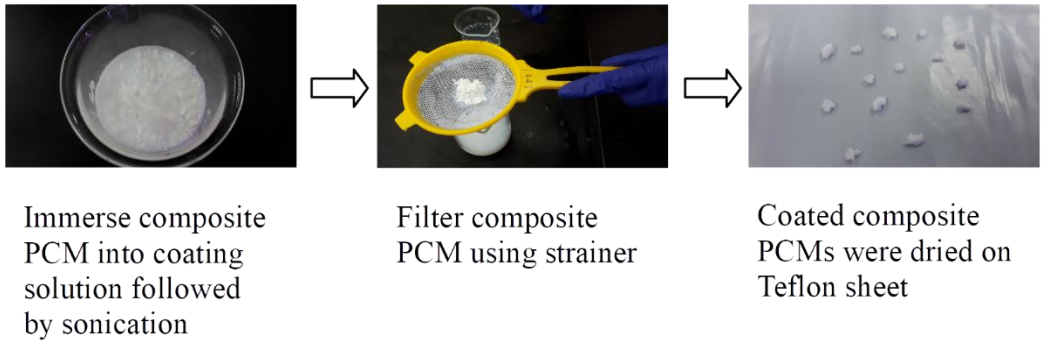

Figure 3.2: Immersion and Filtration Method

3.2.2 Form stable PCM (MA) in pellet form

In phase 2 of the research study, MA was compressed into MA pellet without PMMA supporting material. MA pellets were then coated with two different types

of coating solution which are PA coating solution and NBR coating solution in different combination.

3.2.2.1 Preparation method

MA was weighed in the range from 0.2750 to 0.2800g. After that, MA was ground into powder with pestle in a mortar. Next, MA powder was put in a pellet die. It was followed by compressing MA powder into pellet using hydraulic press at 4000 psi. When the pressure dropped to 3800 kPa, the die was removed from the hydraulic press. The pressed MA pellet was then carefully removed from die and kept in a desiccator. Lastly, the die was cleaned with absolute ethanol and the steps were repeated for next pellet.

3.2.2.2 Dip-coating method

The mass and thickness of the pellet were measured and recorded prior coating. To coat one layer of coating, the MA pellet was immersed into the coating solution for five seconds as shown in Figure 3.3. Next, the MA pellet was taken out and dried in a Teflon sheet at room temperature for 4 days. After the MA pellet was dried, the same steps were then repeated with the same pellet being flipped upside down and dipped into same coating solution. These steps were done to ensure the top and bottom surface of the pellet was well coated and minimize the difference in coating thickness of both sides due to the effect of gravity. The mass and thickness

of the MA pellet was recorded after each layer of coating was done. For MA pellet with two layers of coating, the same steps were repeated for another layer of coating.

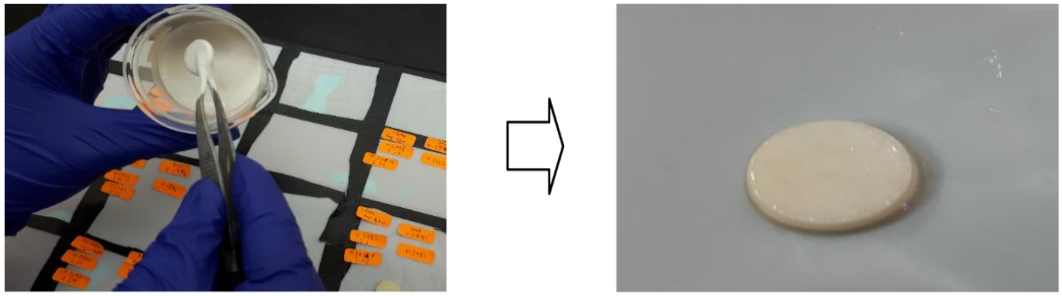

Figure 3.3: Dip Coating Method

3.3 Preparation of FSCPCM to improve light absorption

RGO was synthesized by oxidizing graphite nanofiber (GNF) to graphene oxide (GO) (Hummers and Offeman, 1958) followed by reduction of GO using hydrazine hydrate (Tripathi et al., 2013). After that, RGO was blended with PA coating solution. This coating solution was used to dip coat MA pellet. The dip coating method is same as the method reported in section 3.2.3.2.

3.3.1 Synthesis of RGO

Firstly, GNF was oxidized to GO using the conventional Hummer's method (Hummers and Offeman, 1958). 5 g of GNF was added into a beaker filled with 115

mL of sulfuric acid which was placed and stirred under an overhead stirrer. An ice bath was used to keep the temperature of the reaction at 0 °C. Subsequently, 2.5 g of sodium nitrate was added into the beaker. 15 g of potassium permanganate was added slowly into the beaker once the sodium nitrate was dissolved to prevent overheating of reaction mixture. Visible green suspension formed almost instantaneously. The ice bath was then removed. As the procedure progress, purplish vapour can be seen. The solution was then stirred for 3 hours. 230 mL of deionized water was then added slowly into the solution. After the water was completely added, the mixture was stirred for five minutes before being poured into another 700 mL of deionized water. 12 mL of hydrogen peroxide was added, resulting formation of a light-yellow suspension. The mixture was then left overnight and filtered using Whatman Anodisc membrane. The filtrate cake was first washed with 5% hydrochloric acid and then with deionized water for few times. Washing was carried out repeatedly by using centrifugation followed by decantation of supernatant. As the pH of the supernatant reached the range of 5-7, the product (GO) was dispersed in deionized water and dried overnight in an oven at 60 °C.

The prepared GO was then reduced to RGO. 500 mg of GO was dispersed in 500 mL of deionized water and then exfoliated in ultra-sonicator bath for 1 hour. Subsequently, 5 mL of hydrazine hydrate was added, and the solution was refluxed for 24 hours as shown in Figure 3.4. The solution turned from brown to black precipitate. The product (RGO) was filtered using vacuum filter manifold and then washed with deionized water. Lastly, RGO was dried at 60 °C in vacuum oven.

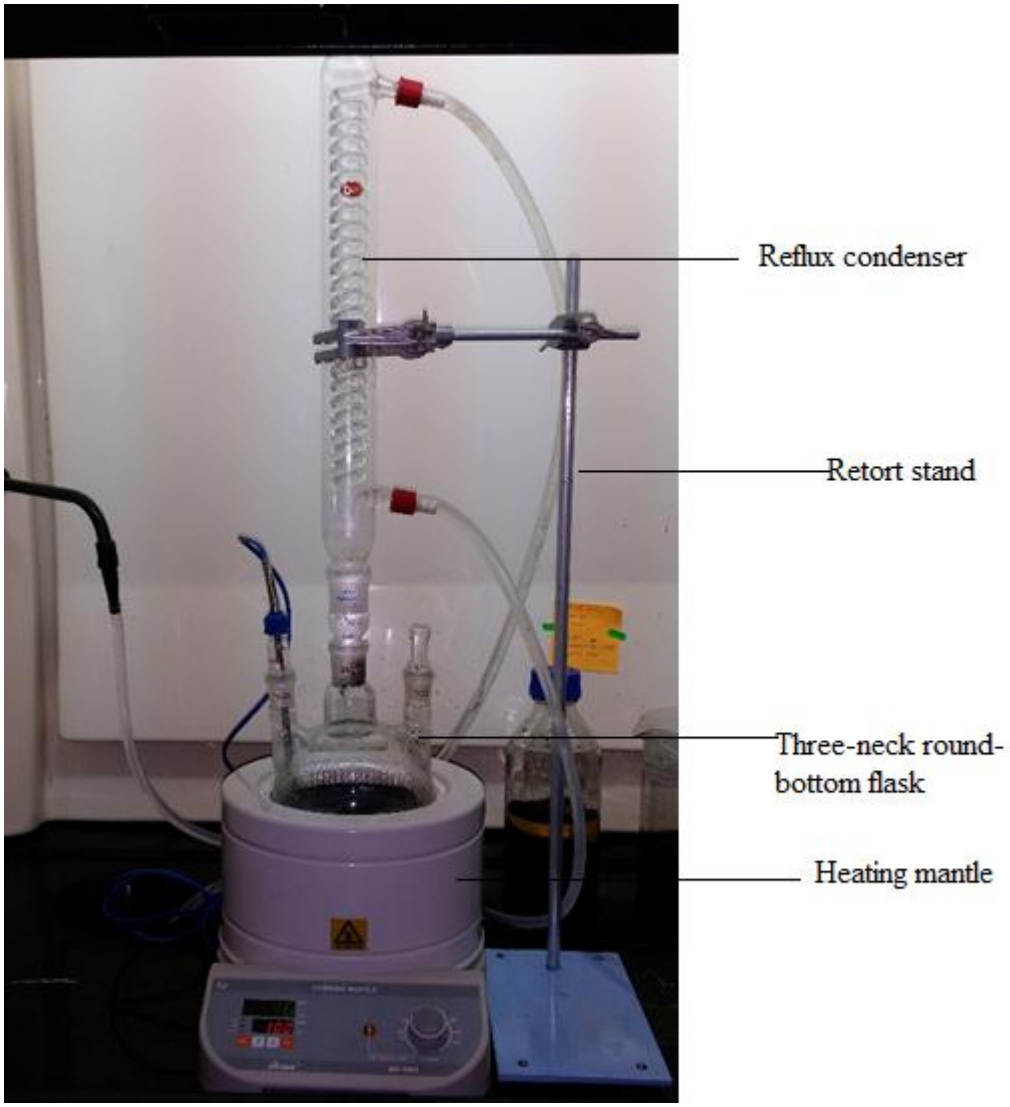

Figure 3.4: Experiment Setup for Reduction of GO to RGO under Reflux

3.3.2 Preparation of RGO blended PA coating solution

RGO obtained from section 3.3.1 was mixed with Triton X-100 prior blending with PA coating solution. The solution was stirred for 1 hour to obtain

homogenous blend solution. The blend was prepared with 0, 0.5, 1.0, 1.5 and 2.0 wt % of RGO.

3.4 Chemical Properties

In this study, characterizations of chemical properties were done using FTIR, XRD, Raman spectroscopy and XPS to identify and confirm the chemical structure of GO and RGO after chemical reaction. FTIR was also used to determine whether FSCPCM are well coated by comparing the FTIR spectra before and after coating.

3.4.1 Fourier transform infrared spectroscopy (FTIR)

Infrared spectra of GNF, GO and RGO were recorded on a FTIR spectrometer (Nicolet photo-spectrometer 8700) to obtain information about the functional groups present. The analysis was carried out using potassium bromide (KBr) pellet to determine the absorption band with a wavelength range of 4000 cm^{-1} to 400 cm^{-1}, 32 scans. Polymer coating films and form stable composite PCM were examined using FTIR photospectrometer (PerkinElmer Spectrum Two FTIR spectrometer) to obtain the information about chemical functional grups. The scanning wavelength range was from 4000 cm^{-1} to 400 cm^{-1} at 4 scans. Attenuated Total Reflectance (ATR) was used because it is a useful sampling accessory that

virtually eliminates the need of sample preparation. Therefore, it can analyse the samples in their natural states without destroying the coating.

3.4.2 X-ray diffraction (XRD)

XRD diffractograms of GNF, GO and RGO were recorded on a X-ray diffractometer (Siemens XRD Diffractometer 5000) to obtain the information about crystalline structures and interlayer spacings of GNF, GO and RGO. The analysis was carried out at room temperature with specular reflection mode. The results were recorded in the scanning range of 2θ between 5° to 90° using copper Kα radiation (0.1542 nm wavelength). The scanning speed was 1 °/min.

3.4.3 Raman spectroscopy

Raman spectra of GO and RGO were recorded on a Raman spectroscopy (NT-MDT NTEGRA Sepctra) to determine structural changes during the reduction of GO to RGO. The analysis was carried out at 473 nm laser power 1.7 mW, 100× objective lens and numerical aperture of 0.9. All powder samples were directly deposited on the glass slide in the absence of solvents.

3.4.4 X-ray Photoelectron spectroscopy (XPS)

XPS data were taken on ULVAC-PHI Quantera II equipped with monochromatic Al Kα (hν = 1486.6 eV) X-ray source. Spectra were collected at room temperature. Calibration was performed by alignment of the spectra with reference to the C 1s line at 284.8±0.2 eV associated with graphitic carbon. XPS was employed to measure the ratio of C and O atomic element composition of GNF, GO and RGO by calculating the peak areas of C and O elements from spectra.

3.5 Tensile

Tensile test was carried out in accordance with the standard test method ASTM D882-02 to measure the E-modulus, tensile strength and elongation at break of polymer film. Polymer film was casted in Teflon mold and dried in room temperature. Polymer film was cut into dumbbell-shape using dumbbell press cutter as shown in Figure 3.5. The average thickness of the film was measured using digital Vernier caliper. The gage length of the specimen is 30 mm. The tensile test was carried out by employing lightweight tensile tester (Tinius Olsen H10KS) with a load cell of 500N, at a crosshead speed of 500 mm/ min. Three tensile tests were performed for each types of polymer film to obtain average values.

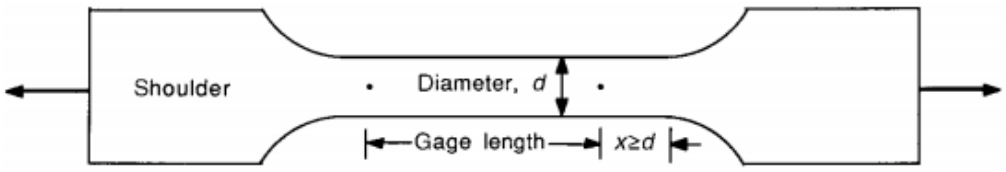

Figure 3.5: Specimen for Tensile Test

3.6 Morphology analysis

Morphology analysis is the analysis using high spatial resolution imaging instrument to produce image of surface structure of substances that cannot be seen with naked eye. In this work, morphology of GNF, GO, RGO and surface of FSCPCM in powder form were studied using FESEM, TEM or AFM in high magnification. Cross section of FSCPCM in pellet also be examined using metallurgical analysis microscope to determine thickness of the coating film.

3.6.1 Metallurgical analysis microscope

Optical micrograph images were taken on metallurgical analysis microscope (BX51M, Olympus) to analyse surface and cross section morphology of FSCPCM at 10x magnifications. For cross section imaging, FSCPCM was freezing by liquid nitrogen gas, followed by cutting using scalpel. Each sample was placed on microscope slide before examining under microscope at room temperature. The

thickness of coating film also can be measured using Vis Plus ver.3.30 image analysis and measurement software.

3.6.2 Field Emission Scanning electron microscopy (FESEM)

Morphologies of GNF, GO, RGO and FSCPCM at different magnifications were captured and recorded using JEOL JSM 6701F field emission scanning electron microscope. Each sample was deposited on a disc with scope tape. All samples were examined after sputter coating with thin layer of platinum to avoid electrostatic charging and poor image resolution.

3.6.3 Transmission electron microscopy (TEM)

TEM images of RGO were recorded using Hitachi HT7700 transmission electron microscope at an accelerating voltage of 100 kV and 60000x magnification. Samples were sectioned in epoxy resin embedment using cryo-ultramicrotomy before being viewed under TEM at room temperature.

3.6.4 Atomic Force Microscope (AFM)

AFM is a very high-resolution type of microscope for studying samples at nanoscale. AFM images were taken on AFM, Park system, XE-70 to analysis three-

dimensional surface topography of RGO/PA film on a 10 x 10 μm^2 area. A non-contact AFM mode was used in this work.

3.7 Thermal properties

Thermal properties are the analysis of the changes in material when heat energy is applied as temperature determines the heat energy level of the atoms. In this work, thermal properties of FSCPCM are studied using DSC to determine phase change temperature and latent heat.

3.7.1 Differential Scanning Calorimetry (DSC)

DSC spectra were measured using Mettler Toledo TOPEM according to test method ASTM D3418 to obtain melting point, freezing point, latent heat of melting and freezing of the FSCPCM. Ideal sample geometries for DSC measurement is in fine powder form. FSCPCM in powder can be ground and directly used in measurement. However, FSCPCM in pellet form was dissolved in chloroform and stirred for 1 hour before dried in a Teflon folded container in order to obtain homogenous fine powder. The powder obtained was then placed into 40 µL crucibles. The weight of the FSCPCM powder were measured and recorded. Next, the crucible was sealed with its lid and ready for analysis. Nitrogen gas was used as the purge gas and the flow rate was 20 ml/min. The DSC measurement of FSCPCM

was carried out at the temperature range of 25-100 °C as well as 5 °C/min heating and cooling rate under a constant stream of nitrogen gas.

3.8 Thermal stability analysis

Thermal stability analysis is to determine the stability of FSCPCM over phase change temperature. In this work, thermal stability analysis was done on litmus paper.

3.8.1 Leakage analysis

The leakage test method is modified from the diffusion-oozing circle test proposed by Ma et al. to evaluate exudation stability of a shape-stabilized PCM (Ma et al., 2013; Kong et al., 2016). The leakage tests of FSCPCM were carried out on litmus papers as the leakage can be observed through the color changes of litmus paper from blue to red. The 13-mm diameter of a standard circle was drawn on litmus papers as shown in Figure 3.6. For FSCPCM in powder form, 0.1g of FSCPCM were uniformly distributed into the standard circle on the litmus papers. Whereas for MA pellet with different polymer coating combination, they were placed on the standard circle on the litmus paper. The thermal stability test was done in oven at temperature of 65 °C. After finish testing, the leakage area of composite PCMs were measured using GIMP 2 and Image J software.

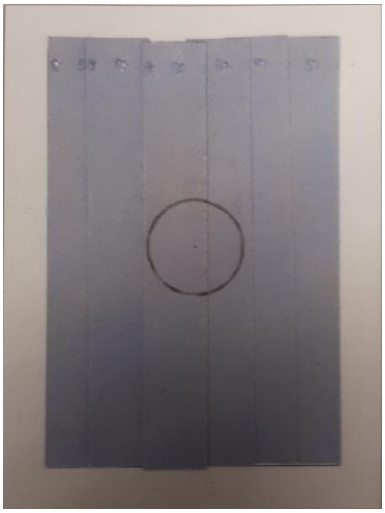

Figure 3.6: Leakage Test Layout

3.9 Durability analyses

In this study, durability analyses were done under thermal cycling setup and weathering at outdoor. Thermal cycling is the analysis of thermal reliability of FSCPCM with respect to repeated melting and freezing cycles. Weathering test is to investigate the UV stability of polymeric film at outdoor.

3.9.1 Thermal cycling

Thermal cycling test was carried out using a thermal cycling system of in-house design by University of Malaya to determine thermal reliability of FSPCMs. The thermal cycling system was designed to operate from 30°C to 80°C. The image

of thermal cycling setup is showed in Figure 3.7. The specific amount of PCMs was put in DSC crucible and then placed in PCM storage box to undergo repeated heating and cooling. The heating and cooling process were done using heater and fan, respectively. The thermal cycling test were done up to 1000 cycles and the temperature variations of FSCPCM was automatically recorded in computer by accuracy of ±0.1 ℃. The DSC spectra before and after thermal cycling were compared to determine the changes of latent heat and melting point of FSCPCM.

Figure 3.7: In house Thermal Cycling Test System

3.9.2 Weathering

FSCPCM and polymer coating film were placed on Teflon sheet in petri dish. All the petri dishes were put in basket and exposed to sunlight for duration of 30 days. The picture of weathering setup is shown in Figure 3.8. The mass and FTIR spectra of all samples were compared before and after weathering test.

Figure 3.8: Experiment Setup for Weathering

3.10 Light absorption measurement

Light absorption measurement is to determine the ability of light absorptive polymeric FSCPCM (RGO-PARB/MA) in conversion of solar energy into heat energy. In this work, UV-VIS absorption analysis was used to determine absorption wavelength of RGO. Outdoor solar energy conversion efficiency experiment was carried out to determine the amount of stored heat and solar energy conversion efficiency of light absorptive polymeric FSCPCM (RGO-PARB/MA).

3.10.1 UV-Vis absorption analysis

UV absorption analysis of RGO was done using UV-Visible Spectrophotometer (UV-1700, Shimadzu) to determine absorption wavelength range of RGO. Before RGO was used for analysis, it was dispersed in distilled water

at concentration of 0.0001g/ml. The solution was then sonicated for 10 minutes to ensure better dispersion of RGO. The scanning wavelength of analysis is in the range of 200 to 700nm. The maximum absorbance of this instrument is 4.0.

3.10.2 Solar energy conversion efficiency

Prior to solar energy conversion efficiency measurement, the specific heat capacity of every sample was measured. The solar energy conversion efficiency measurement was carried out under the sunlight. The experimental apparatus can be divided into 2 main components: solar energy conversion system, as well as data collection and processing devices.

3.10.2.1 Specific heat capacity measurement

The specific heat capacity of MA, PA and NBR were measured by using Mettler Toledo DSC1 differential scanning calorimetry (DSC). The heating of the sample inside the crucible in the DSC is illustrated in Figure 3.9. The DSC measurement setting for MA is same as the setting for FSCPCM in section 3.7.1. For NBR, measurement was carried out at the temperature range of -25-200 °C and 5 °C/min heating rate under a constant stream of nitrogen gas at the flow rate of 20 mL/min. On the other hand, PA was carried out at the temperature range of 10-

200 °C as well as 5 °C/min heating and cooling rate under a constant stream of nitrogen gas at the flow rate of 20 mL/min.

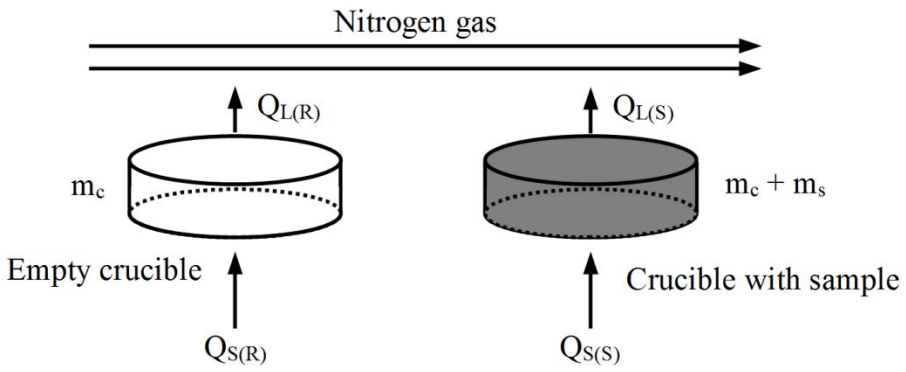

Figure 3.9: Specific Heat Capacity Measured by Using DSC

Eq. (3.1) and Eq. (3.2) are the specific heat equations for the empty crucible and crucible with the sample,

$$Q_{S(R)} - Q_{L(R)} = m_c c_c \Delta T \tag{3.1}$$

$$Q_{S(S)} - Q_{L(S)} = m_s c_s \Delta T + m_c c_c \Delta T \tag{3.2}$$

Where,

$Q_{S(R)}$ = Heat energy supplied to the empty crucible (J);

$Q_{S(S)}$ = Heat energy supplied to the crucible with the sample (J);

$Q_{L(R)}$ = Heat energy loss from the empty crucible (J);

$Q_{L(S)}$ = Heat energy loss from the crucible with the sample (J);

m_c = Mass of the crucible (g);

m_s = Mass of the sample (g);

c_c = Specific heat capacity of the crucible ($Jg^{-1}K^{-1}$);

c_s = Specific heat capacity of the sample ($Jg^{-1}K^{-1}$);

ΔT = Change in temperature (K);

Assuming the heat losses of both crucibles are the same,

$$Q_{L(R)} = Q_{L(S)} \tag{3.3}$$

Substitute Eq. (3.3) into Eq. (3.1) and subtract the resulting equation from Eq. (3.2).

$$\Delta Q = Q_{S(S)} - Q_{S(R)} = m_s c_s \Delta T \tag{3.4}$$

The specific heat capacity can be calculated from the DSC result by using Eq. (3.5) obtained by rearranging Eq. (3.4),

$$c_s = \frac{\Delta Q}{m_s \Delta T} = \frac{\frac{\Delta Q}{\Delta t}}{m_s\left(\frac{\Delta T}{\Delta t}\right)} \tag{3.5}$$

Where,

Δt = The period of time for the change in temperature ΔT (s).

In the DSC result, the unit of the differential heat flow $\Delta Q/\Delta t$ is mW. Therefore, Eq. (3.6) is used to calculate the specific heat capacity at different temperature.

$$c_{sn} = \frac{\frac{y_n}{1000}}{m_s\left(\frac{T_n - T_{n-1}}{t_n - t_{n-1}}\right)}, \quad n \geq 2 \tag{3.6}$$

Where,

$y_n = \frac{\Delta Q}{\Delta t}$ = Differential heat flow from the DSC result (mW).

The calculation of the specific heat capacity is shown in Table 3.2

Table 3.2: Calculation of the Specific Heat Capacity

n	t_n	$y_n = \frac{\Delta Q}{\Delta t}$	T_n	c_{sn}
1	t_1	y_1	T_1	-
2	t_2	y_2	T_2	$c_{s2} = \frac{y_2/1000}{m_s (T_2 - T_1)/(t_2 - t_1)}$
3	t_3	y_3	T_3	$c_{s3} = \frac{y_3/1000}{m_s (T_3 - T_2)/(t_3 - t_2)}$
⋮	⋮	⋮	⋮	⋮
N	t_N	y_N	T_N	$c_{sN} = \frac{y_N/1000}{m_s (T_N - T_{N-1})/(t_N - t_{N-1})}$

To calculate the specific heat capacity at any temperature T, linear interpolation of the results as shown in Figure 3.10 can be used.

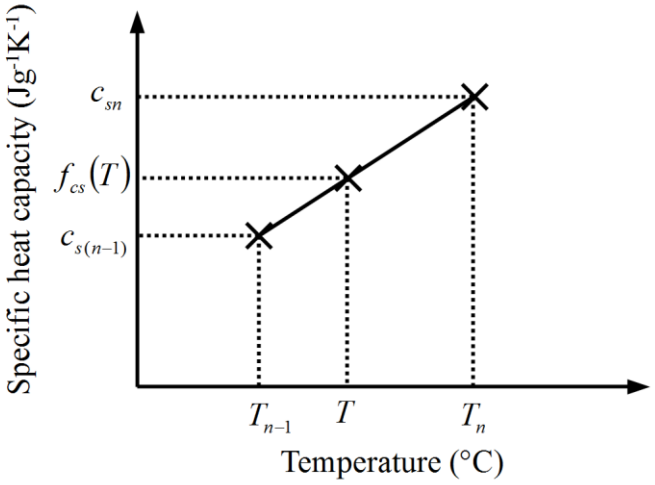

Figure 3.10: Linear Interpolation of C_s at Any Temperature T

From Figure 3.10,

$$\frac{c_{sn}-c_{s(n-1)}}{T_n-T_{n-1}}=\frac{f_{cs}(T)-c_{s(n-1)}}{T-T_{n-1}},\quad T_{n-1}\le T\le T_n \tag{3.7}$$

The function to calculate specific heat capacity f_{cs} at any temperature, T in Eq. (3.8) can be obtained by rearranging Eq. (3.7),

$$f_{cs}(T)=\left[\frac{c_{sn}-c_{s(n-1)}}{T_n-T_{n-1}}\right]T+\frac{T_nc_{s(n-1)}-T_{n-1}c_{sn}}{T_n-T_{n-1}},\quad T_{n-1}\le T\le T_n \tag{3.8}$$

3.10.2.2 Outdoor solar energy conversion efficiency measurement

The solar energy conversion system consists of light absorptive polymeric FSCPCM samples and thermal insulated polystyrene box. The samples were placed in the polystyrene box and exposed under the sunlight as illustrated in Figure 3.11.

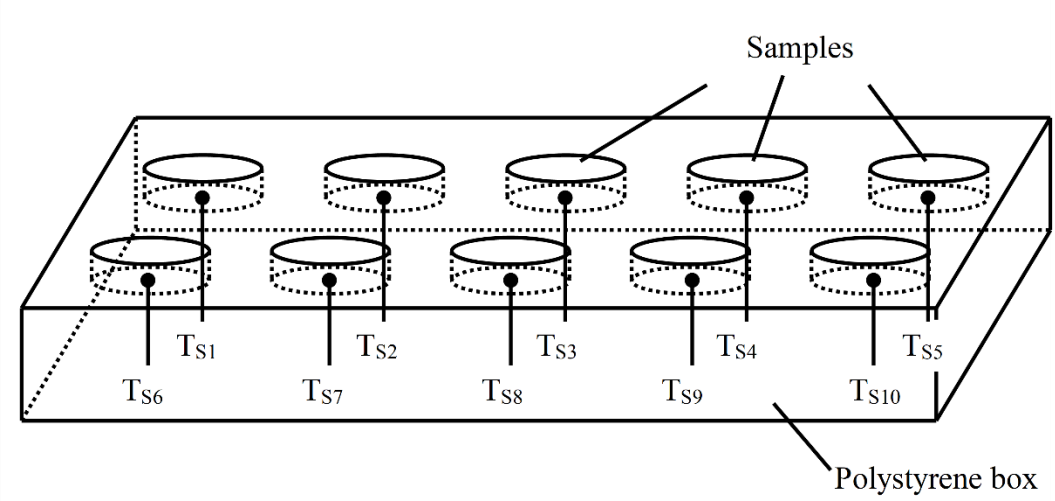

Figure 3.11: Solar Energy Conversion System

The KiPP & Zonen CMP3 Pyranometer was used to record the solar irradiance. The thermopile sensor construction of the pyranometer measured the solar energy per unit area that is received from the sun and the field of view extended to the whole hemisphere (180° field of view). The output was expressed in Watts per meter square. Type-T thermocouples were used in this setup to measure the temperatures of the samples under the sunlight. The thermocouples were connected to Graphtec data logger GL820. All the data was processed and recorded by a

computer. The outdoor experiment setup for solar energy conversion efficiency measurement is shown in Figure 3.12.

The experiment was conducted on three sunny days. The room temperature and the temperature of the polystyrene box were measured. To make a fair comparison of the solar conversion efficiency of all the pellet, only the results from the first 20 minutes are used in the calculation when the temperature difference is less than 5°C. In these periods of time, the effect of the heat loss to the environment which is mainly affected by the difference between the pellet temperature and the temperature inside the PMMA container is the minimum.

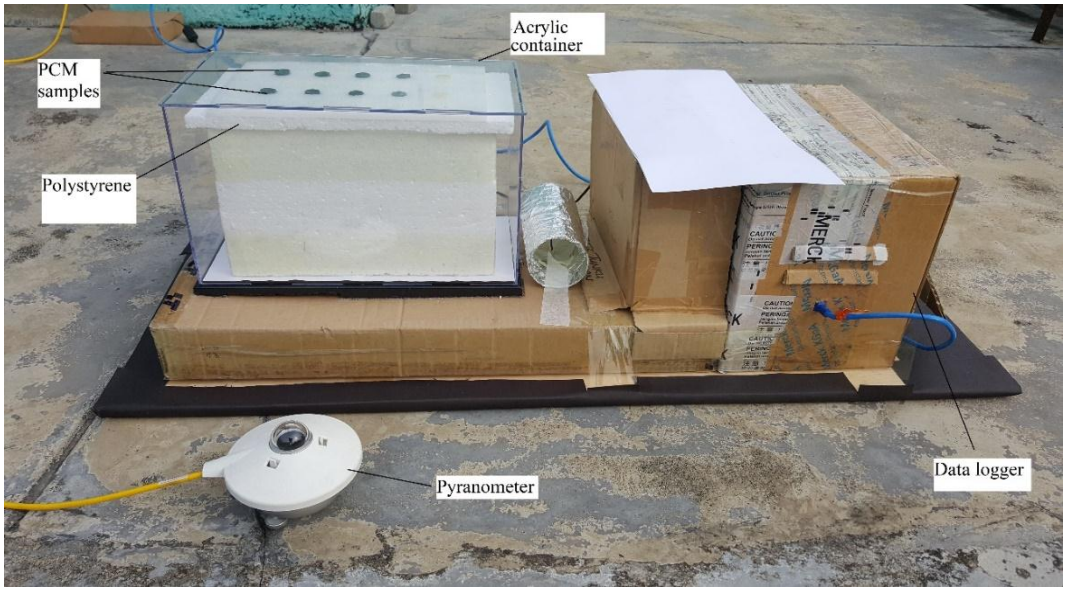

Figure 3.12: The Outdoor Experiment Setup for Solar Energy Conversion Efficiency Measurement

The energy transfer of a sample in the outdoor experiment setup is shown in Figure 3.13. The sample absorbed solar energy E_{solar} from the sunlight at the top surface. A portion of the solar energy was converted into heat energy, E_{heat} which increased the temperature of the sample. The rest of the solar energy was the energy loss: the sunlight reflected by the top surface, as well as the heat energy transferred to the environment via convection and radiative heat transfers.

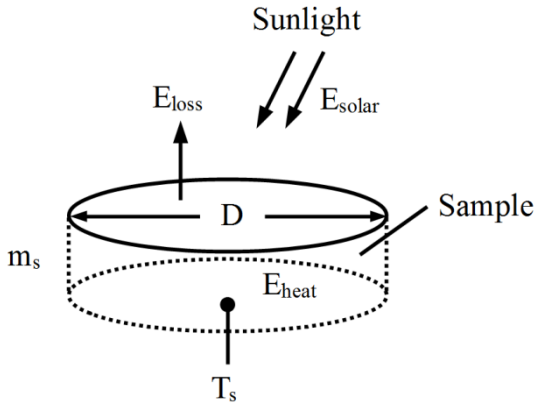

Figure 3.13: Energy Transfer of a Sample

The energy transfer mechanism is represented by Eq. (3.9).

$$E_{heat} = E_{solar} - E_{loss} = m_s c_s \Delta T_s \tag{3.9}$$

Where,

E_{heat} = Heat energy absorbed by the sample which increase the temperature (J);

E_{solar} = Solar energy from the sun (J);

E_{loss} = Energy loss (J);

m_s = Mass of the sample (g);

c_s = Specific heat capacity of the sample ($Jg^{-1}K^{-1}$);

T_s = Temperature of the sample (°C);

The solar energy can be calculated from the solar irradiance measured by the pyranometer and the top surface area of the sample by using Eq. (3.10).

$$E_{solar} = \int_{t=0}^{t_N} I_{solar}(t) \cdot A \, dt \tag{3.10}$$

Where,

I_{solar} = Solar irradiance measured by using the pyranometer (Wm^{-2});

$A = \pi D^2/4$ = Top surface area of the sample (m^2).

The heat energy can be calculated from the result by using Eq. (3.11).

$$E_{heat} = \sum_{n=2}^{N} m_s f_{cs}(T_{sn})\left[T_{sn} - T_{s(n-1)}\right] \tag{3.11}$$

Where,

f_{cs}(T) = The function to calculate specific heat capacity by using Eq. (3.8) ($Jg^{-1}K^{-1}$);

Numerical integration is used to calculate the solar energy from the solar irradiance and top surface area. The integration of solar irradiance using trapezoidal rule is shown in Figure 3.14.

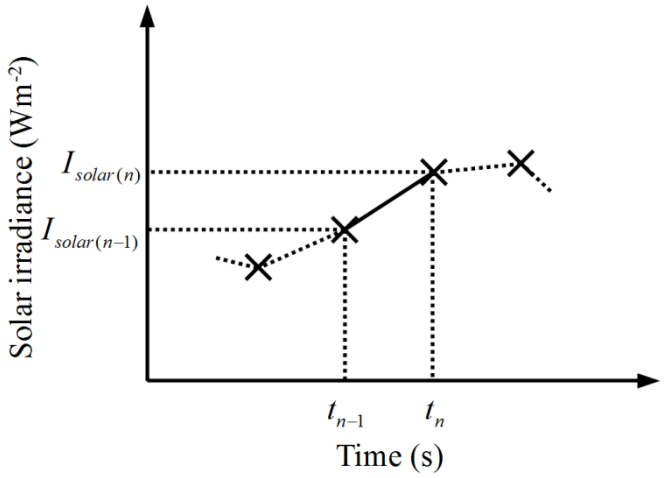

Figure 3.14: Numerical Integration of Solar Irradiance with Respect to Time

The area of trapezoid under the line from t_{n-1} to t_n can be found by,

$$A_{trapezoid} = \frac{1}{2}(t_n - t_{n-1})\left[I_{solar(n)} + I_{solar(n-1)}\right] \tag{3.12}$$

Summing up all the areas and multiplying the result by the top surface area,

$$E_{solar} = \sum_{n=2}^{N} \frac{A}{2}(t_n - t_{n-1})\left[I_{solar(n)} + I_{solar(n-1)}\right] \tag{3.13}$$

The calculation of the solar energy and heat energy using Eq. (3.11) and Eq. (3.13), respectively is shown in Table 3.3.

Table 3.3: Calculation of the Solar Energy and Heat Energy

n	t_n	$I_{solar(n)}$	T_{sn}	$\frac{A}{2}(t_n - t_{n-1})\left[I_{solar(n)} + I_{solar(n-1)}\right]$	$m_s f_{cs}(T_{sn})\left[T_{sn} - T_{s(n-1)}\right]$
1	t_1	$I_{solar(1)}$	T_{s1}	-	-
2	t_2	$I_{solar(2)}$	T_{s2}	$\frac{A}{2}(t_2 - t_1)\left[I_{solar(2)} + I_{solar(1)}\right]$	$m_s f_{cs}(T_{s2})\left[T_{s2} - T_{s1}\right]$
3	t_3	$I_{solar(3)}$	T_{s3}	$\frac{A}{2}(t_3 - t_2)\left[I_{solar(3)} + I_{solar(2)}\right]$	$m_s f_{cs}(T_{s3})\left[T_{s3} - T_{s2}\right]$
⋮	⋮	⋮	⋮	⋮	⋮
N	t_N	$I_{solar(N)}$	T_{sN}	$\frac{A}{2}(t_N - t_{N-1})\left[I_{solar(N)} + I_{solar(N-1)}\right]$	$m_s f_{cs}(T_{sN})\left[T_{sN} - T_{s(N-1)}\right]$

$$E_{solar} = \sum_{n=2}^{N} \frac{A}{2}(t_n - t_{n-1})\left[I_{solar(n)} + I_{solar(n-1)}\right] \qquad E_{heat} = \sum_{n=2}^{N} m_s f_{cs}(T_{sn})\left[T_{sn} - T_{s(n-1)}\right]$$

The solar energy conversion efficiency can be calculated by Eq. (3.14).

$$\eta = \frac{E_{heat}}{E_{solar}} \times 100\% \tag{3.14}$$

Where,

η = solar energy conversion efficiency of the sample (%).

3.11 Summary

In this chapter, specification of the chemicals and materials used in this work are listed. They were purchased from chemical companies and used as received. The methodology to synthesize RGO and develop FSCPCM is also presented in details. The RGO was synthesis in the laboratory, using the published method. All FSCPCMs were constructed in the laboratory. Besides, the characterization tests, instrument and also its setting used in analysis have been presented. The measurement setup for solar energy conversion efficiency was also described.

CHAPTER 4

RESULTS AND DISCUSSION FOR FORM STABLE COMPOSITE PCM WITH SUPPORTING MATERIAL AND COATING TO PREVENT LEAKAGE

This chapter presents the result and discussion for phase 1 of the research study- FSCPCM (MA/PMMA) with supporting material and coating to prevent leakage. The contents of the chapter were outlined into eight subsections. This chapter begins with the introduction of the work flow in this research study. Characterization and performance analysis tests such as leakage analysis, morphology, durability study, thermal, mechanical and chemical properties were presented and discussed. Lastly, summary of this phase was made as well. The suitable coating material used for next phase was identified from the results.

4.1 Introduction

The work flow of this phase research study was summarized in Figure 4.1. Composite PCMs (MA/PMMA) were prepared by blending of PMMA and MA at different weight percentage of MA (20, 40, 60 and 80 wt%). The MA and PMMA were selected as PCM and supporting material, respectively. PMMA was used owing to its compatibility with fatty acid and good thermal stability (Wang et al., 2011a). As liquid MA may leak out during phase change, this study proposes the

use of two coatings, namely PA and conformal coating to solve the leakage problem. Both coatings have high transparency and UV resistance, stable to environment condition and exhibit good barrier properties to moisture (Moghbelli et al., 2014). Despite several researches on PA and conformal coating, there is a lack of study on the application of these coatings for composite PCM (MA/PMMA). Therefore, the objective of this phase is to prepare and characterize coatings on composite PCM (MA/PMMA) for solving the leakage problem. Performance of composite PCM (MA/PMMA) with the coatings would be compared to determine which coating is better in preventing leakage. Leakage analysis was investigated through leakage test technique. Besides, tensile test was also carried out for the coating films to determine their mechanical properties. Chemical compatibility, thermal properties and morphology of composite PCM (MA/PMMA) were studied using DSC, FTIR and FESEM, respectively. Thermal cycling test were also carried out to determine the thermal stability of composite PCM (MA/PMMA) after 1000 melting and freezing cycles.

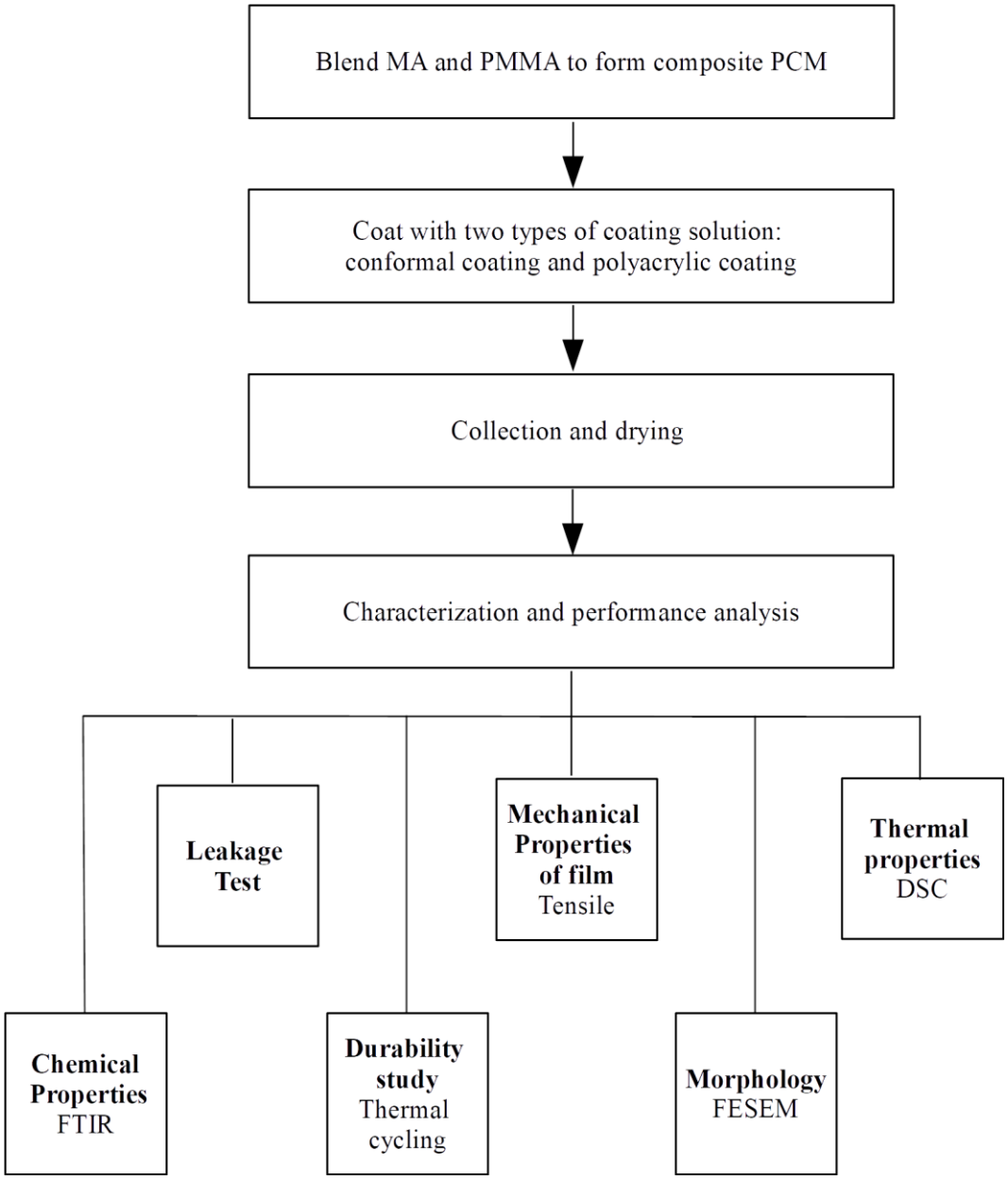

Figure 4.1: Work Flow of Phase 1 Experiment

4.2 Leakage Test

The leakage area of all the composite PCMs (MA/PMMA) after two hours heating in oven at 65 ºC are presented in Table 4.1. The leakage area increased with increasing weight percentage of the MA for all samples. This is due to the weight percentage of PMMA that provides physical hooks between the chains and form a network structure to hold the melted MA reduced (Xiao et al., 2002; Sarı and Karaipekli, 2007). As a result, a continuous and dense polymer network cannot be formed, thus leakage was seen.

Table 4.1: Leakage Area for Composite PCMs (MA/PMMA) with and those without Coatings

MA:PMMA (wt %)	Leakage Area (cm^2)		
	Without Coating	Conformal Coating	PA Coating
20:80	1.68	**0.00**	**0.00**
40:60	4.17	**0.00**	**0.00**
60:40	4.32	1.74	**0.00**
80:20	8.68	1.82	1.61

The effect of the coatings in leakage prevention is apparent in Table 4.1. For instance, the leakage percentage of composite PCM (MA/PMMA, 80/20 wt %) was reduced by at least 80% after coating. This is attributed to the coating films that

form a barrier to prevent leakage during phase change process. It is also noticeable that the PA coating performs slightly better than the conformal coating in preventing leakage. No leakage was seen when the PA coating was used in composite PCM (MA/PMMA, 60/40 wt %), compared to that of conformal coating which leakage area was 1.74 cm^2. The samples did not have leakage were marked bold in Table 4.1.

Figure 4.2 shows the image of MA on blue litmus papers after 2 hours heating at 65 °C. It is clearly seen that MA (melting point, 55.90 °C) is completely melted and turn the blue litmus paper to red. Figure 4.3 (a) shows that the composite PCM (MA/PMMA, 60/40 wt %) remains solid over the melting temperature but a certain amount of MA still leaks out. However, the leaking of composite PCM (MA/PMMA, 60/40 wt %) has been reduced after coating with conformal coating as shown in Figure 4.3 (b). The composite PCM (MA/PMMA, 60/40 wt %) with PA coating shows better thermal stability and no leaking was found as shown in Figure 4.3 (c). Therefore, it can be concluded that the coating can prevent the leaking of composite PCM (MA/PMMA) over the melting temperature.

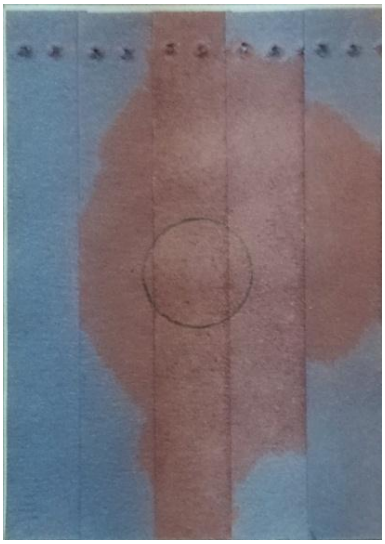

Figure 4.2: Leakage Image of MA After Heating in Oven.

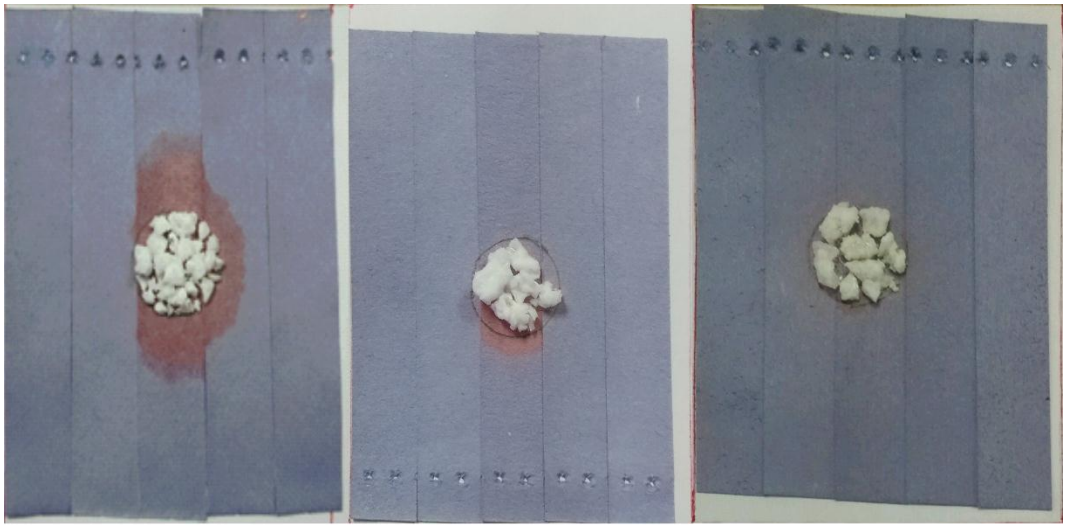

(a) (b) (c)

Figure 4.3: Leakage Comparison for Composite PCM (MA/PMMA, 60/40 wt %): (a) Without Coating (b) With Conformal Coating (c) With PA Coating

4.3 Tensile Properties

Conformal and PA coating were casted into thin sheet film on Teflon mould for tensile test. E-modulus measures stiffness and rigidness of the polymer coating film (Swallowe, 2013). E-modulus is defined as the stress per unit area divided by the strain resulting from the applied force. Therefore, it measures the resistance of polymer film being deformed when a force is applied to it. Figure 4.4 shows stress strain curves for conformal and PA coating. Figure 4.5 shows that PA had 144.61% higher E-modulus than conformal coating. This shows that PA had higher resistance over the volume change of MA during phase change process if compared to conformal coating. The higher the resistance towards deformation, the lesser the chain movement and free volume in the coating and thus PA coating had improved barrier properties and higher leakage resistance.

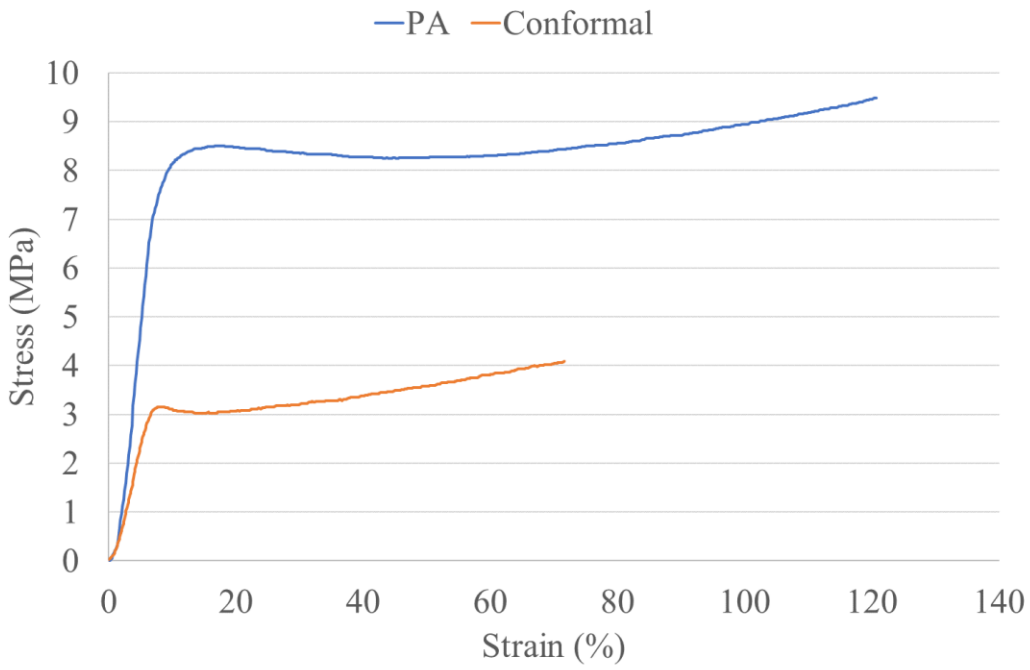

Figure 4.4: Stress Strain Curve for PA and Conformal Coating

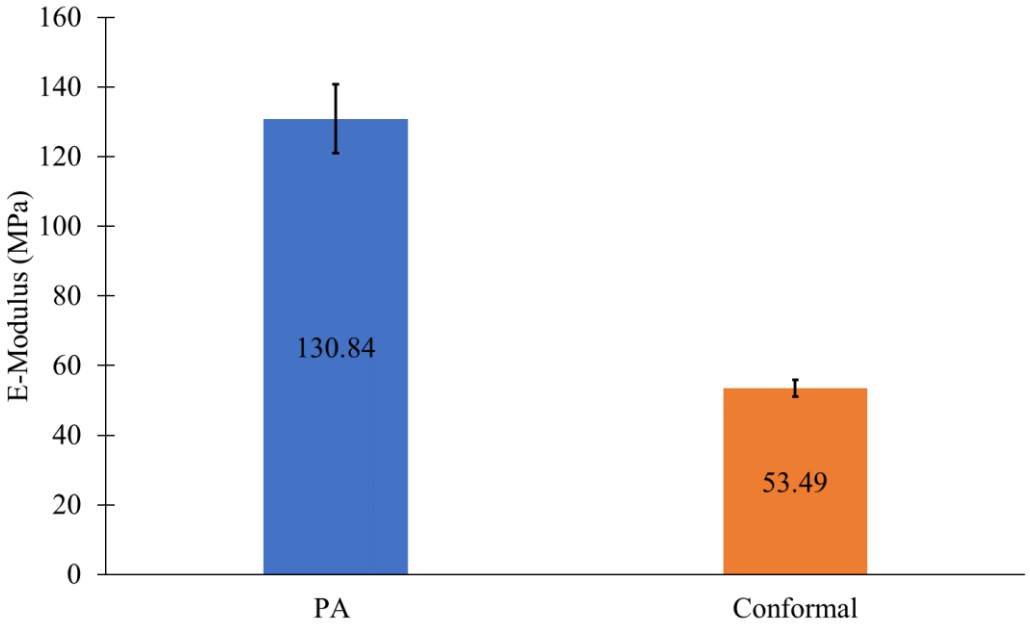

Figure 4.5: E-Modulus of PA and Conformal Coating Film

Tensile strength measures the strength of the polymer film under tension. It also measures maximum strength that a polymer coating film can withstand while being stretched before it ultimately breaks (Davis, 2004). Therefore, a good polymer coating material should have high tensile strength to prevent cracking during phase change process. Figure 4.6 shows that tensile strength for PA and conformal coating were 12.19 MPa and 4.11 MPa, respectively. Thus, PA had 196.59% higher tensile than conformal coating.

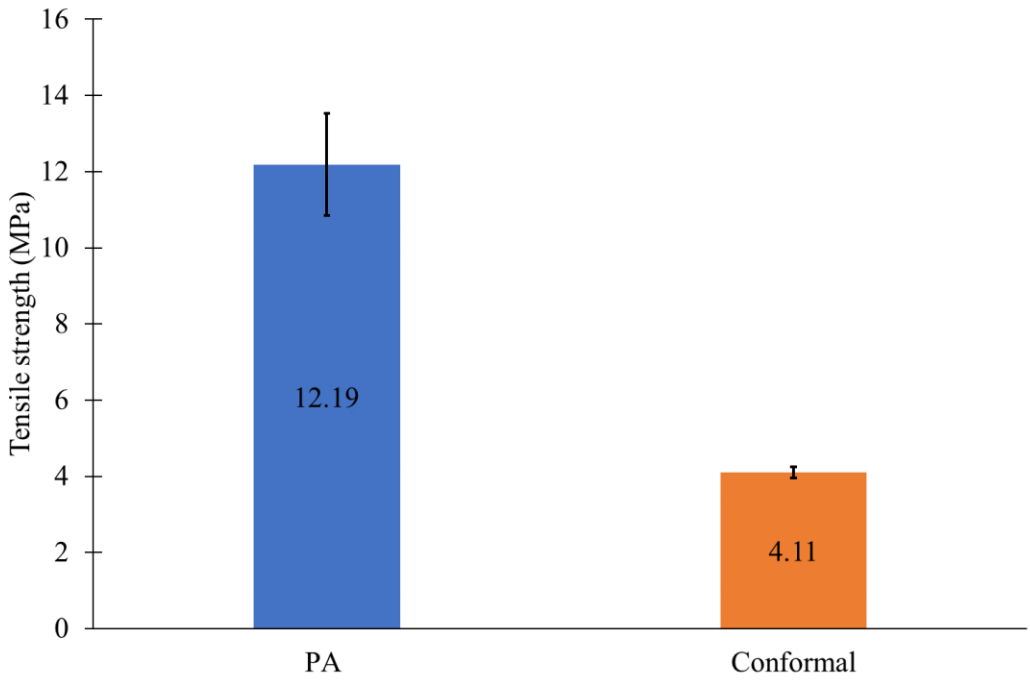

Figure 4.6: Tensile of PA and Conformal Coating Film

Elongation at break measures the elongation that causes the breakage in the test specimen with sufficient tension developed under the particular conditions of

the test (i.e., cross-head speed and initial gauge length)(Brown, 1999). It is also known as the ratio between changed length and initial length after breakage of the test specimen. It is expressed in percentage. Figure 4.7 shows that PA had 137.53% higher elongation at break than conformal coating. This shows that PA coating film can stretch and elongate more during phase change process of MA before it breaks.

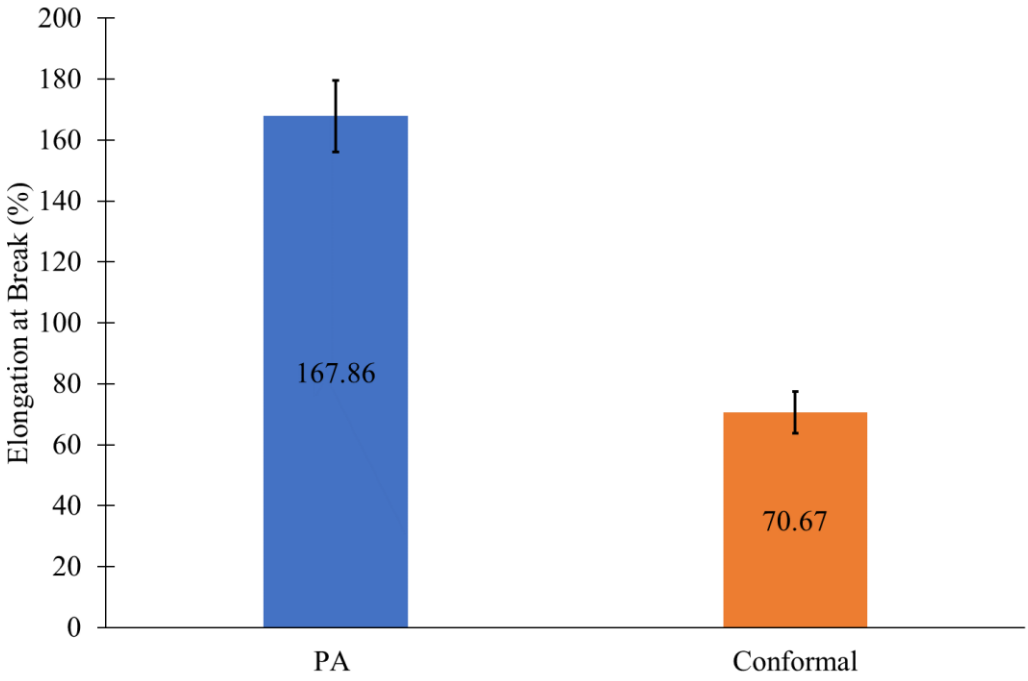

Figure 4.7: Elongation at Break of PA and Conformal

Overall, PA has better mechanical properties in term of E-modulus, tensile strength and elongation at break compared to the conformal coating. Therefore, PA has better performance in preventing leakage. These results support the leakage test result in section 4.2.

4.4 Chemical Properties: Fourier Transform Infrared Spectroscopy (FTIR)

Interaction between MA and PMMA were investigated using FTIR spectroscopy. Figure 4.8 shows the FTIR spectra for pure PMMA, MA and composite PCM (MA/PMMA, 60/40 wt %). For PMMA, the peaks at 2999-2953 cm^{-1}, 1735 cm^{-1}, 1458 cm^{-1} and 1147cm^{-1} are assigned to -CH stretching, C=O stretching, CH_3 stretching and –O-CH_3 stretching vibrations, respectively (Abdelrazek et al., 2016). Other peaks for PMMA at 985-844 cm^{-1} correspond to CH_3 bending (Tomar et al., 2011). For MA, C=O peak and C-H symmetrical stretching peak are occurred at 1697 cm^{-1} and 2917cm^{-1}, respectively (Cellat et al., 2015). The O-H stretching of MA can be observed in the range of 2500 to 3300 cm^{-1} (Wang and Meng, 2010a). The peaks corresponding to the out of plane bending vibration and in-plane swinging vibration of –OH functional group in MA are found at 939 and 720 cm^{-1}, respectively (İnce et al., 2015). The peaks for composite PCM (MA/PMMA, 60/40 wt %) are almost similar as MA due to the high mass fraction of fatty acid in the composite (60% w/w). The hydroxyl peak (O-H) of MA in the range of 2500 to 3300 cm^{-1} has small change in the composite due to the interaction between oxygen atom of carbonyl group (C=O) in PMMA and hydrogen atom of hydroxyl group of MA (Alkan and Sari, 2008). Hydrogen bonding between MA and PMMA increase the compatibility between both components of the composite. However, no new functional group is found. Therefore, it can be concluded that the interaction of MA and PMMA does not involve any chemical reaction.

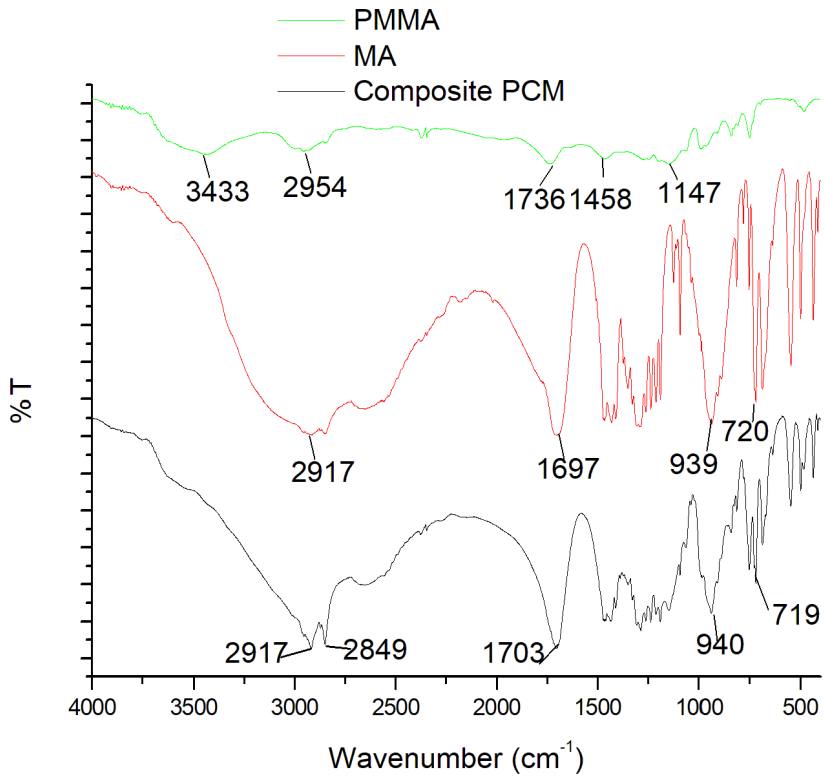

Figure 4.8: FTIR Spectra for the Pure PMMA, Pure MA and Composite PCM (MA/PMMA, 60/40 wt %)

FTIR spectra for the composite PCM (MA/PMMA, 60/40 wt %), pure silicone conformal coating film and composite PCM (MA/PMMA, 60/40 wt %) with conformal coating is shown in Figure 4.9. The silicone conformal coating film's peaks at 2965 cm^{-1}, 1426 cm^{-1}, 1257 cm^{-1}, 1014 cm^{-1} and 792 cm^{-1} are assigned to C-H stretching, C-H bend, Si-CH_3, Si-O bond, and Si-C, respectively (Park et al., 2012). Silicone conformal coating has very intense peak in the region of 1500 to 700 cm^{-1} due to the interaction of Si atom. The result shows that composite PCM (MA/PMMA, 60/40 wt %) with conformal coating has similar peak

wavelength as conformal coating film. Therefore, composite PCM (MA/PMMA, 60/40 wt %) is well coated because only conformal coating peak is detected after coating.

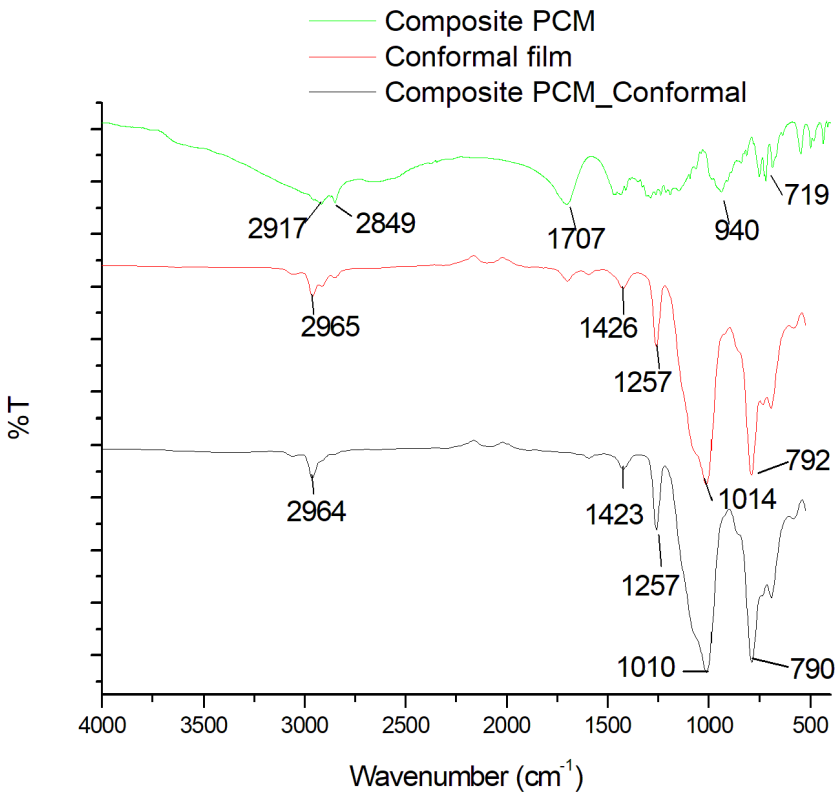

Figure 4.9: FTIR Spectra for Composite PCM (MA/PMMA, 60/40 wt %), Pure Silicone Conformal Coating Film and Composite PCM (MA/PMMA, 60/40 wt %) with Conformal Coating

FTIR spectra for the composite PCM (MA/PMMA, 60/40 wt %), pure PA coating film and composite PCM (MA/PMMA, 60/40 wt %) with PA coating is shown in Figure 4.10. PA coating peaks at 3225 cm^{-1}, 2955-2851 cm^{-1}, 1726 cm^{-1},

1448 cm^{-1} and 1142cm^{-1} are assigned to O-H stretching, CH stretching, C=O stretching, CH_3 stretching and –O-CH_3 stretching vibrations, respectively (Shanti et al., 2017). Similar with previous result, composite PCM (MA/PMMA, 60/40 wt %) with PA only showed PA coating peak and none of the MA peak is detected.

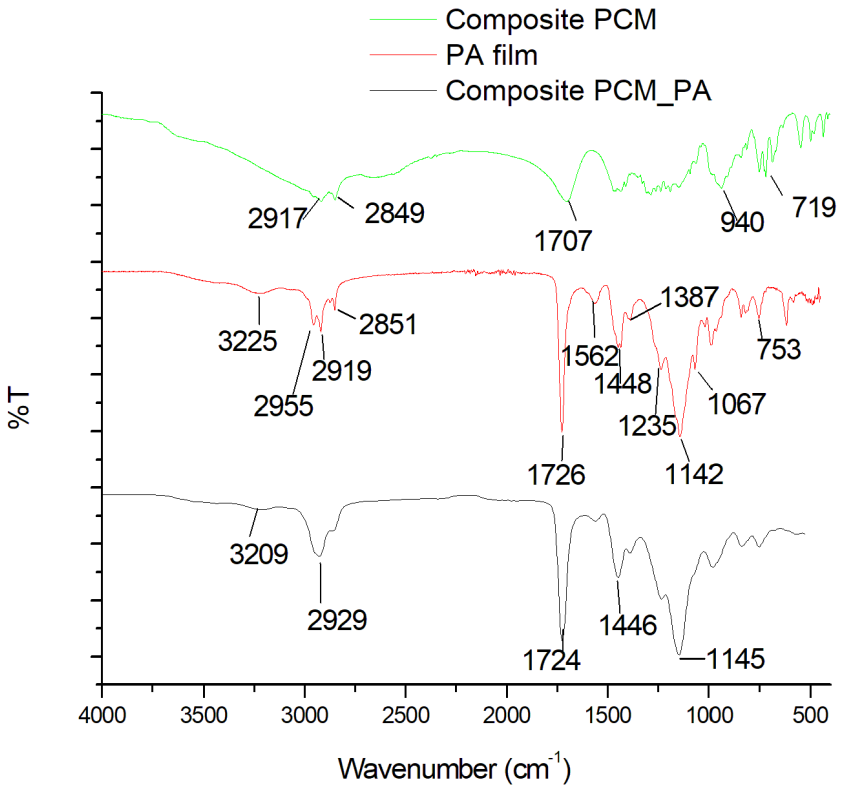

Figure 4.10: FTIR Spectra for the Composite PCM (MA/PMMA, 60/40 wt %), Pure PA Film and Composite PCM (MA/PMMA, 60/40 wt %) with PA Coating

4.5 Morphology Analysis: Field Emission Scanning Electron Microscope (FESEM)

Surface morphology analysis of composite PCMs (MA/PMMA, 60/40 wt %) were conducted by using FESEM at 500 times magnification. Figure 4.11 shows fibrous surface morphology for composite PCM without coating. The surface of composite PCM was rough and uneven.

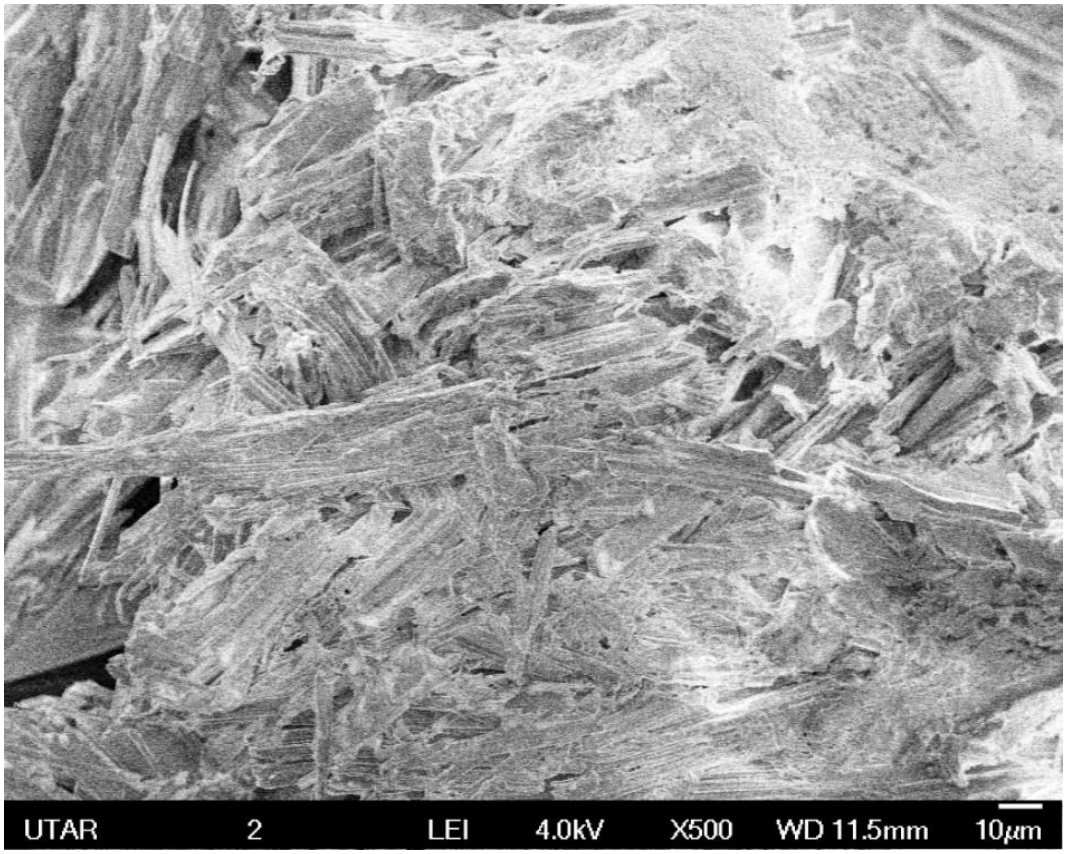

Figure 4.11: FESEM Photograph of Composite PCM (MA/PMMA, 60/40 wt %)

Figure 4.12 (a) and (b) shows that the surface of composite PCM becomes flat and smooth after coatings. This is because a thin layer of film without cracks and holes were formed on surface of composite PCM. The observation verified that both coating acted as barrier to prevent the leakage of MA during phase change process.

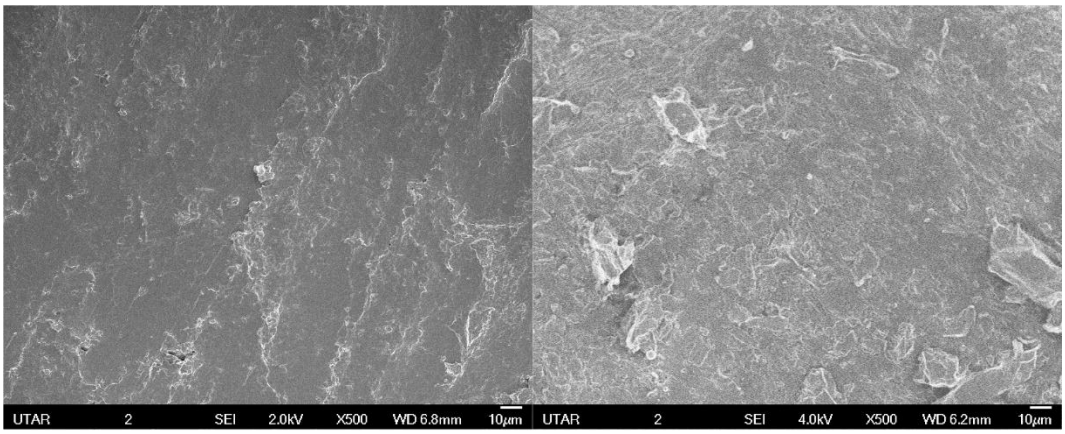

(a) (b)

Figure 4.12: FESEM Photograph of Composite PCM (MA/PMMA, 60/40 wt %): (a) with Conformal Coating and (b) with PA Coating

4.6 Thermal Properties: Differential Scanning Calorimetry (DSC)

Thermal properties of MA and composite PCMs (MA/PMMA) at different weight percentage of MA were studied using DSC. The melting point, freezing point, latent heat of melting and freezing are shown in Table 4.2 and Figure 4.13. In composite PCMs (MA/PMMA), the latent heat of melting and freezing increased

with increasing weight percentage of the MA. This is because MA contribute to latent heat. The differences of melting and freezing temperature between composite PCMs (MA/PMMA) and MA are small and thus insignificant.

Table 4.2: Thermal Properties of Composite PCMs (MA/PMMA) at Different Weight Percentage of MA

Composite PCMs (MA:PMMA, wt.%)	Melting Point (°C)	Latent heat of melting (J/g)	Freezing Point (°C)	Latent heat of freezing (J/g)
20:80	55.53±0.58	30.77±2.26	52.35±0.50	29.61±2.45
40:60	55.15±0.13	76.83±3.59	52.90±0.21	73.9±4.63
60:40	55.45±0.06	129.04±5.63	53.06±0.24	128.76±5.59
80:20	55.87±0.19	163.77±5.29	52.65±0.35	163.77±5.49
Pure MA	55.97±0.12	215.65±4.69	52.72±0.27	218.44±5.02

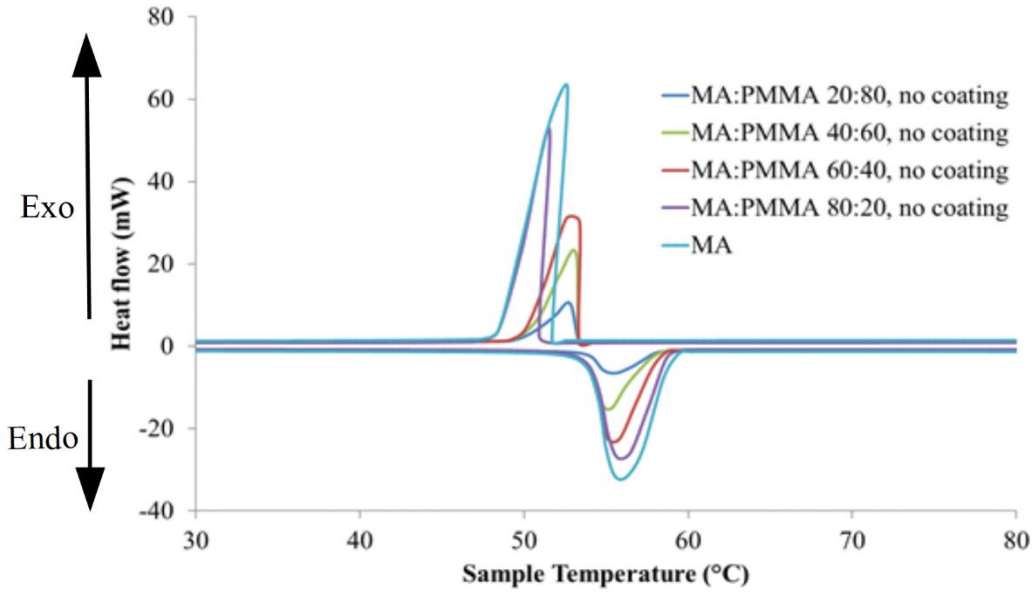

Figure 4.13: DSC Curves of Composite PCM (MA/PMMA) at Different Weight Percentage of MA

Thermal properties of composite PCMs (MA/PMMA) with coating at different weight percentage of MA are summarized in Table 4.3. Overall, both coatings: conformal and PA coating reduced the latent heat of melting and freezing as shown in Figure 4.14 and Figure 4.15, respectively. The latent heat is the amount of heat energy per unit mass of the substance undergoing a change of state (Bond and Hughes, 2013). In the pure fatty acid all the substance mass is the fatty acid. On the other hand, the substance mass of the composite consists of the coating, fatty acid and PMMA. Only part of the substance mass is the fatty acid which contributes to the latent heat. Therefore, the latent heat reduces when more composite material or coatings were added to the fatty acid. However, DSC results also show that the coating does not affect much on melting and freezing point of PCMs.

Composite PCMs (MA/PMMA) which did not have leakage during leakage test were marked bold in Table 4.3. Among all leakage-free samples, composite PCMs (MA/PMMA, 60/40 wt %) with PA exhibit the highest latent heat. The melting and freezing temperature of composite PCM (MA/PMMA, 60/40 wt %) with PA measured by DSC as 54.94±0.23 ºC and 51.39±0.61 ºC, respectively, while the melting and freezing latent heat were 91.42±7.22 J/g and 91.38±8.13 J/g, respectively. If compared to MA, the latent heat of composite PCM (MA/PMMA, 60/40 wt %) with PA was reduced about 57.61%.

Table 4.3: Thermal Properties of Composite PCMs (MA/PMMA) in Different Weight Percentage of MA

Coating	MA:PMMA (wt %)	Melting Point (°C)	Latent Heat of Melting (J/g)	Freezing Point (°C)	Latent Heat of Freezing (J/g)
Conformal coating	**20:80**	**56.43±0.51**	**20.76±5.61**	**49.39±0.34**	**20.94±6.07**
	40:60	**57.95±0.88**	**46.39±7.33**	**50.49±0.76**	**46.6±6.92**
	60:40	55.39±0.09	85.39±8.44	52.2±0.39	85.58±8.21
	80:20	60.25±0.89	114.98±2.05	47.52±0.72	116.06±3.42
PA coating	**20:80**	**55.49±0.13**	**21.03±3.30**	**47.57±0.53**	**18.73±2.85**
	40:60	**54.90±0.03**	**55.59±2.31**	**51.04±0.67**	**55.05±3.05**

60:40	**54.94±0.23**	**91.42±7.22**	**51.39±0.61**	**91.38±8.13**
80:20	54.79±0.41	112.78±8.59	50.66±0.38	112.34±9.03

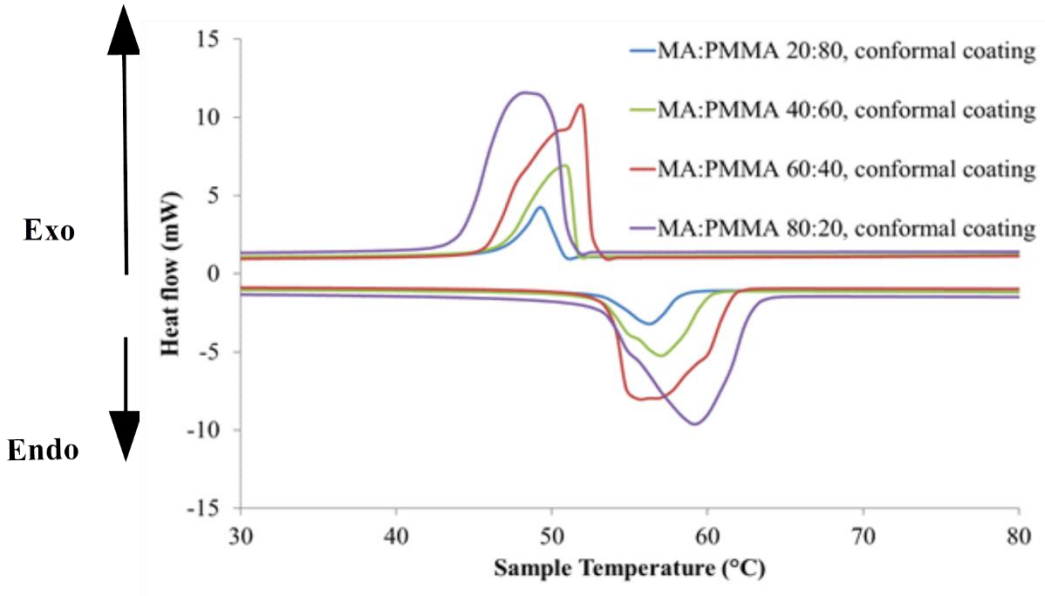

Figure 4.14: DSC Curves of Composite PCMs (MA/PMMA) with Conformal Coating in Different Weight Percentage of MA

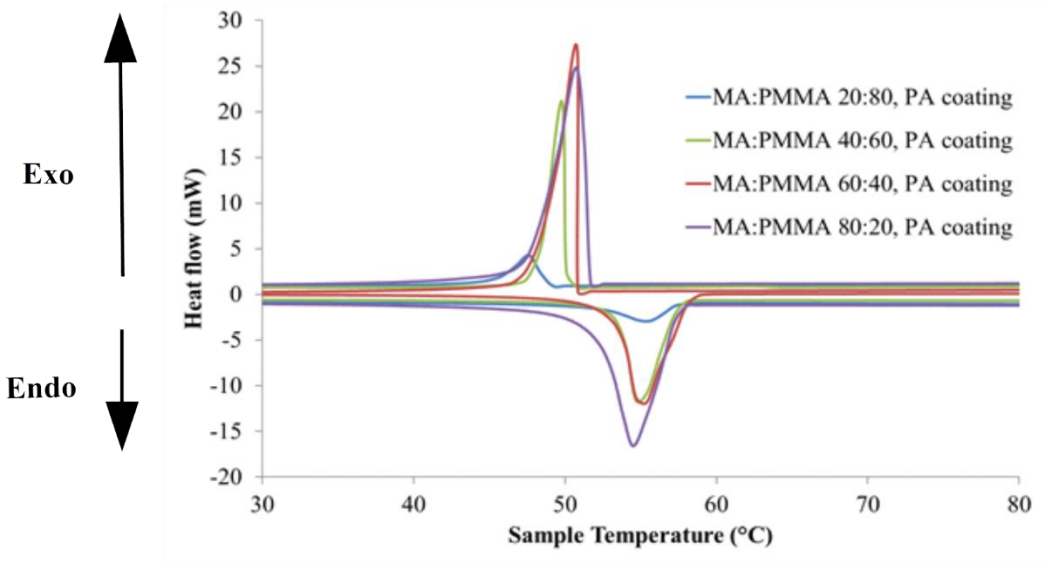

Figure 4.15: DSC Curves of Composite PCMs (MA/PMMA) with PA Coating in Different Weight Percentage of MA

4.7 Durability: Thermal cycling

For thermal reliability, the thermal properties of composite PCM (MA/PMMA, 80/20 wt %) with and without coating after 1000 times thermal cycling test were analyzed by DSC. Table 4.4 shows that the variances in melting and freezing temperatures of all samples before and after thermal cycling were small and less than 2%.

Table 4.4: DSC Results of Melting and Freezing Point before and after 1000 Thermal Cycling.

PCM composite (MA:PMMA) 80:20	Melting point (°C)			Freezing point (°C)		
	Before	After	Changes percentage (%)	Before	After	Changes percentage (%)
Without coating	56.62	56.23	0.68	51.86	51.51	0.68
With conformal	58.84	58.79	0.09	49.73	49.64	0.18
With PA	54.19	54.18	0.02	48.47	47.79	1.40

Table 4.5 shows the changes of latent heats of melting and freezing for composite PCM without coating were 2.85% and 3.53%, respectively. The changes of latent heats of melting and freezing for same composite PCM (MA/PMMA) with coating dropped within a narrow range of 0.16%–1.22% after thermal cycling, indicating the good thermal reliability of the composite PCM (MA/PMMA) after coating. The DSC curves before and after repeated thermal cycling of composite PCM with and without coating are given in Figure 4.16 and Figure 4.17.

Table 4.5: DSC Results of Melting and Freezing Latent Heat before and after 1000 Thermal Cycling.

PCM composite (MA:PMMA) 80:20	Latent heat of melting (J/g)			Latent heat of freezing (J/g)		
	Before	After	Changes percentage (%)	Before	After	Changes percentage (%)
Without coating	170.65	165.79	2.85	171.89	165.82	3.53
With conformal	106.12	105.95	0.16	106.75	106.40	0.33
With PA	103.14	102.09	1.02	103.27	102.01	1.22

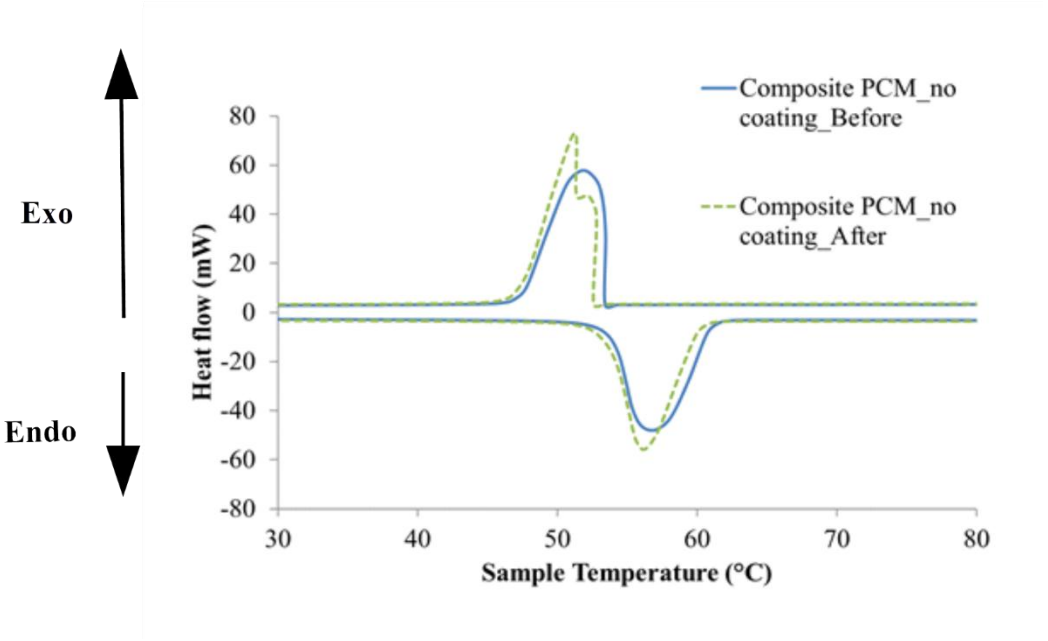

Figure 4.16: DSC Curves of Composite PCMs (MA/PMMA, 80/20 wt%) without Coating before and after 1000 Thermal Cycling

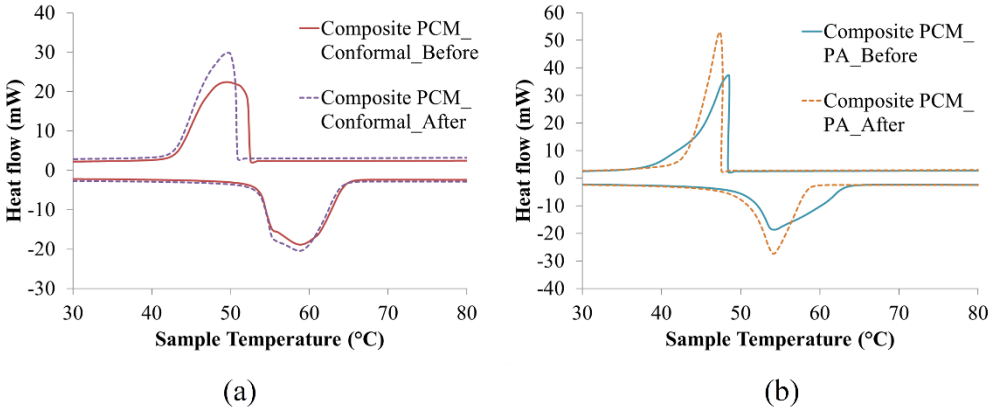

Figure 4.17: DSC Curves of Composite PCMs (MA/PMMA, 80/20 wt%): (a) with Conformal Coating and (b) with PA Coating before and after 1000 Thermal Cycling

4.8 Summary

Composite PCMs (MA/PMMA) with conformal coating and PA coating have been produced in this work. Characterization test results are summarized in Table 4.6. Leakage test indicated that the coating can be used to prevent and minimize the leaking of composite PCMs (MA/PMMA). PA performs better compared to conformal coating as no leakage was found on composite PCM (MA:PMMA, 60:40 wt%) with PA coating compared to those with conformal coating whose leakage area was 1.74 cm^2 under the same weight percentage of MA/ PMMA. This result was supported by tensile result as PA showed 144.64%, 196.76% and 137.56% higher E-modulus, tensile strength and elongation at break (%), respectively, as compared to conformal coating. FTIR result shows that the

composite PCM (MA/PMMA) was well coated with coating because only coating film peak was detected after coating. This finding was supported by FESEM images because the surface morphology of composite PCM with coating was smooth as a thin layer of coating without crack was form on the surface of composite PCM. DSC result shows that the coating did not affect much on melting and freezing point but it will reduce latent heat of melting and freezing of composite PCMs. Among all leakage-free samples, composite PCMs (MA/PMMA, 60/40 wt %) with PA had the highest latent heat. The melting and freezing temperature of composite PCM (MA/PMMA, 60/40 wt %) with PA were 54.94±0.23 ºC and 51.39±0.61 ºC, respectively, while the melting and freezing latent heat were 91.42±7.22 J/g and 91.38±8.13 J/g, respectively. Furthermore, composite PCMs with coating were thermal reliable as the changes of melting and freezing latent heat after 1000 thermal cycling was in the range of 0.16% - 1.22%.

Table 4.6: Summary of the Outcome of the Characterization Tests

No	Characterization Tests	Outcome
1.	Leakage analysis	PA had better performance in preventing leakage.
2.	Tensile properties	PA had better mechanical properties than conformal coating.

3.	FTIR Analysis	Both composite PCMs are well coated because only the coating functional groups were detected on the PCM after coating.
4.	FESEM	Surface morphology of composite PCM with coating was smooth because a thin layer of coating film was form on the surface of composite PCM.
5	DSC	Latent heat of composite PCM were reduced after adding coating. However, coating did not affect much on melting and freezing point of composite PCM.
6	Thermal cycling	Composite PCMs with coating were thermal reliable as the changes of melting and freezing latent heat after 1000 thermal cycling was in the range of 0.16% - 1.22%.

Based on the results above, it can be concluded that PA is ideal to be used as a coating material on preventing leakage. However, the latent heat of composite PCM was reduced significantly after adding coating and PMMA supporting material. Therefore, next phase will be focused on developing the enhanced polymer coating combination that can be applied directly on MA pellet without PMMA supporting material to maximize latent heat.

CHAPTER 5

RESULT AND DISCUSSION FOR FORM STABLE COMPOSITE PCM WITH ENHANCED COATINGS COMBINATION TO MAXIMIZE LATENT HEAT

This chapter presents the result and discussion for phase 2 of the research study – FSCPCM with enhanced coating combination to maximize latent heat. In this phase, coatings with different mechanical properties are directly applied on MA pellet without PMMA supporting material to maximize latent heat. The contents of the chapter were outlined into eight subsections. This chapter begins with the introduction of the work flow used in this phase. Characterization and performance analysis tests such as leakage analysis, tensile, FTIR, FESEM, DSC and thermal cycling were also presented. Lastly, summary of this phase was made. The polymer coating combination which gave the best thermal stability for MA pellet was identified from the results.

5.1 Introduction

The work flow in this phase of research study was summarized in Figure 5.1. First, MA flakes were compressed into pellet using hydraulic press. Then, MA pellet was dip coated with two types of polymer coating solution which were PA and nitrie butadiene rubber (NBR) in different combinations. MA pellet was used as PCM core

to store latent heat while polymer coating was used as a shell to contain the PCM. In this phase, PA was continued to be used because it had higher mechanical strength to withstand the pressure during the volume change as reported in phase1. Whereas NBR was used because it is lightweight, resistant to corrosion, possess high tensile strength and able to perform under wide range of temperatures -20 to +125 ° (Singh et al., 2012; Board, 2013). It also has good flexibility at low temperature (Lawindy et al., 2002). Therefore, it was proposed to be used on MA pellet to withstand the expansion of melted MA during phase change process. Despite several researches on PA and NBR, there is a lack of study on the application of these two coatings for PCM. Besides, most of the researchs were done by applying polymer coating on PCM with supporting material, resulting reduction of latent heat. This is supported by phase 1 result which also showed significant reduction of latent heat after adding PMMA suporting material and polymer coating. Therefore, the objective of this phase is to maximize the latent heat by directly applying polymer coating on MA pellet without supporting material. Hence, the latent heat of PCM is expected to increase. Performance of MA pellet with different polymer coating combination would be compared to determine which combination gave the best thermal stability. The thermal stability was investigated through leakage test analysis. Besides, tensile properties of the coating films were analysed to determine their mechanical properties. Chemical compatibility, thermal properties and morphology analysis of MA pellet with different polymer coating combinations were characterized using

DSC, FTIR and FESEM, respectively. Thermal cycling test were also carried out to determine the thermal stability of samples after 1000 melting and freezing cycles.

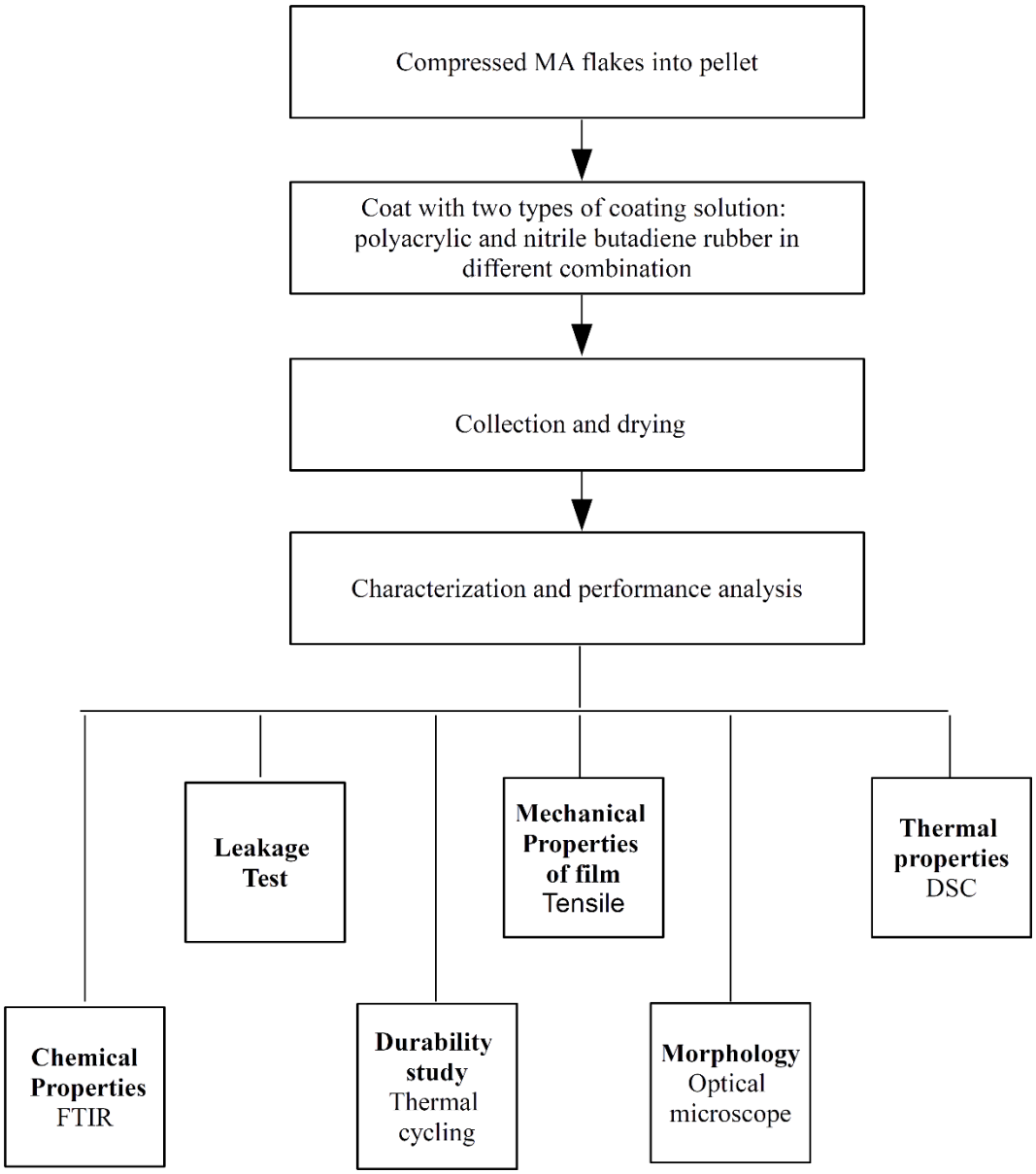

Figure 5.1: Work flow of Phase 2 Experiment

5.2 Leakage Analysis

Leakage analysis was carried out in oven at 65 ºC. Leakage area of all samples were measured every 2 hours for a duration of 10 hours as shown in Figure 5.2. The leakage area of all samples after 10 hours heating in oven is summarized in Table 5.1. The samples that did not have leakage were marked bold in Table 5.1. 2NBR/MA pellet and PANBR/MA pellet were most thermally stable over phase change temperature as no leakage were found.

Table 5.1: Leakage Area for MA pellet with Different Polymer Coating Combination after 10 Hours Heating

Abbreviation	Types of coating	Leakage area (cm^2)
MA	No coating	22.71
PA/MA	1-layer PA	22.84
NBR/MA	1-layer NBR	18.91
2PA/MA	2-layers PA	16.56
2NBR/MA	**2-layers NBR**	**0.00**
PANBR/MA	**1-layer PA (outer layer) and 1- layer NBR (inner layer)**	**0.00**

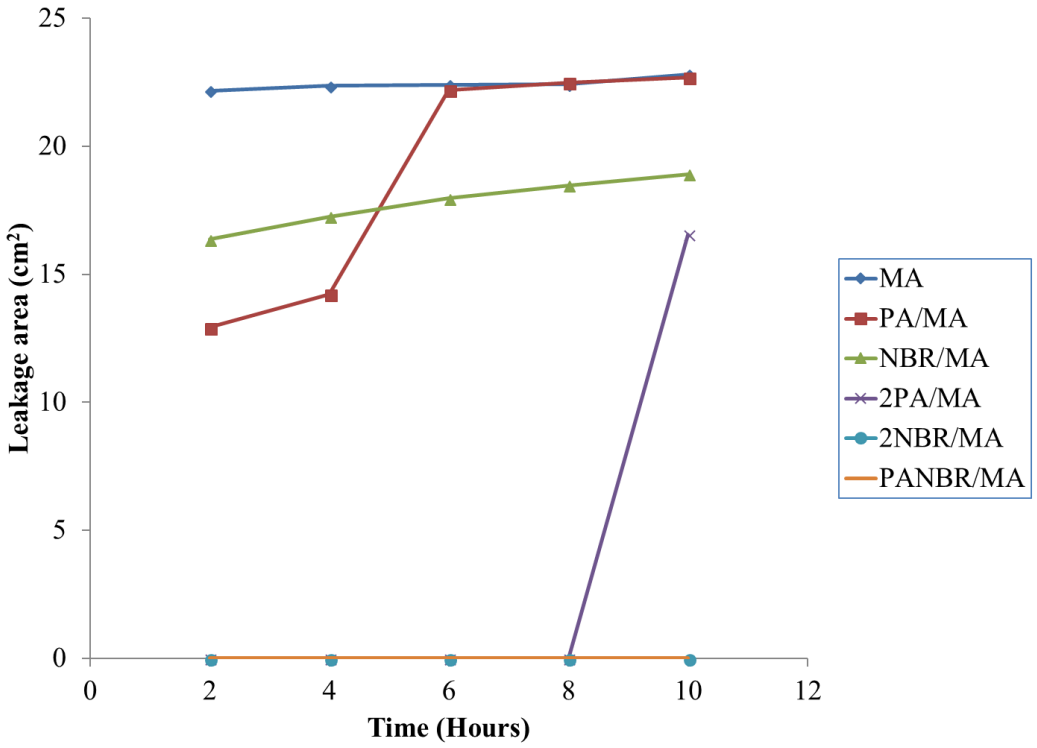

Figure 5.2: Changes of Leakage Area for Samples Over 10 Hours

Figure 5.2 shows that MA pellet without coating (melting point, 55.90 °C) was completely melted in first 2 hours. PA/MA pellet and NBR/MA pellet with 1-layer coating exhibit smaller leakage area in first 2 hours duration of heating in oven if compared to pure MA pellet. This shows that 1-layer coating can minimize the leakage but still not strong enough to hold the volume change of melted MA during phase change process. 2PA/MA pellet with 2-layers of PA coating was stronger and only started to leak after 8 hours of heating in oven. Moreover, 2NBR/MA pellet and PANBR/MA pellet did not show any leakage after 10 hours of heating. The leakage can be evidenced by leakage comparison image for all samples after heating

10 hours in oven as shown in Figure 4.2. In overall, the leakage area after 10 hours heating in oven were reduced with increasing number of coating layers. Therefore, it can be concluded that 2 layers of coating perform better than the 1-layer of coating.

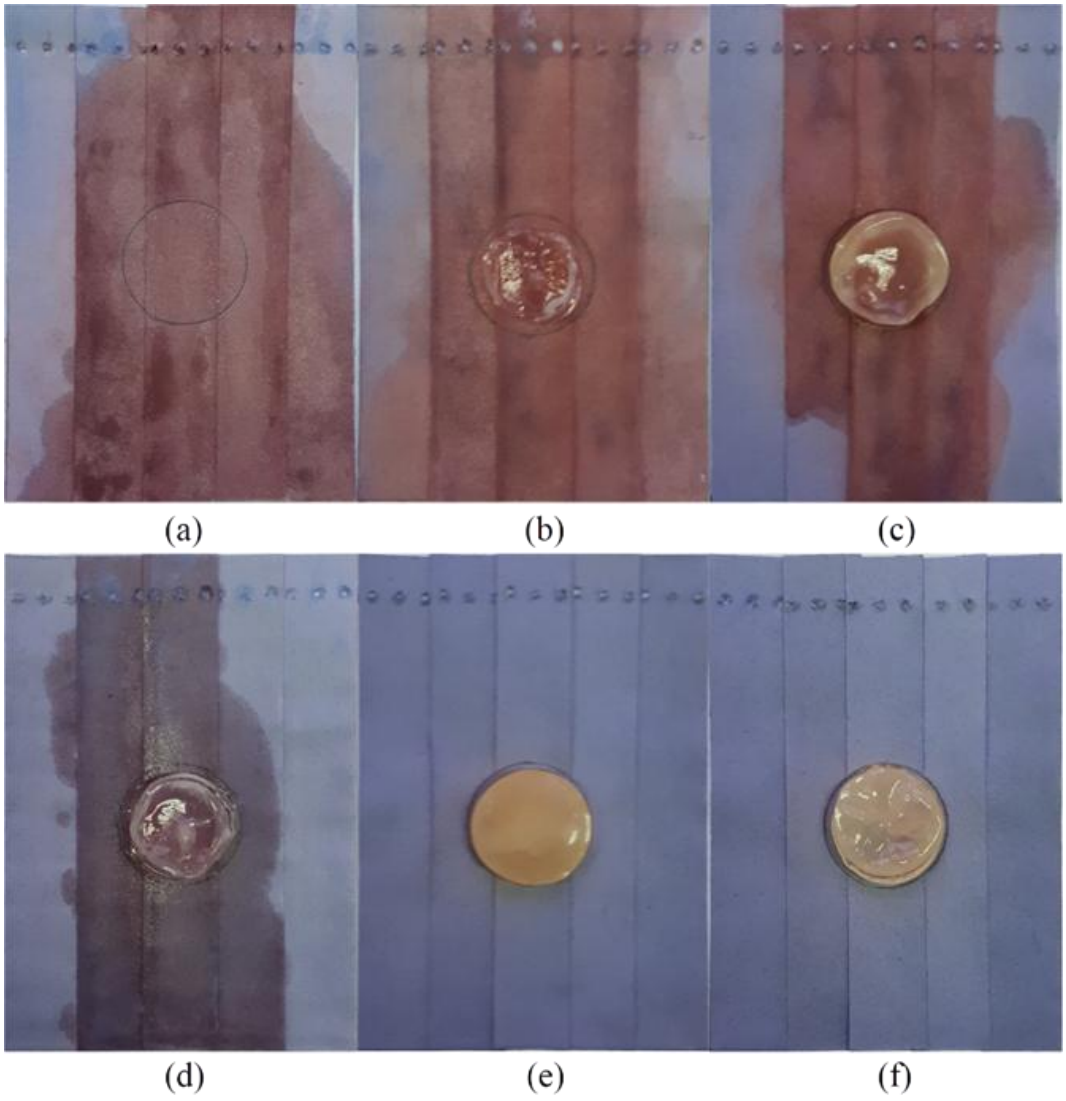

Figure 5.3: Leakage Comparison for (a) MA Pellet, (b) PA/MA Pellet, (c) NBR/MA, (d) 2PA/MA, (e) 2NBR/MA (f) PARB/MA after Heating in Oven at 65°C for 10 Hours

Among all samples, 2NBR/MA pellet and PANBR/MA pellet were the most thermally stable samples. Therefore, these 2 samples were put in oven continuously for 24 hours to further verify thermal stability. Lastly, PANBR/MA pellet which was coated with 1 inner NBR layer and 1 outer PA layer showed better performance and no leakage after 24 hours heating in oven as shown in Figure 5.4. Hence, it can be concluded that the combination of NBR and PA is the best polymer coating combination for MA pellet in preventing leakage.

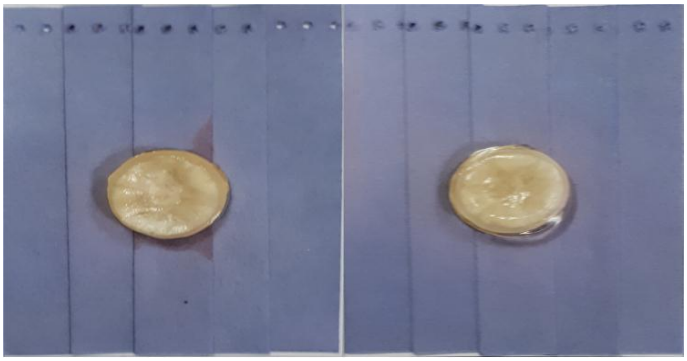

(a) (b)

Figure 5.4: Leakage Comparison for (a) 2NBR/MA Pellet and (b) PANBR/MA Pellet after Heating in Oven at 65°C for 24 Hours

5.3 Mechanical Properties of Film: Tensile

NBR, PA and combination of PA and NBR (PA+NBR) coating were casted into thin sheet film on Teflon mould for tensile test. Figure 5.5 shows stress strain curve for PA, NBR and PA+NBR. NBR film had extremely low E-modulus and tensile strength but very high elongation at break. This was because NBR is an

elastomer with very long polymer chains that could be stretched under tension (Zhao et al., 2007). Whereas PA film is a thermoplastic with higher E- modulus and tensile strength but lower elongation at break than NBR. A good coating film must have moderate E-modulus, tensile strength and elongation at break to hold and sustain the expansion of melted of PCM (Zhou et al., 2012). Therefore, NBR and PA film were combined to enhance the mechanical properties.

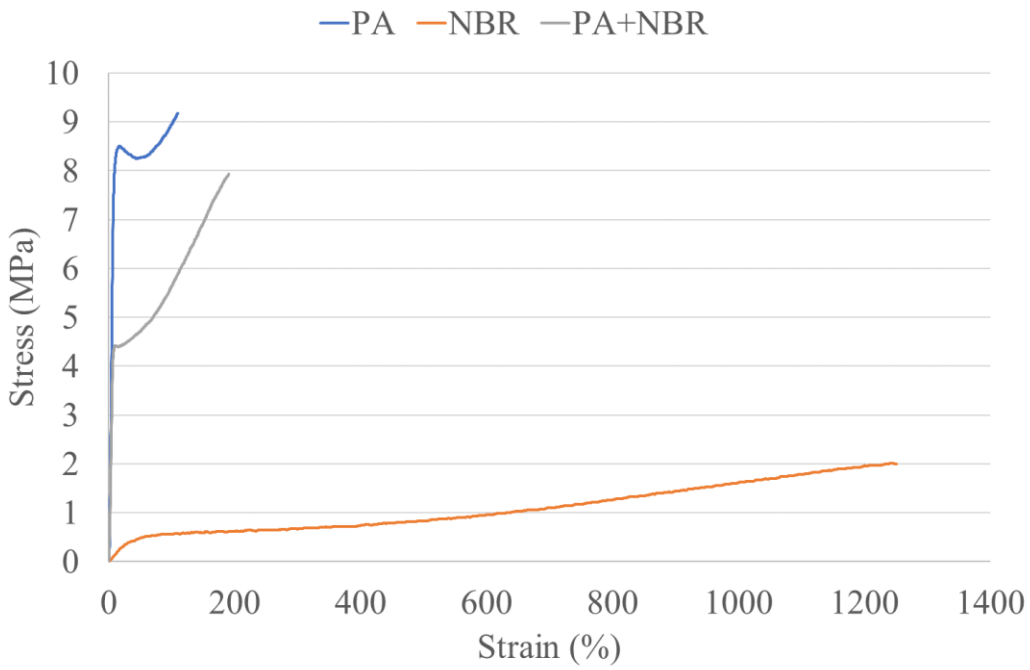

Figure 5.5: Stress Strain Curve for PA, NBR and PA+NBR

Table 5.2 shows that PA had high E-modulus (130.84 ± 9.88 MPa) whereas NBR had very low E-modulus ($9.22 \times 10^{-2} \pm 3.94 \times 10^{-3}$ MPa). Thus, PA as outer layer of coating had higher resistance to deformation over the volume change of MA during phase change process if compared to NBR. The combination of PA and NBR

gave a moderate E-modulus (76.10 ± 5.43 MPa). PA as outer layer of coating also had high tensile strength to prevent cracking during phase change process. The combination of PA and NBR gave a moderate tensile strength ($8.21 \pm 3.14 \times 10^{-1}$ MPa). NBR (1250.22 ± 10.01%) had higher elongation at break than PA (167.86 ± 11.76%). This shows that NBR as inner layer of coating able to stretch and elongate more during phase change process of MA before it breaks. The combination of PA and NBR gave a moderate elongation at break (193.92 ± 2.88%).

Overall, combination of PA and NBR improved the mechanical properties of the film in the aspect of E-modulus, tensile strength and elongation at break. Therefore, this combination had better performance in preventing leakage. These results support the leakage test result in section 5.2.

Table 5.2: Tensile Properties of Polymer Coating Films

Polymer coating	E-modulus (MPa)	Tensile Strength (MPa)	Elongation at break (%)
NBR	$9.22 \times 10^{-2} \pm 3.94 \times 10^{-3}$	$2.32 \pm 2.88 \times 10^{-1}$	1250.22 ± 10.01
PA	130.84 ± 9.88	12.19 ± 1.34	167.86 ± 11.76
PA+NBR	76.10 ± 5.43	$8.21 \pm 3.14 \times 10^{-1}$	193.92 ± 2.88

5.4 Chemical Properties: Fourier Transform Infrared Spectroscopy (FTIR)

Figure 5.6 shows the FTIR spectra of pure MA pellet, pure PA film and pure NBR film. For MA, C=O and C-H stretching peaks are recorded at 1697 cm^{-1} and 2917 cm^{-1}, respectively (Cellat et al., 2015). The peaks corresponding to the out of plane bending vibration and in-plane swinging vibration of –OH functional group for MA are found at 939 cm^{-1} and 720 cm^{-1}, respectively (Wang and Meng, 2010b). For PA film, the peaks at 3225 cm^{-1}, 2957-2800 cm^{-1}, 1728 cm^{-1}, 1449 cm^{-1} and 1146 cm^{-1} are corresponding to O-H stretching, CH stretching, C=O stretching, CH_3 stretching and –O-CH_3 stretching vibrations, respectively (Shanti et al., 2017). For NBR, characteristic peaks occur at the broad range of 3200-3550 cm^{-1} for O-H symmetric stretching vibration and N-H stretching vibration. The peaks at 2922 cm^{-1} and 2848 cm^{-1} correspond to asymmetric stretching vibration of methylene in the saturated hydrocarbon backbone and symmetric stretching vibration of methylene, respectively (Liu et al., 2016) . Besides, peak at 2237 cm^{-1}, 1698 cm^{-1}, 1642 cm^{-1}, 1440 cm^{-1} and 967 cm^{-1} are corresponded to C≡N bond, C=O stretching, C=C stretching vibration, CH_2 deformation vibration and CH deformation vibration, respectively (Aly, 2016).

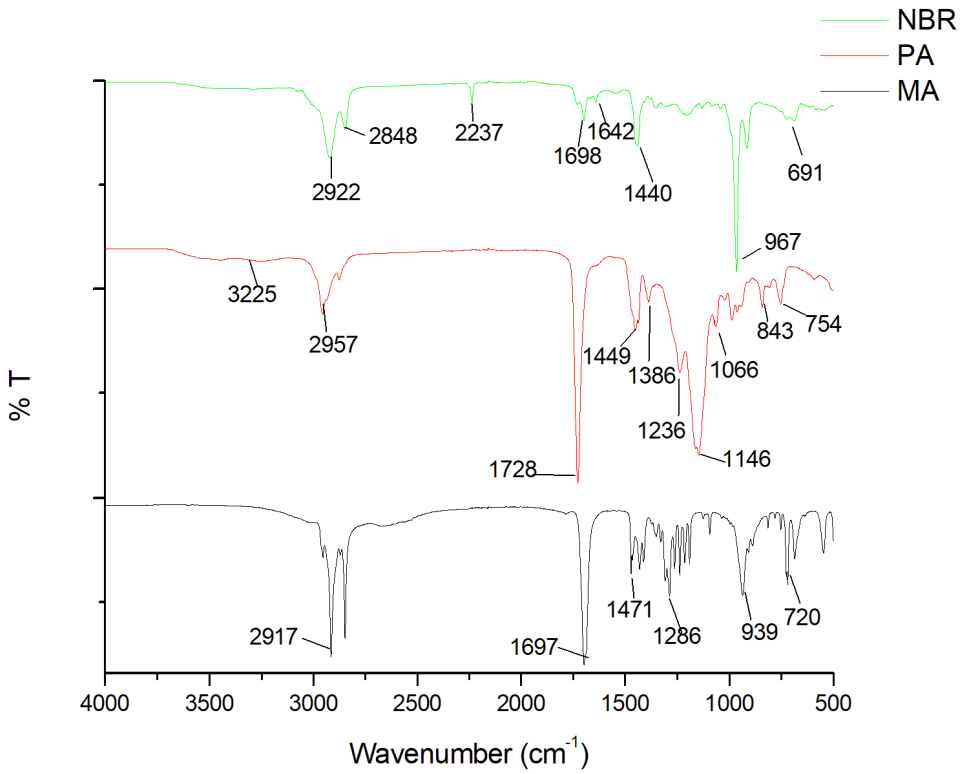

Figure 5.6: FTIR Spectra for the NBR Film, PA Film and MA Pellet

The FTIR spectra for PA film, PA/MA pellet, 2PA/MA pellet and PANBR/MA pellet are shown in Figure 5.7. The result shows that all MA pellet coated with PA coating has similar peak shape and frequency value as PA film. It indicates that MA pellets are well coated because only the functional groups of outer layer of polymer coating materials are detected after coating (Sarı et al., 2014).

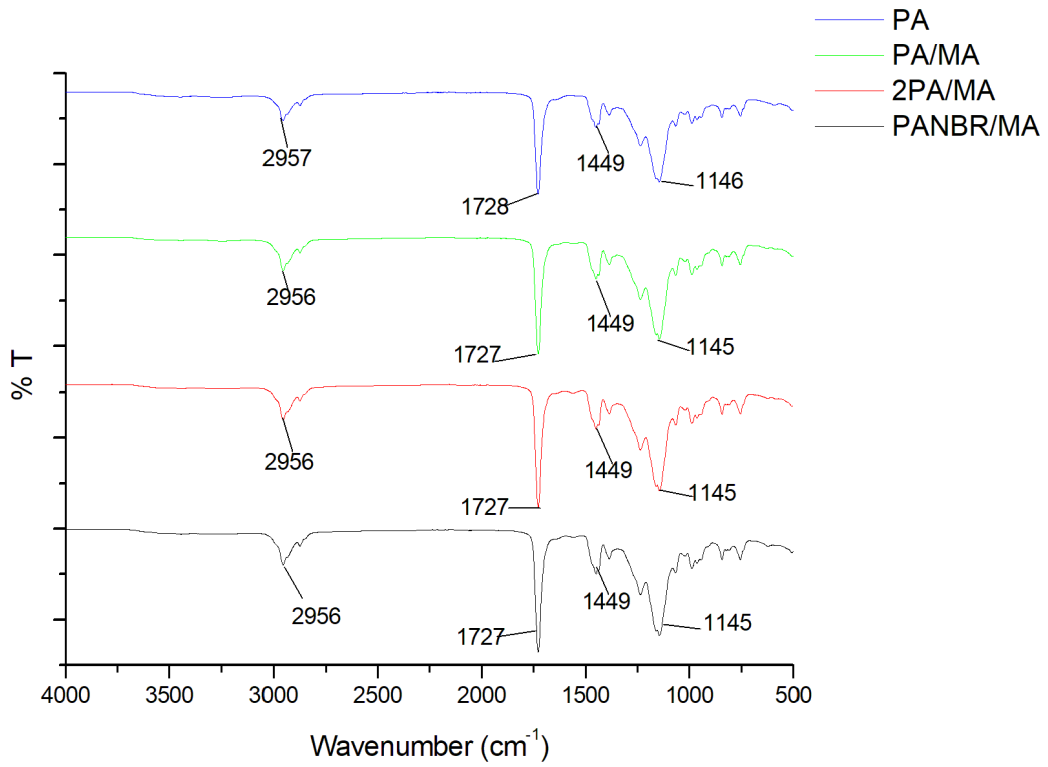

Figure 5.7: FTIR Spectra for PA Film, PA/MA Pellet, 2PA/MA Pellet and PANBR/MA Pellet

The FTIR spectra for NBR film, NBR/MA pellet and 2NBR/MA pellet is shown in Figure 5.8. Similar with previous result, MA pellet coated with NBR only shows NBR coating peak and none of the MA peak is detected. Therefore, it can be concluded that MA pellet was well coated with coating. Moreover, both spectra: Figure 5.7 and Figure 5.8 show that no new functional groups are found on FTIR spectra of dip coated MA pellet. It further confirms that the dip coating method is physical method with no chemical reaction between MA pellet with coating film.

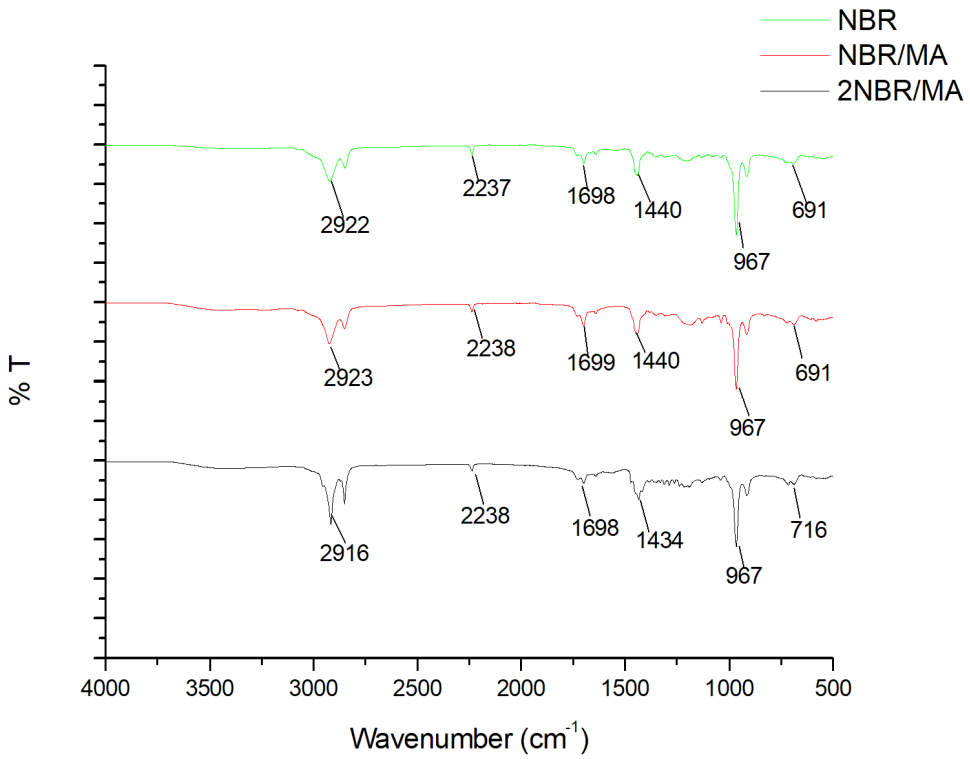

Figure 5.8: FTIR Spectra for NBR Film, NBR/MA Pellet and 2NBR/MA Pellet

5.5 Morphology Analysis: Microscope

Cross-section of the dip coated MA pellet was observed using metallurgical microscope at 10 times magnification. Figure 5.9 - Figure 5.11 show that all polymer coating films adhere compactly to the core MA material in the pellet as no defects such as holes, gaps, and cracks could be observed at the interface between the coating film and MA pellet.

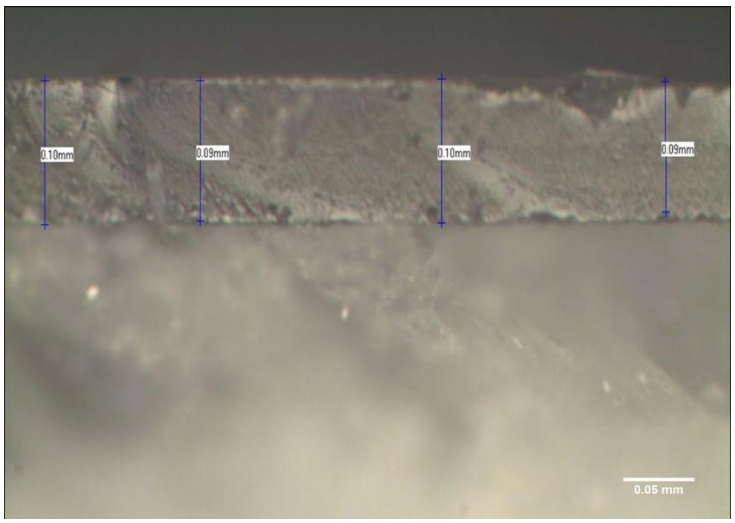

Figure 5.9: Optical Micrograph of the Cross Section of PA/MA Pellet

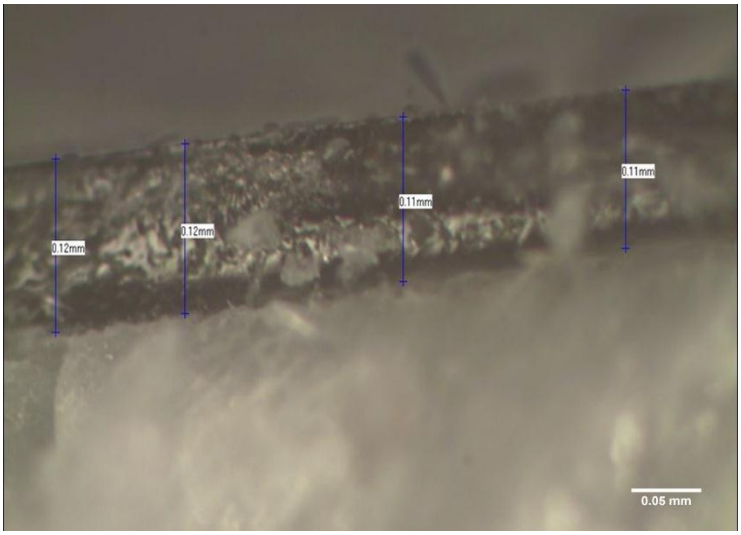

Figure 5.10: Optical Micrograph of the Cross Section of NBR/MA Pellet

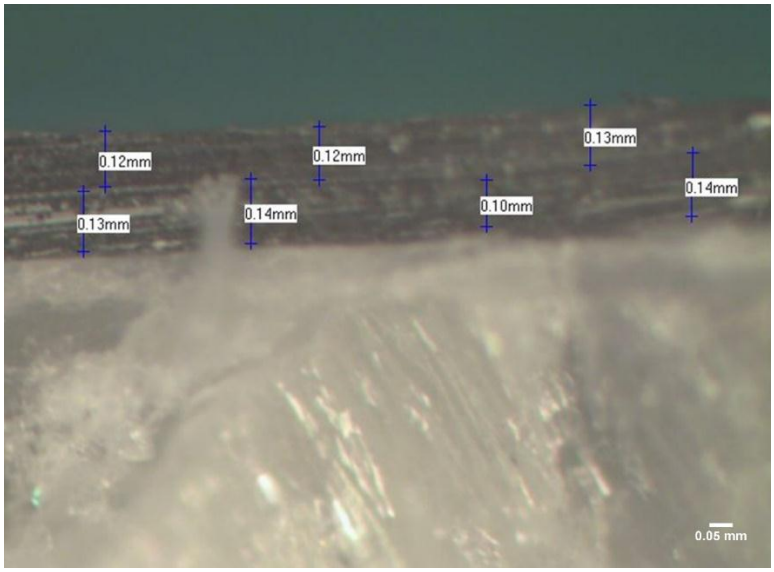

Figure 5.11: Optical Micrograph of the Cross Section of PANBR/MA Pellet

The thickness of the coating film for all samples were measured using digital Vernier Caliper. The thickness of pellet before and after coating for each sample were measured and recorded 3 times, then the average thickness was calculated from the readings recorded. The coating film thickness can be calculated by Eq. (5.1)

$$T_{film} = \frac{T_{AC} - T_{BC}}{2} \tag{5.1}$$

Where,

T_{film} = Thickness of one side coating film

T_{AC} = Thickness of pellet after coating

T_{BC} = Thickness of pellet before coating

The average thickness of 1-layer PA and NBR coating for 20 samples measured using Vernier Caliper were 0.104038±0.029853 mm and 0.114851±0.032975 mm respectively. These measurement results were further confirmed by the measurement from microscope image using the Plus ver.3.30 image analysis and measurement software. Figure 5.9 shows the thickness of 1-layer PA coating was in the range of 0.09-0.10 mm. Whereas Figure 5.10 shows that the thickness of 1-layer NBR coating was in the range of 0.11-0.12 mm. Figure 5.11 shows that the thickness for inner layer of NBR coating and outer layer of PA were in the range of 0.10-0.14 mm and 0.12-0.13 mm, respectively. These optical micrograph measurement results obtained were in the range of measurement result obtained using Vernier Caliper. Therefore, Vernier Caliper can be used to measure thickness of coating for large number of PCM samples with coating.

5.6 Thermal Properties: Differential Scanning Calorimetry (DSC)

Thermal properties of dip coated MA pellet with different polymer coating combination were studied using DSC. The melting point, freezing point, latent heat of melting and freezing are shown in Table 5.3 and Figure 5.12. When compared to phase change temperatures of the dip coated MA pellet with pure MA, the changes in melting point was -0.53, -0.88, -0.84, -1.31, and -1.25 °C and the changes in freezing point was -0.18, -0.79, -0.98, -0.91, and -1.16 °C for PA/MA, NBR/MA,

2PA/MA, 2NBR/MA and PANBR/MA, respectively. These small changes indicated that both coatings did not significantly affect the melting and freezing point of pure MA. However, latent heat decreased with the increased of coating weight percentage. It can be seen that dip coated MA pellet with two layers of coating had lower latent heat. This is because the coating material fraction reduce the mass percentage of MA which contribute to latent heat (Alkan and Sari, 2008).

Table 5.3: Thermal Properties of Dip Coated MA Pellet with Different Polymer Coating Combination

PCM	Coating layers	Coating (wt%)	PCM (wt%)	Melting Point (ºC)	Latent heat of melting (J/g)	Freezing Point (ºC)	Latent heat of freezing (J/g)
MA	No coating	0	100	55.97± 0.12	216.04 ±4.72	52.72± 0.27	216.85± 4.54
PA/MA	1-layer PA	18.62	81.38	55.44± 0.18	161.62 ±4.06	52.54± 0.16	160.91± 3.85
NBR/ MA	1-layer NBR	19.87	80.13	55.09± 0.33	157.52 ±9.10	51.93± 0.73	157.80± 9.61
2PA/MA	2-layers PA	36.43	63.57	55.13± 0.11	130.53 ±6.09	51.74± 0.16	129.16± 7.94
2NBR/ MA	2-layers NBR	38.84	61.16	54.66± 0.24	124.83 ±7.78	51.81± 0.42	124.22± 8.29
PANBR/ MA	**1-layer NBR + 1-layer PA**	**37.78**	**62.22**	**54.72± 0.27**	**131.84 ±5.76**	**51.56± 0.58**	**130.97± 7.40**

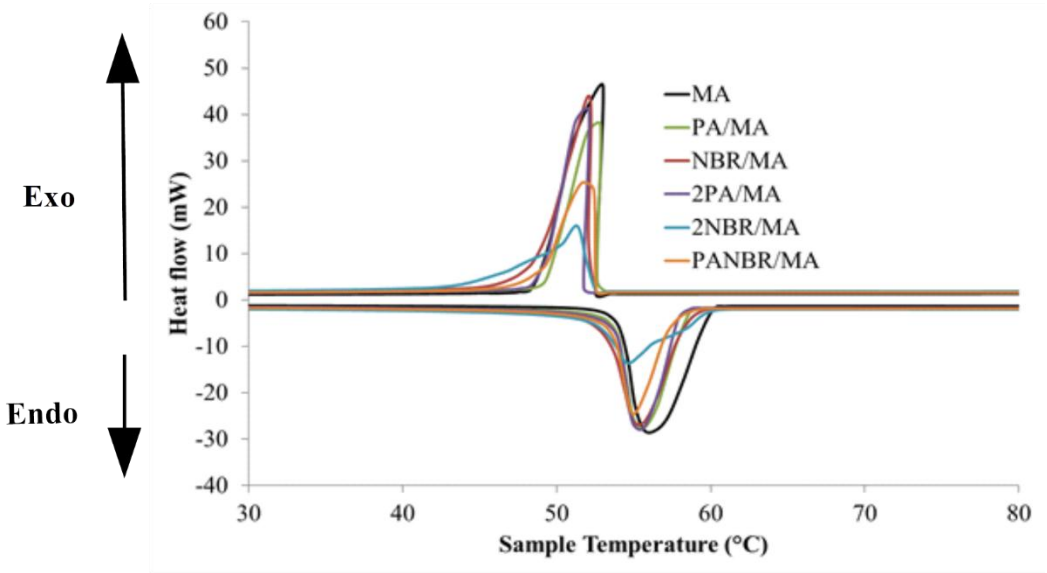

Figure 5.12: DSC Curves of Dip Coated MA Pellet with Different Polymer Coating Combination

PANBR/MA pellet is the most thermally stable sample as indicated earlier in Table 5.3. The melting and freezing temperature of PANBR/MA pellet measured by DSC as 54.72±0.27 ºC and 51.56±0.58 ºC, respectively, while the melting and freezing latent heat were 131.84±5.76 J/g and 130.97±7.40 J/g, respectively. If compared to the latent heat of the most thermal stable sample in chapter 4 (Phase I of the research study), PANBR/MA pellet (131.84±5.76 J/g) exhibit 30.66% higher latent heat.

5.7 Durability: Thermal cycling

For durability analysis, the thermal properties of PANBR/MA pellet after 1000 times repeated thermal cycling test were analyzed by DSC as shown in Figure 5.13. The DSC curve shape for PANBR/MA pellet did not change much after 1000 thermal cycles. Table 5.4 shows that the variances in melting temperature, freezing temperatures, latent heat of melting and freezing for PANBR/MA pellet before and after thermal cycling were small and less than 2 %. Therefore, it can be concluded that PANBR/MA pellet had good thermal reliability.

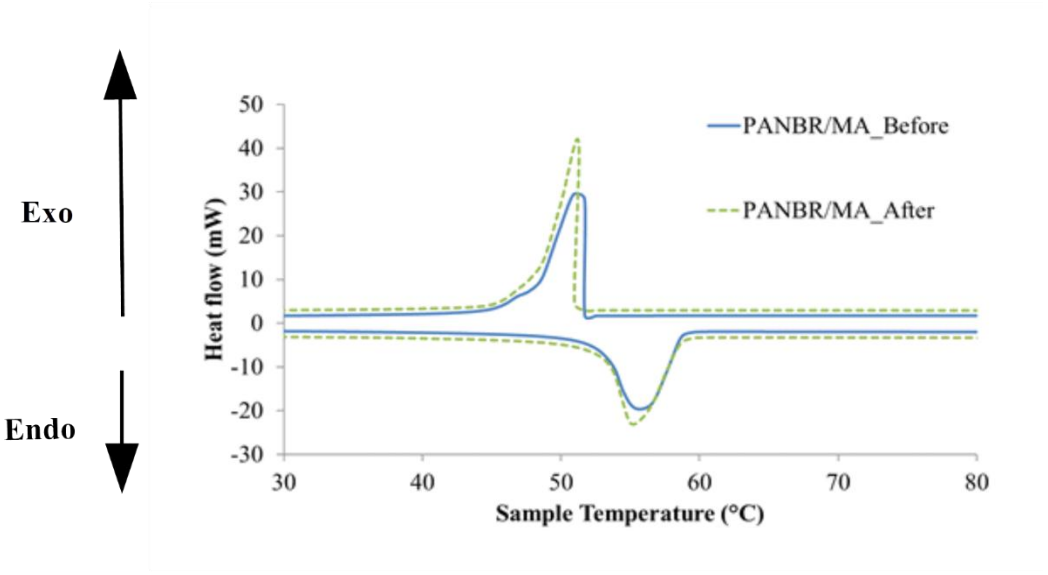

Figure 5.13: DSC Curves of PANBR/MA Pellet before and after 1000 Thermal Cycling

Table 5.4: DSC Results of PANBR/MA Pellet before and after 1000 Thermal Cycling

	Melting Point (°C)	Latent heat of melting (J/g)	Freezing Point (°C)	Latent heat of freezing (J/g)
Before	55.79	131.77	51.70	130.98
After	55.27	129.66	51.28	129.77
Changes percentage (%)	0.93	1.60	0.81	0.92

5.8 Summary

Dip coated MA pellet with PA and NBR in different combination have been produced in this work. Characterization test results are summarized in Table 5.5. Leakage test showed that the MA pellets coated with 2-layers of coating were more stable if compared to those without coating and coated with 1-layer of coating. Among all samples, PANBR/MA pellet with the combination of NBR (inner layer) and PA (outer layer) performed better as no leakage was found after heating in oven for 24 hours. Besides, tensile test showed that the combination of NBR and PA had moderate mechanical properties. NBR as inner layer of coating was elastic and able to withstand the volume change of PCM inside the core, while PA as outer layer of coating was able to provide good structure to hold the PCM from deforming. FTIR result shows that the MA pellet was well coated because only polymer coating's functional group was detected after the coating. This finding was supported by

optical micrograph as polymer coating film were compact and adhered well to the MA pellet. No defects such as holes, gaps, and cracks could be observed at the interface between film and MA pellet. For thermal performance, melting temperature and latent heat of PANBR/MA pellet were recorded at 54.72±0.27 ºC and 131.84 ±5.76 J/g, respectively. The latent heat of PANBR/MA pellet in this phase was 30.66% higher than previous phase where latent heat of composite PCM (MA/PMMA, 60/40 wt %) with PA coating was 91.42±7.22 J/g. Furthermore, PANBR/MA pellet was thermal reliable as the changes of melting and freezing latent heat after 1000 thermal cycling was less than 2 %.

Table 5.5: Summary of the Outcome of the Characterization Tests

No	Characterization Tests	Outcome
1.	Leakage Analysis	PANBR/MA pellet with the combination of NBR (inner layer) and PA (outer layer) had better performance in preventing leakage.
2.	Tensile	Combination of NBR and PA had moderate mechanical properties.
3.	FTIR Analysis	MA pellet are well coated because only the coating functional groups were detected after coating.
4.	Microscope	Polymer coating film was compact and adhered well to the MA pellet as no gaps could be observed at the interface between film and MA pellet.
5	DSC	Latent heat of PANBR/MA pellet was 131.84±5.76 J/g.

6	Thermal cycling	PANBR/MA pellet were thermal reliable as the changes of melting and freezing latent heat after 1000 thermal cycling was less than 2 %.

Based on the results above, the objective of this phase was achieved as the latent heat was increased by directly applying polymer coating on PCM without supporting material. Therefore, PANBR/MA pellet is the most ideal form stable composite PCM because it had high latent heat and good thermal reliability. This combination will be continue used on phase 3 by adding RGO to enhance light absorption of PCM.

CHAPTER 6

RESULT AND DISCUSSION FOR FORM STABLE COMPOSITE PCM WITH ENHANCED COATINGS BLENDED WITH RGO TO IMPROVE LIGHT ABSORPTION

This chapter presents the result and discussion for phase 3 of research study– FSCPCM with enhanced coatings blended with RGO to improve light absorption. The contents of the chapter were outlined into five subsections. This chapter begins with the introduction of the work flow used in this phase. Characterization of RGO through FTIR, XPS, Raman spectroscopy, XRD, FESEM, TEM and UV-Visible absorption analysis were presented and discussed. Dispersion of RGO in coating were studied using XRD, FESEM and AFM. Characterization and performance analysis of FSCPCM with RGO such as solar energy conversion efficiency, DSC, FTIR, thermal cycling test and weathering test were discussed as well. Lastly, summary of this phase was made. The optimum RGO loading which gave the highest solar energy conversion efficiency was identified from the results.

6.1 Introduction

Work flow in this phase of research study was summarized in Figure 6.1. First, RGO was synthesized by oxidizing graphite nanofiber (GNF) via conventional Hummer's method (Hummers and Offeman, 1958) followed by reduction using

hydrazine hydrate (Tripathi et al., 2013). Then, a few analyses such as FTIR, XPS, Raman, XRD, FESEM and TEM were used to determine successful oxidation of GNF and reduction of graphene oxide (GO) to RGO. Absorption wavelength of RGO was also determined using UV-Visible spectroscopy. Next, RGO was mixed with Triton X-100 prior blending with PA coating solution. The dispersion of RGO in PA film was studied using XRD, AFM and FESEM. The polymer coating combination which gave the best thermal stability in phase 2 will be continued to be used in this phase. MA pellet was coated with one layer of NBR first then followed by second layer of PA coating blended with RGO. MA was used as PCM core to store latent heat; polymer coating was used as a shell to contain the PCM; RGO was used as light absorptive materials. RGO is proposed to be used in this phase because RGO is efficient in light absorption. RGO has large optical absorptivity, tunable bandgap and band-position (Mukhopadhyay and Gupta, 2012; Sadasivuni et al., 2015). Besides, a new in-house design setup for measuring solar conversion efficiency is presented. This work is carried out at outdoor setup to determine solar energy conversion efficiency and the total amount of stored heat energy. Then the chemical compatibility and thermal properties of FSCPCM with RGO (RGO-PANBR/MA) were characterized using DSC and FTIR, respectively. Thermal cycling test were also carried out to determine the thermal reliability of RGO-PANBR/MA pellet after 1000 melting and freezing cycles. Moreover, RGO-PANBR/MA pellets were also exposed to sunlight for weathering test.

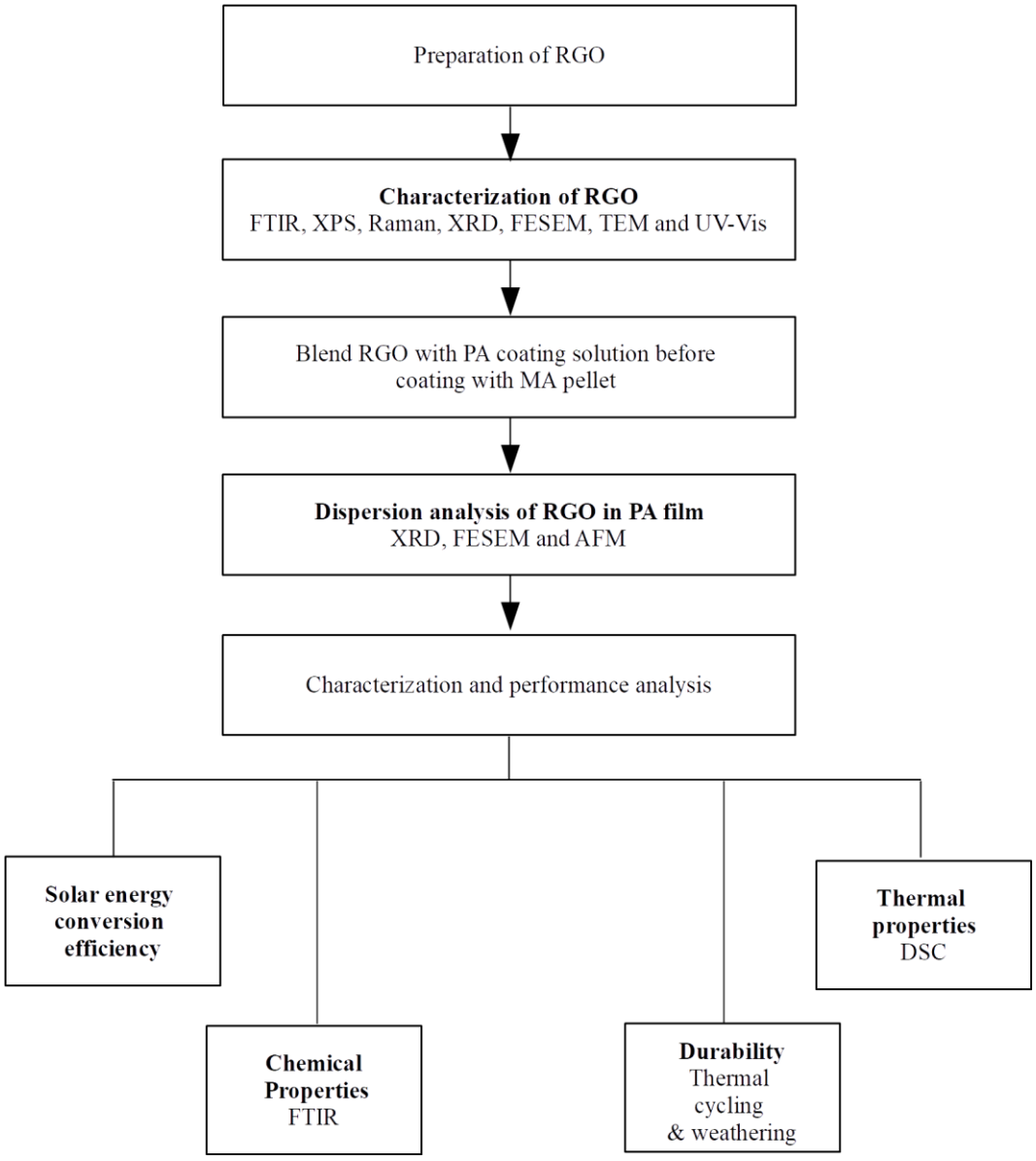

Figure 6.1: Work Flow of Phase 3 Experiment

6.2 Characterization of RGO

The chemical composition and morphology of GNF, GO and RGO were studied using following instruments such as FTIR, XPS, Raman spectroscopy, XRD, FESEM and TEM. These characterization analyses were carried out to confirm GO was reduced to RGO successfully. Characterisation analysis such as FTIR, XPS, Raman, XRD is to determine chemical structure of RGO. FESEM and TEM is to determine morphology of RGO. Besides, UV-Vis analysis is to determine light absorption properties of RGO.

6.2.1 Fourier Transform Infrared Spectroscopy (FTIR)

Figure 6.2 shows the FTIR spectra of GNF, GO and RGO. The peak of GNF at 1565 cm^{-1} corresponds to the C=C aromatic ring chain stretching. The FTIR spectrum of GO represents the characteristic peaks corresponding to the oxygen functionalities such as C=O stretching, C-O stretching and C-O bending vibration at 1723, 1256 and 1032 cm^{-1}, respectively (Deshmukh and Joshi, 2014). The peak at 3402 and 1386 cm^{-1} corresponds to hydroxyl groups (OH) and the broad range from 2500 to 3500 cm^{-1} confirms the presence of carboxylic group (COOH). The peak at 1623 cm^{-1} represents the unoxidized graphitic domain (C=C) (Shen et al.,

2013). The GO spectrum shows that the oxidation of GNF using Hummer's method was successful through the incorporation of oxygen functional group. The reduction of GO was proved by the FTIR spectrum of RGO where the peak intensity of all oxygen functionality group (C=O and C-O) was reduced significantly as shown in the square box in Figure 6.2. The peak at 3435 cm^{-1} in the FTIR spectrum of RGO represents the hydroxyl groups (OH) which indicates the incomplete reduction of GO (Konios et al., 2014).

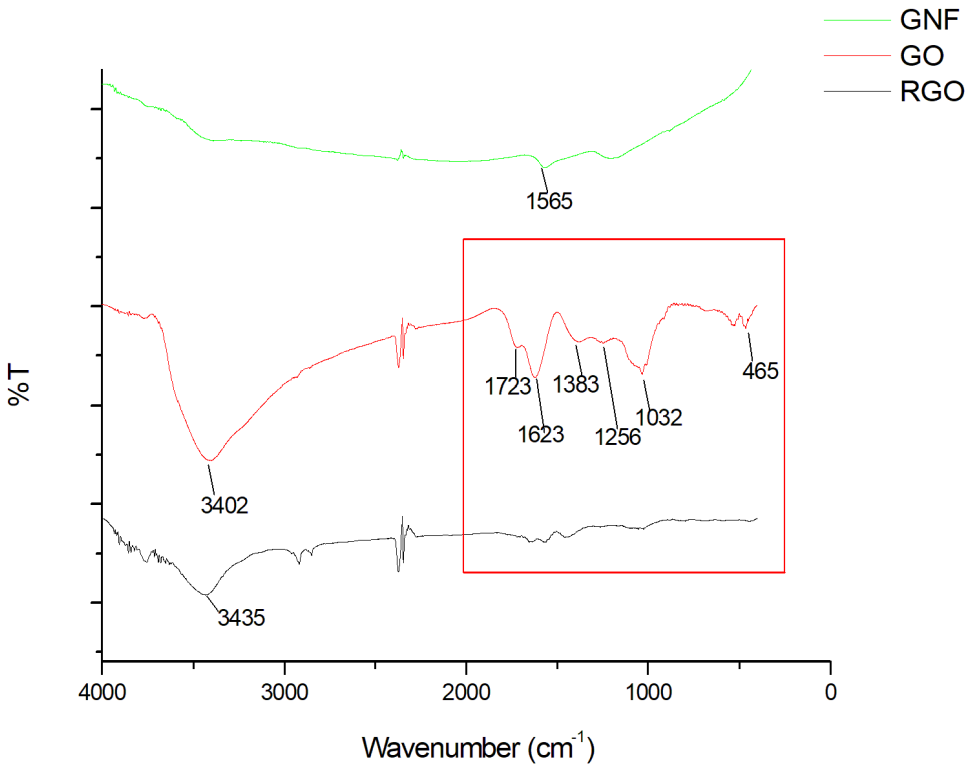

Figure 6.2: FTIR Spectra of GNF, GO and RGO

6.2.2 X-Ray Diffraction (XRD)

XRD patterns of GNF, GO and RGO are shown in Figure 6.3. The strongest peak of GNF was found at 2 theta degree (2θ) value of 26.3281° which represents the typical graphitic structure, similar to the XRD pattern of graphite found in other publications (Peng et al., 2013; Spyrou and Rudolf, 2014). The interlayer spacing of GNF was 3.382Å. By comparing the XRD patterns of GNF and GO, GO has less intense and broad-diffraction peak at the region of 9°-12°, corresponding to the increase in the interlayer spacing from 3.382Å in GNF to 7.110-9.732Å in GO. The results were similar to those obtained by previous works (Wang and Hu, 2011; Ashori et al., 2015). This is because oxygen functional groups were attached to both sides of the single graphene layer during its oxidation and enlarged the interlayer spacing (Lerf et al., 1998; Jeong et al., 2008; Szabó et al., 2006; Boukhvalov and Katsnelson, 2008). The results can be further supported by the FTIR spectra shown in Figure 6.2. Several oxygen functional group can be found on the FTIR spectrum due to the oxidation of GNF. Besides, RGO had very low intensity peak at 2θ value of 26.3867°. The interlayer spacing of RGO was 3.378Å. The decrease in interlayer spacing is due to the removal of oxygen during reduction process (Thema et al., 2012). Therefore, it confirms GO was reduced to RGO successfully.

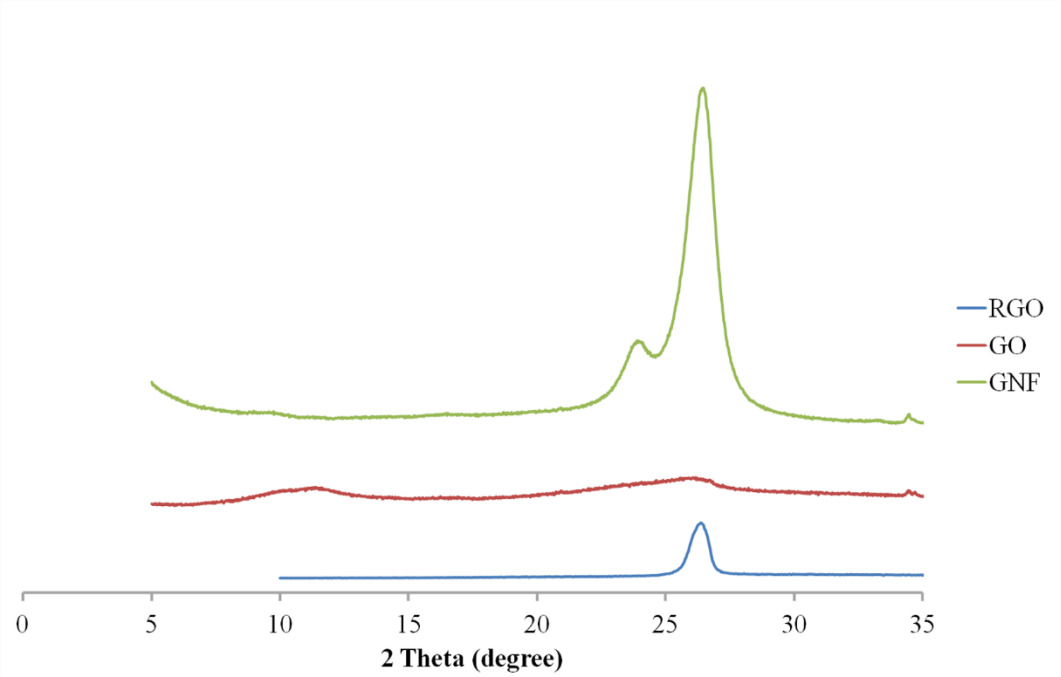

Figure 6.3: XRD Diffractogram of GNF, GO and RGO

6.2.3 X-ray Photoelectron Spectroscopy (XPS)

Figure 6.4 shows the core-level shift (Cls) XPS spectra of GO and RGO, respectively. In Figure 6.4 (a), it is clearly showed that GNF was oxidized to GO successfully. The Cls XPS spectrum of GO are represented by the characteristic peaks corresponding to carbon atom with different functional groups: the non-oxygenated ring C (C-C, 284.80 eV), ether C (C-O, 286.93 eV), carbonyl C (C=O, 288.55 eV) and carboxylate C (COOH, 291.01 eV) (Zhang et al., 2014). The Cls spectrum of RGO also exhibits these same oxygen functionalities. However, their peak intensities are much smaller than those in GO which indicates the reduction of

oxygen functional groups. There is also an additional peak at 285.79 eV corresponding to nitrogen bound to carbon atom (Yang et al., 2009). Therefore, the results indicated that the reduction of GO to RGO using hydrazine hydrate will incorporate nitrogen to the carbon atom (Ren et al., 2011).

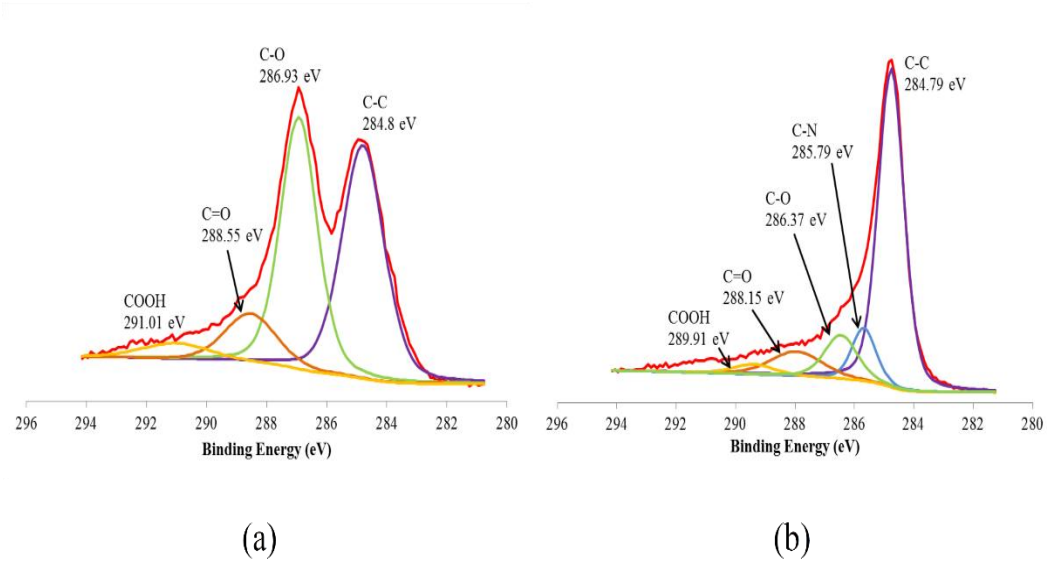

Figure 6.4: The C1s XPS Spectrum of (a) GO; (b) RGO

6.2.4 Raman Spectroscopy

Figure 6.5 shows that both the GO and RGO have strong G and D peaks, suggesting that they have very small crystal sizes (Childres et al., 2013). In the Raman spectrum of GO, the G and D bands are at 1597 cm^{-1} and 1353 cm^{-1}. The G band corresponds to the first-order scattering of the E2g mode while the D peak indicates the reduction in size of the in-plane sp^2 domain. This is due to the extensive oxidation and the attachment of hydroxyl and epoxide groups on the carbon basal

plane. The Raman spectrum of the RGO also contains both G and D bands at 1603 cm^{-1} and 1363 cm^{-1}, respectively). However, with an increased D/G intensity ratio compared to that in GO. This change suggests a decrease in the average size of the sp^2 domains upon reduction of the exfoliated GO, and can be explained if new graphitic domains were created that are smaller in size to the ones present in GO before reduction, but more numerous in number (Stankovich et al., 2007)

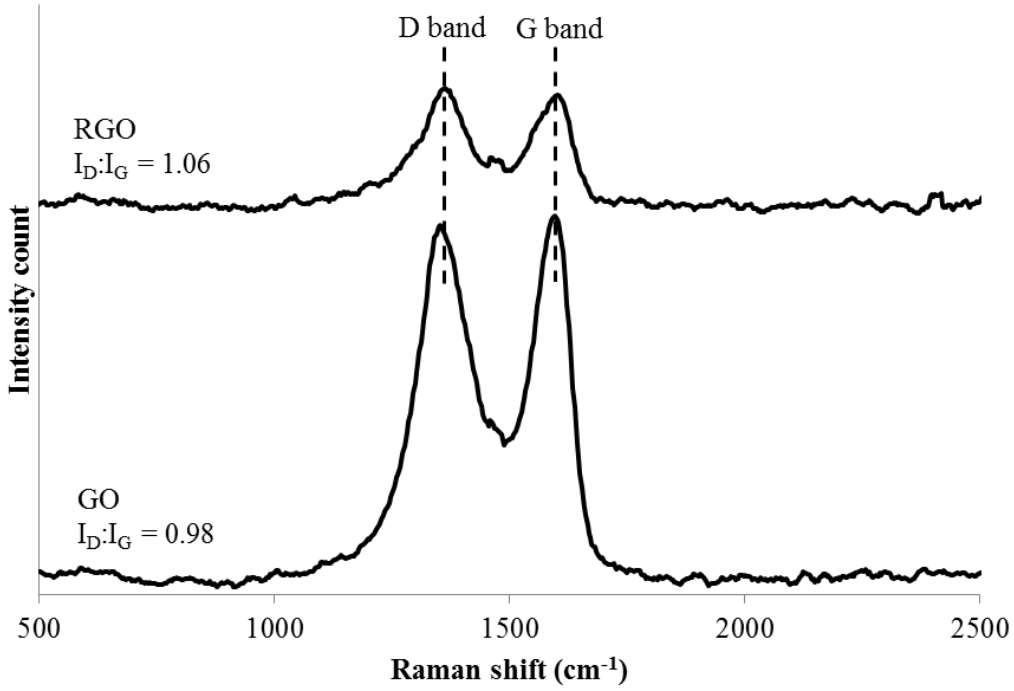

Figure 6.5: Raman Spectra of GO and RGO

6.2.5 Morphology Analysis: Field Emission Scanning Electron Microscopy (FESEM)

Figure 6.6 - Figure 6.8 show the FESEM image of GNF, GO and RGO at

20,000 times magnification, respectively. It can be seen that both GNF and GO possessed hair-like fiber structure. However, GO fiber structure was torn into smaller pieces and the surface was rougher as compared to GNF. This could be attributed by the oxygen-containing groups present on the surface of the graphitic layer. Figure 6.8 shows that RGO has different morphology where the surface is smooth and it is in layered form. This FESEM image confirm the RGO is in thin sheet structure.

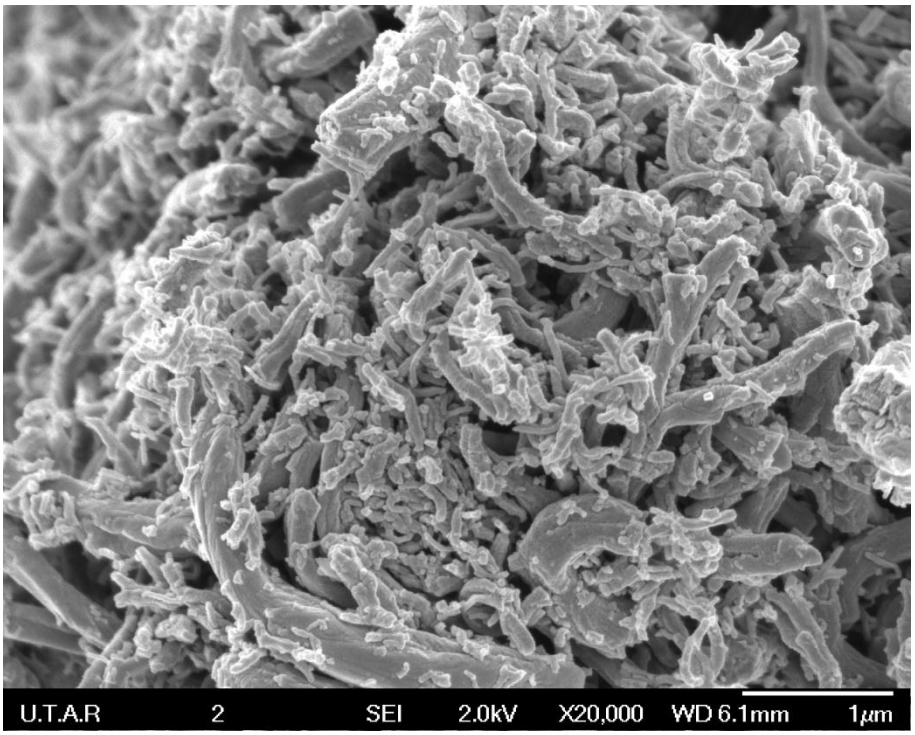

Figure 6.6: FESEM Image of GNF

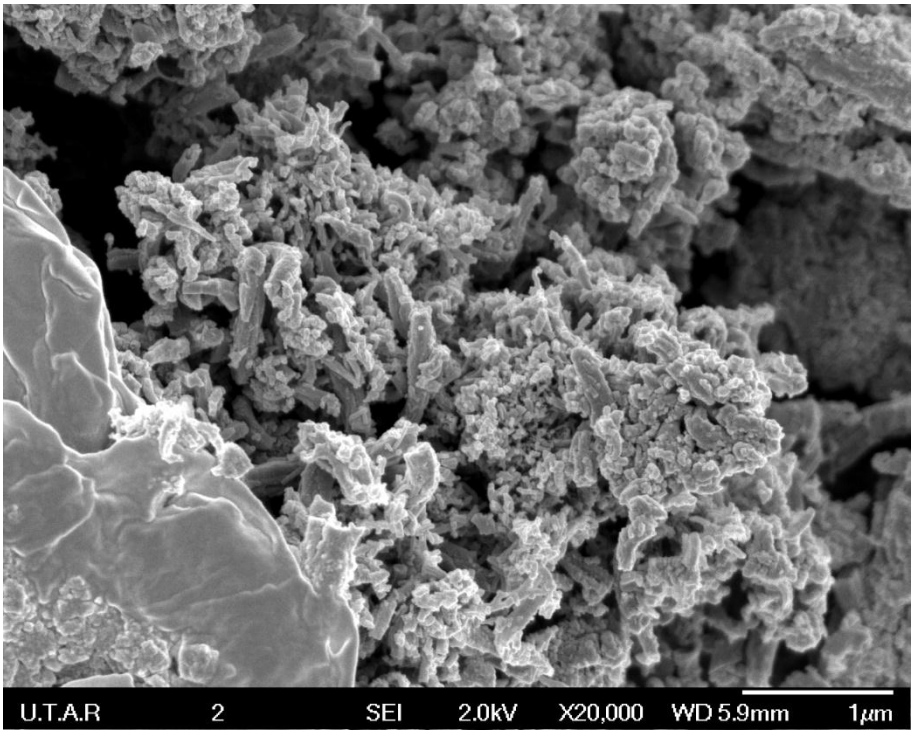

Figure 6.7: FESEM Image of GO

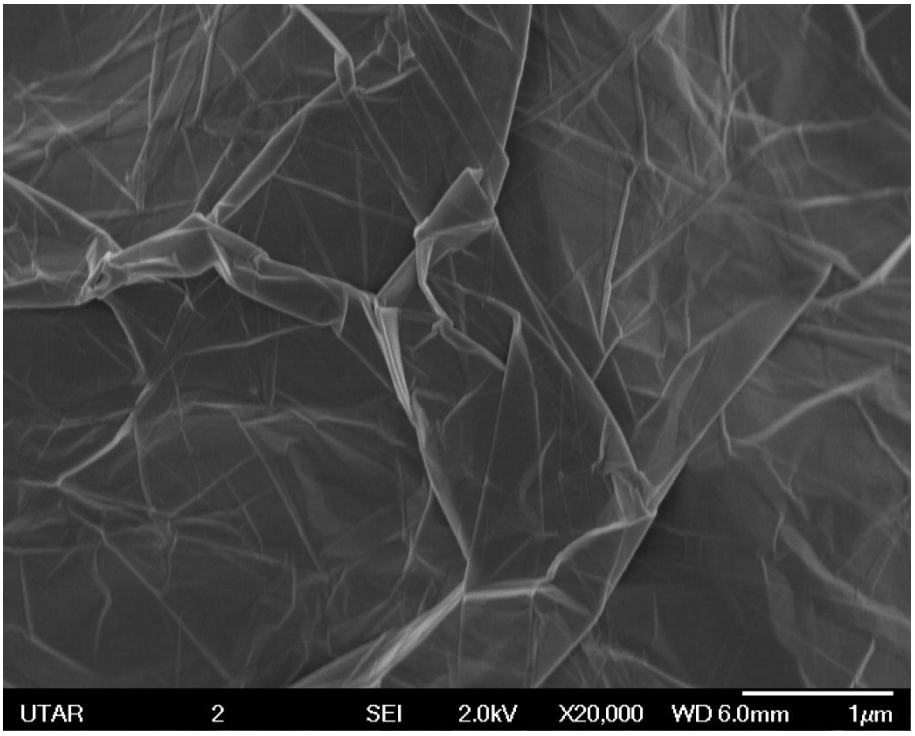

Figure 6.8: FESEM Image of RGO

6.2.6 Transmission Electron Microscopy (TEM)

Figure 6.9 shows the TEM image of RGO at 60,000 times magnification. TEM image further confirm that RGO is a smooth and thin layer of graphene sheets stacked together. The number of layers ranges from 2 to 4 by visual inspection, and the average length is found to be 738.5 ± 141.1 nm. This finding is important as RGO in thin sheet structure is expected to have larger surface area and higher light absorption.

Figure 6.9: Cross Section TEM Image of RGO

6.2.7 UV-Visible Absorption Analysis

Figure 6.10 shows the absorption peak of RGO in aqueous dispersion which was at 255.10 nm but it still absorbed significant amount of visible light. The absorption peak around 260 nm was generally regarded as the excitation of p-plasmon of graphitic structure (Wang et al., 2008b). This finding indicated that RGO is able to absorb UV and visible light. Therefore, RGO is suitable to be used as light absorption material to absorb sunlight and convert it to thermal energy.

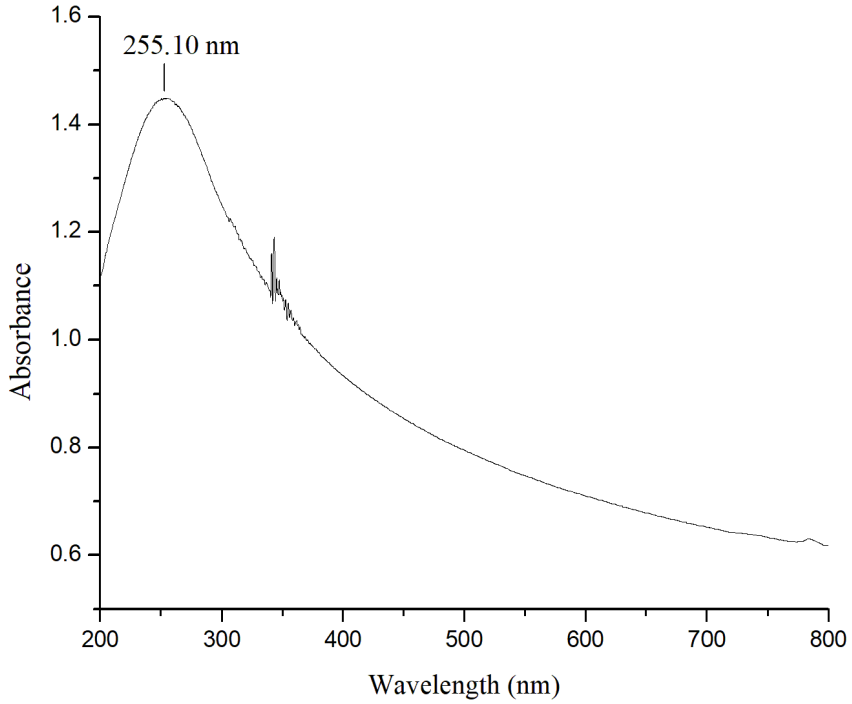

Figure 6.10: UV-Visible Spectrum of RGO Disperse in Water

6.3 Dispersion Analysis of RGO in PA film

The dispersion of various loading of RGO in PA film was studied using XRD and FESEM and AFM.

6.3.1 X-ray Powder Diffraction (XRD)

XRD diffractogram of RGO and PA at various RGO loading is shown in Figure 6.11. The XRD pattern for pure PA showed no diffraction peaks which indicated amorphous nature of PA (Flora et al., 2012). While RGO had a peak at 2θ value of 26.3867°, indicating RGO nanosheets had packed into an ordered structure. PA with 0.5 wt%, 1.0 wt% and 1.5 wt% of RGO loading had a small peak at 2θ value of 26°. Large reduction of RGO characteristic peaks in PA at 0.5, 1.0 and 1.5 wt% loading could be observed. Another broad and less intense peak could be observed at 2θ value of 23 -15˚ for all the three samples. This indicates an expansion of interlayer spacing of RGO from 2.05 Å to 4.50 Å. Thus RGO is more likely to be intercalated inside the PA matrix rather than exfoliated. The regular and ordered structure of RGO layers had been expanded with insertion of polymeric chains (Liang et al., 2009).

PA with 2.0 wt% RGO loading had an intense peak at 2θ value of 26.25052°, indicating that the RGO was not well dispersed. Similar results were obtained for polymer nanocomposites incorporated with other multilayer nanofillers such as clay at high loading (Liu et al., 2003). PA with 2.0 wt% of RGO also contain smaller amount of RGO exhibit larger interlayer spacing at 2θ value of 23.6329°. This indicates the formation of intercalated structure of RGO in PA at certain extend.

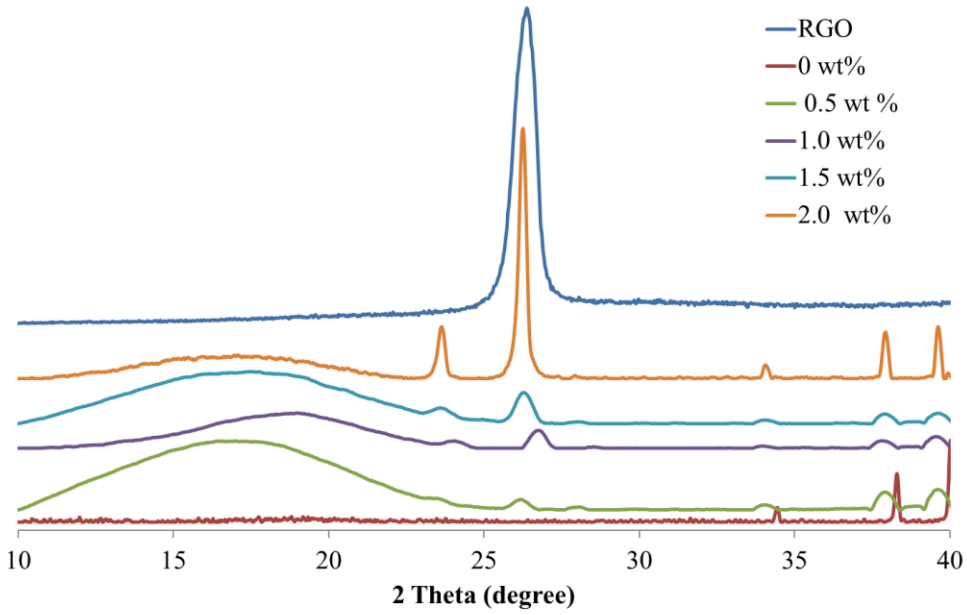

Figure 6.11: XRD Diffractogram of RGO and PA at Various RGO Loading

6.3.2 Field Emission Scanning Microscopy (FESEM)

Cross section FESEM images of PA at 1.5 wt% and 2.0 wt% RGO loading are shown in Figure 6.12 (a) and (b), respectively. Apparently, PA with 2.0 wt% RGO loading has more agglomerated multi-layer RGO if compared to PA with 1.5 wt% RGO, as indicated by the darker image of multilayer RGO. This indicated that 2.0 wt% RGO is not well dispersed in PA and formed agglomerates. This images further support the results obtained from XRD diffractogram where the 2Θ value peak for 2.0 wt% RGO filled PA was similar as the 2Θ value peak for original RGO.

Agglomeration of RGO will reduce the effective surface area for sun light absorption.

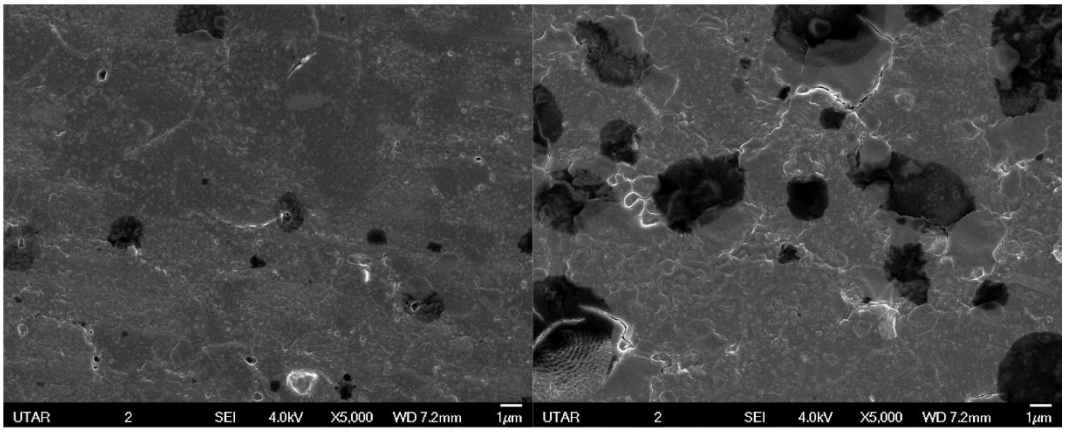

(a) (b)

Figure 6.12: Cross Section FESEM Images of PA at Various RGO Loading. (a) 1.5 wt% RGO Loading. (b) 2.0 wt% RGO Loading

6.3.3 Atomic Force Microscope (AFM)

AFM images of PA at 1.5 wt% and 2.0 wt% RGO loading are shown in Figure 6.13 (a) and (b), respectively. The roughness values for PA at 1.5 wt% and 2.0 wt% RGO are 18.60 nm and 76.80 nm, respectively. PA with 2.0 wt% RGO loading has rougher surface if compared to PA with 1.5 wt% RGO. This indicated that PA with 2.0 wt% RGO loading is not well dispersed and has more aggregate number of multi-layer RGO.

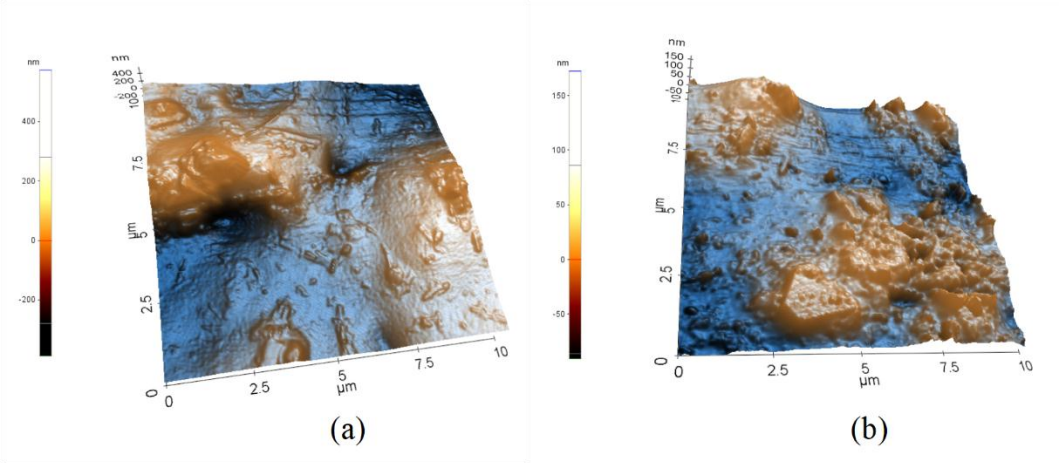

Figure 6.13: AFM Images of PA at Various RGO Loading. (a) 1.5 wt% RGO Loading. (b) 2.0 wt% RGO Loading

6.4 Characterization and Performance Analysis of Light Absorptive Polymeric Form Stable Composite PCM

Characterization and performance analysis of light absorptive polymeric FSCPCM can be studied via solar energy conversion efficiency, FTIR analysis, DSC and reliability analysis.

6.4.1 Solar Energy Conversion Efficiency

To verify the light absorption of RGO, PCM samples with different RGO loading were placed under sunlight. The outdoor environment measurement setup is shown in Figure 3.12. Compared with pure PANBR/MA pellet (0.0 wt% RGO), the temperature of all RGO-PANBR/MA pellet rapidly increased upon sunlight

irradiation. This is because RGO in PANBR coating absorb sunlight and transform it into heat through non-radiation thermal decay. Similar finding was reported by Tang et al. (2016) who used dye as light absorptive material on PCM. Figure 6.12 shows that 1.5 wt% RGO-PANBR/MA pellet had higher temperature (61.1 °C) than pure PANBR/MA pellet (55.2 °C) after exposing to sunlight for 8000 seconds. An increment of 10.69% in temperature was recorded.

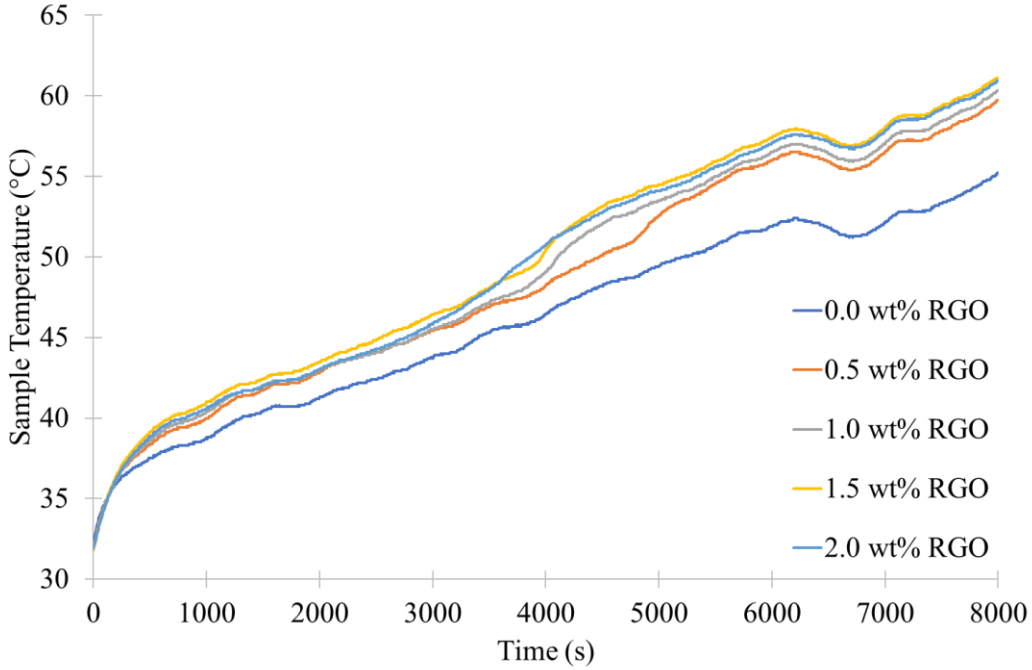

Figure 6.12: Temperature of RGO-PANBR/MA Pellets with Various Loading after Exposing to Sunlight for 8000 seconds

The total heat energy stored in RGO-PANBR/MA pellet with different RGO loading is shown in Figure 6.13. The total stored heat energy is calculated by Eq. (3.9) in section 3.10.2 over the period of 3 sunny days. The RGO-PANBR/MA pellet

with 1.5 wt% RGO loading stored the highest amount of heat energy among the pellets: 49 wt% higher than the PANBR/MA pellet without RGO. The total stored heat energy was lower when the RGO loading is further increased to 2.0 wt%. This is because RGO is agglomerate at 2.0 wt% loading and thus reduce the effective surface area for sunlight absorption.

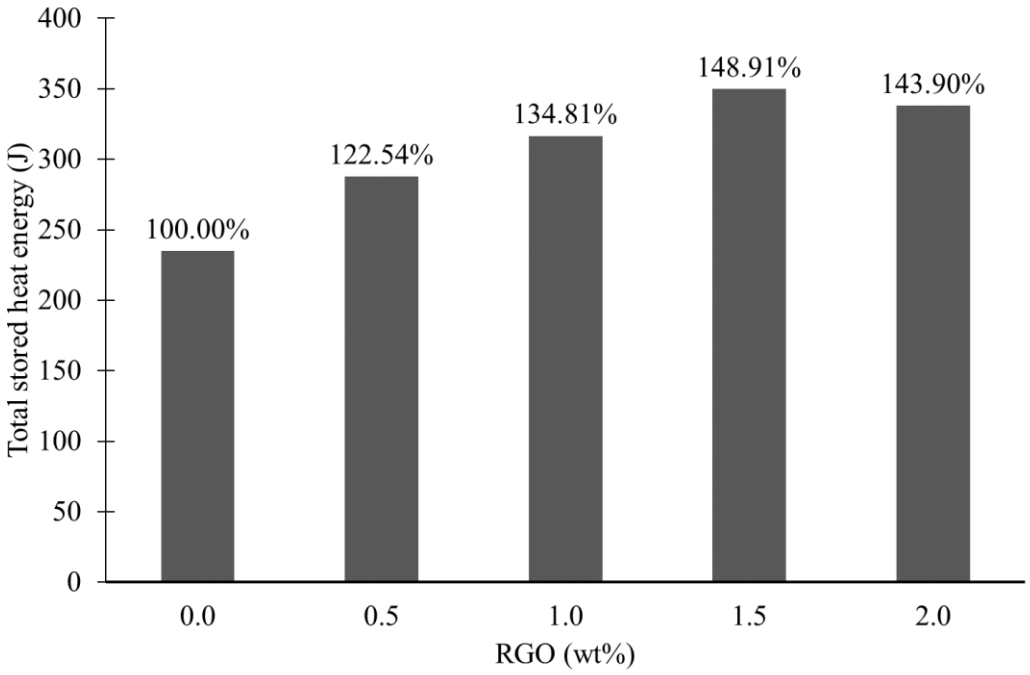

Figure 6.13: Total Stored Heat Energy in RGO-PANBR/MA Pellets with Various Loading

Solar energy conversion efficiency calculated by Eq. (3.14) in section 3.10.2 for RGO-PANBR/MA pellets with different loading is shown in Figure 6.14. The efficiency is dependent on the solar energy absorbed by the top surface as well as

heat loss to the environment which is mainly affected by the difference between the pellet temperature and the temperature inside the PMMA container. All pellets absorb the same amount of solar energy on their top surfaces. However, the heat loss is the same at the beginning of the experiment on each day, but the hotter pellets has significantly higher heat losses than the colder pellets after a short period of time. Therefore, to make a fair comparison of the solar energy conversion efficiency of all the pellets, only the results from the first 20 minutes are used in the calculation when the temperature difference is less than 5°C. The result shows that the 1.5 wt% RGO-PANBR/MA pellet had the highest solar energy conversion efficiency which was 21%. This is because 1.5 wt% RGO-PANBR/MA has the highest loading of RGO before RGO start to aggregate.

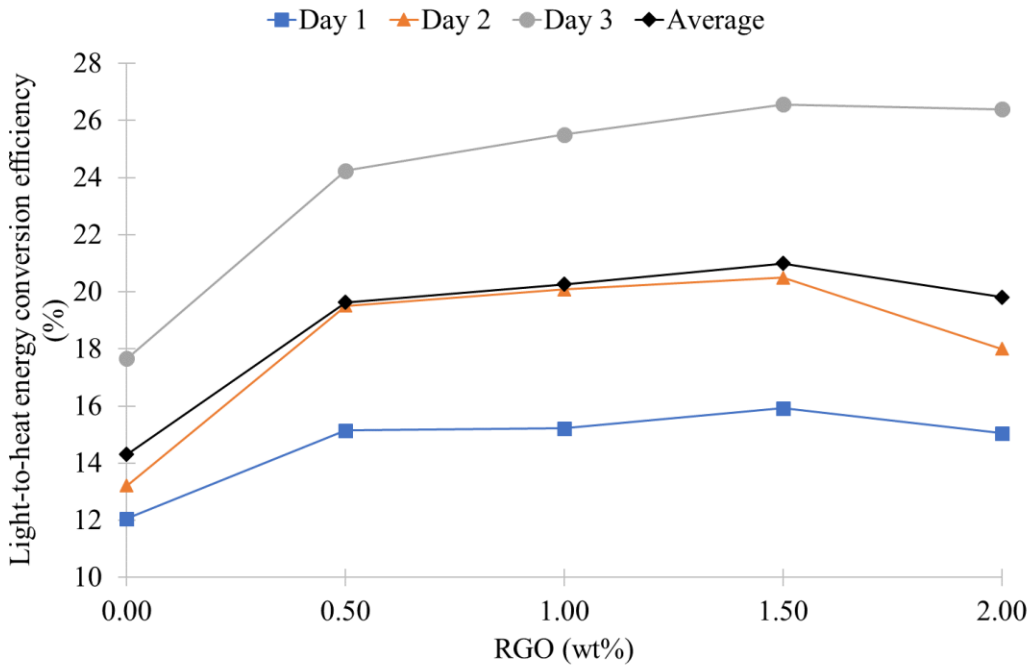

Figure 6.14: Solar Energy Conversion Efficiency of RGO-PANBR/MA Pellets with Various Loading

6.4.2 Chemical Properties: Fourier Transform Infrared Spectroscopy (FTIR)

Figure 6.15 shows the FTIR spectra of RGO, PANBR/MA pellet and 1.5 wt% RGO-PANBR/MA pellet. As can be seen, 1.5 wt% RGO-PANBR/MA pellet had broader and more intense peak at 3435 cm^{-1} due to the presence of hydroxyl group in the RGO as compared to the neat PANBR/MA pellet without RGO. In addition,

interaction of PMMA and RGO does not involve chemical reaction because no new functional group was found. Therefore, it can be concluded that the blending of RGO with PA is physical blending. Besides, FTIR result also shows that the MA pellet was well coated with coating because only polymer coating's functional group was detected after coating.

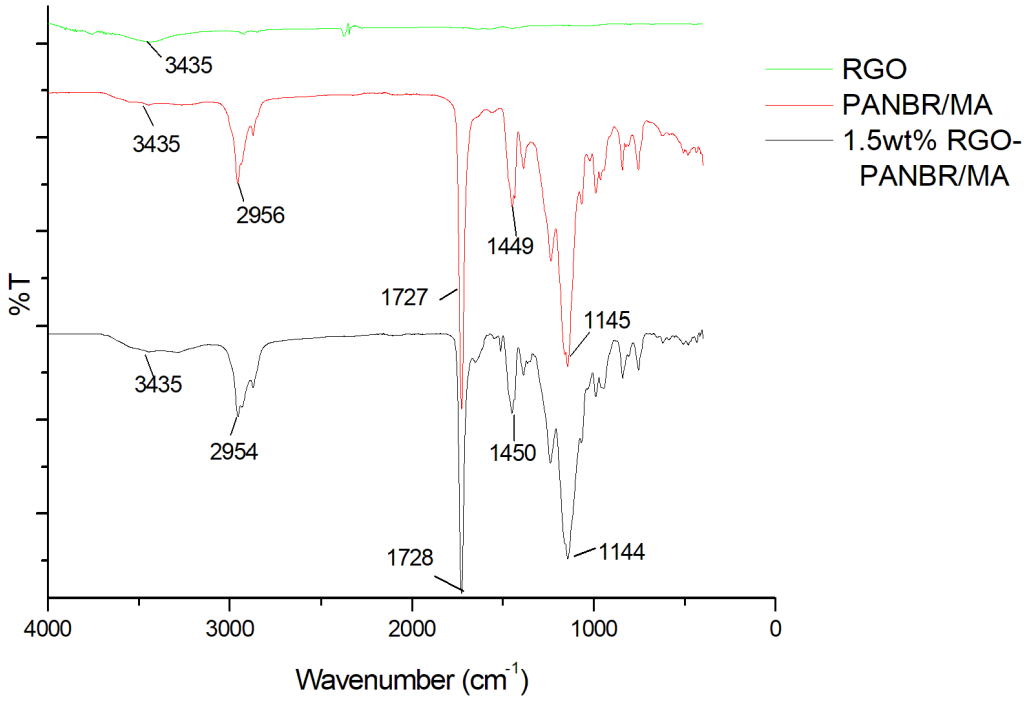

Figure 6.15: FTIR Spectra of RGO, PANBR/MA Pellet and 1.5 wt% RGO-PANBR/MA Pellet

6.4.3 Thermal Properties: Differential Scanning Calorimetry (DSC)

Thermal properties of PANBR/MA pellet at different RGO loading were studied using DSC. The melting point, freezing point, latent heat of melting and freezing are shown in Table 6.1 and Figure 6.16. When compared to phase change temperatures of the PANBR/MA pellet at different RGO loading with pure MA pellet, the changes in melting point was -1.25, -0.77, -1.32, -1.18, and -1.04 °C and the changes in freezing point was -1.16, -0.30, -0.54, -0.34, and -0.64 °C for PANBR/MA pellet, 0.5 wt% RGO-PANBR/MA pellet, 1.0 wt% RGO-PANBR/MA pellet, 1.5 wt% RGO-PANBR/MA pellet and 2.0 wt% RGO-PANBR/MA pellet, respectively. These small changes indicated that coatings and RGO did not significantly affect the melting and freezing point of pure MA. However, RGO-PARB/MA pellet had lower latent heat of melting and freezing than pure MA pellet. This is because RGO and coating material reduced mass percentage of MA which contribute to latent heat (Alkan and Sari, 2008).

Table 6.1: Thermal Properties of RGO-PARB/MA Pellets in Various RGO Loadings

PCM	RGO (wt%)	Coating (wt%)	PCM (wt%)	Melting Point (ºC)	Latent heat of melting (J/g)	Freezing Point (ºC)	Latent heat of freezing (J/g)
MA pellet	0	0	100.00	55.97±0.12	216.04±4.72	52.72±0.27	216.85±4.54
PARB/MA	0	37.78	62.22	54.72±0.27	131.84±5.76	51.56±0.58	130.97±7.40
0.5wt% RGO-PARB/MA	0.5	40.12	59.88	55.20±0.10	118.72±4.89	52.42±0.15	117.91±5.19
1.0wt% RGO-PARB/MA	1.0	39.79	60.21	54.65±0.13	121.02±5.06	52.18±0.20	120.76±5.07
1.5wt% RGO-PARB/MA	**1.5**	**39.83**	**60.17**	**54.79±0.07**	**119.91±6.67**	**52.38±0.24**	**119.66±6.60**
2.0wt% RGO-PARB/MA	2.0	39.23	60.77	54.93±0.19	121.05±6.19	52.08±0.06	121.13±6.49

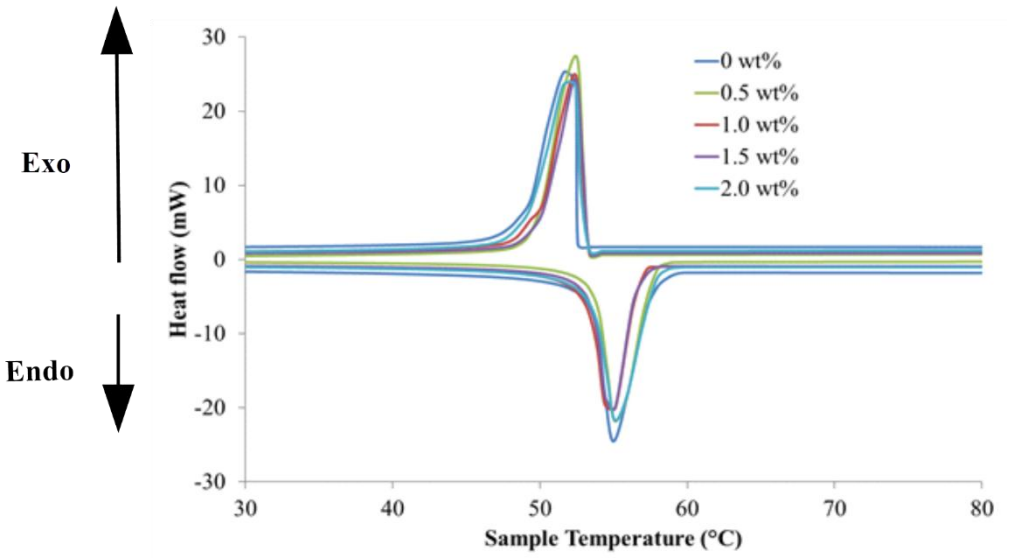

Figure 6.16: DSC Curves of PANBR/MA Pellet with Different RGO Loadings

1.5 wt% RGO-PANBR/MA pellet had the highest solar energy conversion efficiency and the amount of stored heat energy were marked bold in Table 6.1. The latent heat obtained from present work is comparable with other works done by other researchers as shown in Table 6.2. Therefore, it is ideal to be used as light absorptive PCM.

Table 6.2: Comparison Survey of Thermal Performance for Light Absorptive PCM

No	PCM/ PCM Composite	Light Absorptive Materials	Melting Point (°C)	Latent Heat of Melting (J/g)	References

1	Methoxypolyethylene glycol (MPEG-750) + polyethylene polyamine	Yellow dye	32.70	103.70	(Wang et al., 2012c)
2	PEG 6000	1,4-bis((2-hydroxyethyl) amino) anthracene-9,10-dione dye	54.80	78.70	(Wang et al., 2012d)
3	PEG + silicon dioxide (SiO_2)	Titanium black (Ti_4O_7)	59.8	129.80	(Tang et al., 2017a)
4	MA + PANBR coating	RGO	54.79± 0.07	119.91 ± 6.67	Present study

6.4.4 Durability

Durability of RGO-PANBR/MA pellet was examined under thermal cycling and weathering test.

6.4.4.1 Durability: Thermal cycling

For thermal reliability, the thermal properties of 1.5 wt% RGO-PANBR/MA pellet after 1000 times repeated thermal cycling were analyzed by DSC as shown in Figure 6.17. The DSC curve shape for 1.5 wt% RGO-PANBR/MA pellet did not change much after 1000 thermal cycles. Table 6.3 shows that the variances in melting temperature, freezing temperatures, latent

heat of melting and freezing for 1.5 wt% RGO-PANBR/MA pellet before and after thermal cycling were small and less than 2 %. Therefore, it can be concluded that 1.5 wt% RGO-PANBR/MA pellet had good thermal reliability and it can be used for 1000 days (about 2.7 years) without any changes in performance, assuming that it undergoes 1 thermal cycle per day.

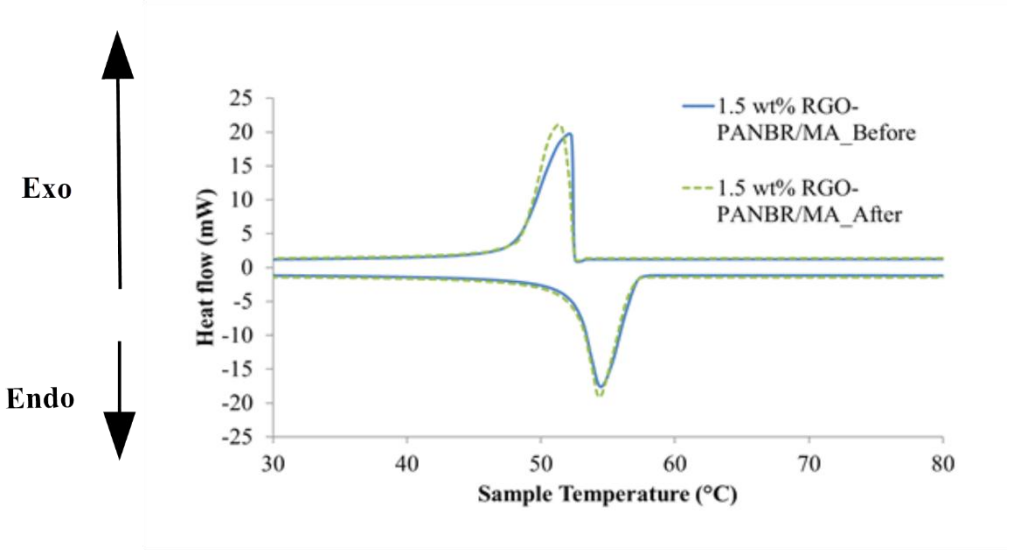

Figure 6.17: DSC Curves of RGO-PANBR/MA Pellet before and after 1000 Thermal Cycling

Table 6.3: DSC Results of RGO-PANBR/MA Pellet before and after 1000 Thermal Cycling

	Melting Point (°C)	Latent heat of melting (J/g)	Freezing Point (°C)	Latent heat of freezing (J/g)
Before	54.44	122.97	51.98	123.78
After	54.31	121.69	51.48	122.28
Changes percentage (%)	0.24	1.04	0.96	1.21

6.4.4.2 Durability: Weathering

Weathering test is carried out for a duration of 30 days to the reliability of 1.5wt% RGO-PANBR/MA pellet at actual outdoor environment.Thermal reliability of 1.5wt% RGO-PANBR/MA pellet can be determined by calculating mass loss percentage of sample through weathering test. The mass of PCM determine the latent heat and thermal storage performance of PCM. Therefore, a good TES material must has small mass loss percentage to maintain its high TES performance in practical outdoor application. The mass loss percentage of 1.5 wt% RGO-PANBR/MA pellet can be calculated by Eq. (6.1).

$$M_{loss}\,(\%) = \frac{M_{AW} - M_{BW}}{M_{BW}} \times 100\% \tag{6.1}$$

Where,

M_{loss} = mass loss percentage (%)

M_{AW} = mass pellet after weathering

M_{BW} = mass pellet before weathering

The mass loss percentage of 1.5wt% RGO-PANBR/MA pellet after weathering test was only 2.1%. It is considered as acceptable as the mass loss percentage did not exceed the maximum value of 5% (Huang et al., 2013). It also

indicates t no leakage of PCM during phase change process when exposed to actual outdoor environment.

Besides, the changes in chemical functional groups of 1.5wt% RGO-PANBR/MA pellet can be measured using FTIR spectroscopy to determine the effect of natural environmental factors on chemical structure of polymer coating film. Figure 6.18 shows no significant peak shifting after weathering test. However, minor changes in the peak intensities were found, indicating minor chemical changes in the polymer coating upon UV irradiation. The peaks at 2876-2954 cm^{-1} (C-H stretching), 1727cm^{-1} (C=O stretching), 1449 cm^{-1} (C-H bending) and 1142 cm^{-1} (C-O-C stretching) were slightly reduced. The reduction of C=O peak is associated to the photo destruction of π bond in C=O (Shanti et al., 2017). The decrease C-O-C and C-H peak are might due to side chain scission of ester group and chain scission, respectively (Torikai et al., 1990; Yang et al., 2001). The increase in intensity of the peak at 3442 cm^{-1} (OH stretching) might due to moisture absorption by the samples.

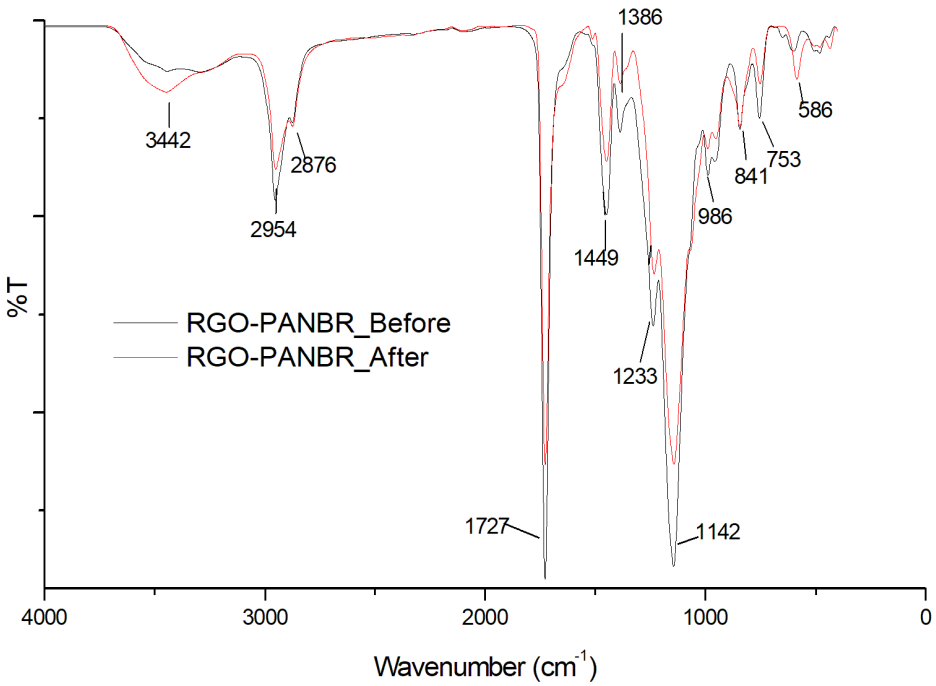

Figure 6.18: FTIR spectra of 1.5 wt% RGO-PANBR before and after weathering test

6.5 Summary

Light absorptive polymeric FSCPCM (RGO-PANBR/MA pellet) was developed in this phase. Characterization test of RGO and performance analysis of RGO-PANBR/MA pellet are summarized in Table 6.4. FTIR, XRD, XPS, and Raman tests confirmed the chemical structure of RGO as all oxygen functional groups were reduced. UV-Visible absorption analysis showed that absorption peak of RGO in aqueous dispersion was at 255.10 nm but it still absorbed significant amount of visible light. Among all samples, 1.5 wt% RGO-PANBR/MA pellet had the highest amount of stored heat energy which was

48.91% higher than pure sample. The solar energy conversion efficiency of 1.5 wt% RGO-PANBR/MA pellet was 21%. XRD, FESEM and AFM results also showed that 1.5 wt% of RGO well dispersed in PA coating film. For thermal performance, melting temperature and latent heat of PANBR/MA pellet were recorded at 54.79±0.07 ºC and 119.91±6.67 J/g, respectively. 1.5 wt% RGO-PANBR/MA pellet were thermal reliable as the changes of melting and freezing latent heat after 1000 thermal cycling was less than 2 %. Moreover, 1.5 wt% RGO-PANBR/MA pellet also stable under exposure to natural environment as the mass loss percentage was only 2.1% after 30 days weathering test. FTIR spectra also showed that RGO-PANBR film only had minor changes of peak intensity after weathering test.

Table 6.4: Summary of the Outcome of the Characterization Tests

No	Characterization Tests	Outcome
1.	FTIR, XRD, XPS, and Raman	Confirm the reduction of GO to RGO.
2.	FESEM and TEM	RGO is in thin layer with high surface area.
3.	UV-Visible	Peak absorption of RGO was observed at 255.10 nm but it still absorbed significant amount of visible light.
4.	XRD, FESEM and AFM	0.5, 1.0 and 1.5 wt% of RGO intercalated in PA. 2.0 wt% of RGO was not well dispersed and maintain the original ordered structure RGO with little intercalation.

5	Solar Energy Conversion Efficiency	1.5 wt% RGO-PANBR/MA pellet had the highest amount of stored heat energy which was 48.91% higher than pure sample. The solar energy conversion efficiency of 1.5 wt% RGO-PANBR/MA pellet was 21%.
6	FTIR	Blending of PA and RGO is physical method as no new functional group was found.
7	DSC	Latent heat of 1.5 wt% RGO-PANBR/MA pellet was 119.91±6.67 J/g.
8	Thermal cycling	1.5 wt% RGO-PANBR/MA pellet was thermal reliable as the changes in melting and freezing latent heat after 1000 thermal cycling was less than 2 %.
9	Weathering test	1.5 wt% RGO-PANBR/MA pellet was stable under natural environment as the mass loss percentage was only 2.1% after 30 days weathering test. FTIR also showed that RGO-PANBR film only had minor changes of peak intensity after weathering test

Based on the results above, the objective of this phase was achieved as RGO is able to absorb sunlight and convert it to heat energy. The optimum RGO loading for RGO-PARB/MA pellet was 1.5 wt% because it had the highest amount of stored heat energy and solar energy conversion efficiency. Therefore, 1.5 wt% RGO-PANBR/MA pellet has the potential to be used as light absorptive polymeric form stable composite PCM.

CHAPTER 7

CONCLUSION & FUTURE WORK

7.1 Conclusions

In conclusion, light absorptive polymeric FSCPCM was developed successfully using blending and dip coating method. The main experiment works can be divided into 3 phases:

I. Apply PA and conformal coating on composite PCM (MA/PMMA) to determine which coating can be used to prevent leakage.
II. Develop the best polymer coating combination and applied directly on MA pellet without PMMA supporting material to maximize latent heat.
III. Synthesis and blend RGO into FSCPCM to improve light absorption.

A series of experiments were done in phase 1 to produce FSCPCM using new coating materials such as conformal coating and PA. Leakage test indicated that these two polymeric coating can be used to prevent and minimize the leakage. The PA coating performs better compared to conformal coating as no leakage was found on composite PCM (MA:PMMA, 60:40 wt%) with PA coating compared to those with conformal coating whose leakage area was 1.74 cm^2 under the same weight percentage of MA/ PMMA. This result was supported by tensile result as PA had 144.64%, 196.76% and 137.56% higher E-

modulus, tensile strength and elongation at break (%), respectively compared to the conformal coating. Among all leakage-free FSCPCM, composite PCMs (MA/PMMA, 60/40 wt %) with PA coating had the highest melting latent heat (91.42±7.22 J/g). However, the latent heat is reduced about 57.61% if compared to pure MA (215.65±4.69 J/g). This is due to the addition of supporting material and coating material which reduced the mass percentage of MA which contribute to the latent heat.

In phase 2, different polymer coating combination of PA and NBR was directly applied on MA pellet without PMMA supporting material to maximize latent heat. Among all samples, PANBR/MA pellet with the combination of NBR (inner layer) and PA (outer layer) was thermally stable as no leakage was found after heating in oven for 24 hours. This is because NBR as inner layer of coating was elastic and able to withstand the volume change of MA inside the core, while PA as outer layer of coating was able to provide good structure to hold the MA from deforming. Moreover, PANBR/MA pellet was thermally reliable as the changes of melting and freezing latent heat after 1000 thermal cycling was less than 2 %. DSC results also showed that the latent heat of PANBR/MA pellet (131.84 ±5.76 J/g) was 30.66% higher than composite PCM (MA/PMMA, 60/40 wt %) with PA coating (91.42±7.22 J/g) produced in phase 1. Therefore, it can be concluded that PANBR/MA pellet is a new polymeric coating FSCPCM which has high latent heat, thermal stability and reliability.

In phase 3, PANBR/MA pellet is blended with RGO to improve light absorption. UV-Visible absorption analysis showed that absorption peak of RGO in aqueous dispersion was at 255.10 nm but it still absorbed significant amount of visible light. Among all samples, 1.5 wt% RGO-PANBR/MA pellet had the highest amount of stored heat energy which was 48.91% higher than pure sample. The solar energy conversion efficiency of 1.5 wt% RGO-PANBR/MA pellet was 21%. For thermal performance, melting temperature and latent heat of 1.5 wt% RGO-PANBR/MA pellet were recorded at 54.79±0.07 ºC and 119.91±6.67 J/g, respectively. 1.5 wt% RGO-PANBR/MA pellet were thermally reliable as the changes of melting and freezing latent heat after 1000 thermal cycling was less than 2 %. Moreover, 1.5 wt% RGO-PANBR/MA pellet is also stable under exposure to natural environment as the mass loss percentage was only 2.1% after 30 days weathering test. FTIR spectra also showed that RGO-PANBR film only had minor changes in peak intensity after weathering test.

As a conclusion, 1.5 wt% RGO-PANBR/MA pellet was formed as a new light absorptive polymeric FSCPCM which is thermally stable and able to convert light to heat energy. This novel light absorptive polymeric FSCPCM is suitable to be used as TES in solar heating application, solar green house and green building.

7.2 Future Work

The focus of the future work in this research is the enhancement of latent heat of light absorptive polymeric FSCPCM. Therefore, future research can be carried out to improve mechanical properties of polymeric coating film by adding crosslinking agent. Crosslink polymeric coating film is expected to have higher tensile and elasticity to withstand the volume change of MA. Therefore, this strong and elastic film will reduce the mass percentage of coating materials and hence it can maintain high latent heat with elimination of leakage and reduction of volume expansion.

Besides, practical application of this light absorptive polymeric FSCPCM has not been studied in this research yet. Therefore, future research can be carried out by applying it in solar water heater tank or PV cooling to test its thermal performance. Optimization work for improving performance efficiency of this light absorptive polymeric FSCPCM in practical application will be carried out also.

REFERENCES

Abdelrazek, E.M., Hezma, A.M., El-khodary, A. and Elzayat, A.M., 2016. Spectroscopic studies and thermal properties of PCL/PMMA biopolymer blend. *Egyptian Journal of Basic and Applied Sciences*, 3(1), pp.10–15.

Agyenim, F., Hewitt, N., Eames, P. and Smyth, M., 2010. A review of materials, heat transfer and phase change problem formulation for latent heat thermal energy storage systems (LHTESS). *Renewable and Sustainable Energy Reviews*, 14(2), pp.615–628.

Akgün, M., Aydın, O. and Kaygusuz, K., 2007. Experimental study on melting/solidification characteristics of a paraffin as PCM. *Energy Conversion and Management*, 48(2), pp.669–678.

Alkan, C., Günther, E., Hiebler, S. and Himpel, M., 2012. Complexing blends of polyacrylic acid-polyethylene glycol and poly(ethylene-co-acrylic acid)-polyethylene glycol as shape stabilized phase change materials. *Energy Conversion and Management*, 64, pp.364–370.

Alkan, C. and Sari, A., 2008. Fatty acid/poly(methyl methacrylate) (PMMA) blends as form-stable phase change materials for latent heat thermal energy storage. *Solar Energy*, 82(2), pp.118–124.

Aly, R.O., 2016. Influence of gamma irradiation on mechanical and thermal properties of waste polyethylene/nitrile butadiene rubber blend. *Arabian Journal of Chemistry*, 9, pp.S1547–S1554.

Amarnath, C.A. et al., 2011. Efficient synthesis of graphene sheets using pyrrole as a reducing agent. *Carbon*, 49(11), pp.3497–3502.

de Andres, P.L., Ramírez, R. and Vergés, J.A., 2008. Strong covalent bonding between two graphene layers. *Physical Review B*, 77(4), p.045403.

Ashori, A., Rahmani, H. and Bahrami, R., 2015. Preparation and characterization of functionalized graphene oxide/carbon fiber/epoxy nanocomposites. *Polymer Testing*, 48, pp.82–88.

Bablich, A., Kataria, S. and Lemme, M.C., 2016. Graphene and Two-Dimensional Materials for Optoelectronic Applications. *Electronics*, 5(1), p.13.

Baetens, R., Jelle, B.P. and Gustavsen, A., 2010. Phase change materials for building applications: A state-of-the-art review. *Energy and Buildings*, 42(9), pp.1361–1368.

Bhuyan, M.S.A., Uddin, M.N., Islam, M.M., Bipasha, F.A. and Hossain, S.S., 2016. Synthesis of graphene. *International Nano Letters*, 6(2), pp.65–83.

Board, N., 2013. *Handbook on Rubber and Allied Products (with Project Profiles) (Photostate Edition)*, Niir Project Consultancy Services.

Bond, T. and Hughes, C., 2013. *O-level Physics Critical Guide (Concise) (Yellowreef)*, Yellowreef Limited.

Borreguero, A.M. et al., 2011. Synthesis and characterization of microcapsules containing Rubitherm®RT27 obtained by spray drying. *Chemical Engineering Journal*, 166(1), pp.384–390.

Boukhvalov, D.W. and Katsnelson, M.I., 2008. Modeling of Graphite Oxide. *Journal of the American Chemical Society*, 130(32), pp.10697–10701.

Bramhaiah, K. and John, N.S., 2012. Facile synthesis of reduced graphene oxide films at the air–water interface and in situ loading of noble metal nanoparticles. *Advances in Natural Sciences: Nanoscience and Nanotechnology*, 3(4), p.045002.

Brodie, B., 1860. Sur le poids atomique du graphite. *Ann. Chim. Phys*, 59(466), p.e472.

Brown, R., 1999. *Handbook of polymer testing: physical methods*, CRC press.

Cabeza, L.F., Castell, A., Barreneche, C., de Gracia, A. and Fernández, A.I., 2011. Materials used as PCM in thermal energy storage in buildings: A review. *Renewable and Sustainable Energy Reviews*, 15(3), pp.1675–1695.

Cárdenas, B. and León, N., 2013. High temperature latent heat thermal energy storage: Phase change materials, design considerations and performance enhancement techniques. *Renewable and Sustainable Energy Reviews*, 27, pp.724–737.

Cellat, K. et al., 2015. Thermal enhancement of concrete by adding bio-based fatty acids as phase change materials. *Energy and Buildings*, 106, pp.156–163.

Chen, K., Yu, X., Tian, C. and Wang, J., 2014. Preparation and characterization of form-stable paraffin/polyurethane composites as phase change materials for thermal energy storage. *Energy Conversion and Management*, 77, pp.13–21.

Chen, L. et al., 2012. Electro- and Photodriven Phase Change Composites Based on Wax-Infiltrated Carbon Nanotube Sponges. *ACS Nano*, 6(12), pp.10884–10892.

Childres, I., Jauregui, L.A., Park, W., Cao, H. and Chen, Y.P., 2013. Raman spectroscopy of graphene and related materials. *Developments in photon and materials research*, pp.978–981.

Choi, W., Lahiri, I., Seelaboyina, R. and Kang, Y.S., 2010. Synthesis of Graphene and Its Applications: A Review. *Critical Reviews in Solid State and Materials Sciences*, 35(1), pp.52–71.

Cui, H., Liao, W., Memon, S.A., Dong, B. and Tang, W., 2014. Thermophysical and Mechanical Properties of Hardened Cement Paste with Microencapsulated Phase Change Materials for Energy Storage. *Materials*, 7(12), pp.8070–8087.

Cui, L., Gao, J., Xu, T., Zhao, Y. and Qu, L., 2016. Polymer/Graphene Hybrids for Advanced Energy- Conversion and- Storage Materials. *Chemistry–An Asian Journal*, 11(8), pp.1151–1168.

Dai, L., Chang, D.W., Baek, J.-B. and Lu, W., 2012. Carbon Nanomaterials for Advanced Energy Conversion and Storage. *Small*, 8(8), pp.1130–1166.

Das, T.K. and Prusty, S., 2013. Graphene-Based Polymer Composites and Their Applications. *Polymer-Plastics Technology and Engineering*, 52(4), pp.319–331.

Davis, J.R., 2004. *Tensile Testing, 2nd Edition*, ASM International.

Deshmukh, K. and Joshi, G.M., 2014. Thermo-mechanical properties of poly (vinyl chloride)/graphene oxide as high performance nanocomposites. *Polymer Testing*, 34, pp.211–219.

Dow Corning, 2018, *DOWSIL™ 1-2620 Low VOC Conformal Coating* [Online]. Available at: https://consumer.dow.com/en-us/pdp.dowsil%201-2620%20low%20voc%20conformal%20coating.03096874z.html?tab=overview&id=03096874z [Accessed: 6 June 2018].

Fan, X. et al., 2008. Deoxygenation of Exfoliated Graphite Oxide under Alkaline Conditions: A Green Route to Graphene Preparation. *Advanced Materials*, 20(23), pp.4490–4493.

Fang, G., Chen, Z. and Li, H., 2010a. Synthesis and properties of microencapsulated paraffin composites with SiO2 shell as thermal energy storage materials. *Chemical Engineering Journal*, 163(1), pp.154–159.

Fang, Y., Kang, H., Wang, W., Liu, H. and Gao, X., 2010b. Study on polyethylene glycol/epoxy resin composite as a form-stable phase change material. *Energy Conversion and Management*, 51(12), pp.2757–2761.

Fei, B. et al., 2008. Multi-functional microcapsules produced by aerosol reaction. *Journal of Aerosol Science*, 39(12), pp.1089–1098.

Feng, L. et al., 2011. Preparation and characterization of polyethylene glycol/active carbon composites as shape-stabilized phase change materials. *Solar Energy Materials and Solar Cells*, 95(2), pp.644–650.

Ferrer, G., Solé, A., Barreneche, C., Martorell, I. and Cabeza, L.F., 2015. Corrosion of metal containers for use in PCM energy storage. *Renewable Energy*, 76, pp.465–469.

Flora, X.H., Ulaganathan, M. and Rajendran, S., 2012. Influence of lithium salt concentration on PAN-PMMA blend polymer electrolytes. *Int. J. Electrochem. Sci*, 7(8), pp.7451–7462.

Fu, X., Liu, Z., Xiao, Y., Wang, J. and Lei, J., 2015. Preparation and properties of lauric acid/diatomite composites as novel form-stable phase change materials for thermal energy storage. *Energy and Buildings*, 104, pp.244–249.

Ge, H., Li, H., Mei, S. and Liu, J., 2013. Low melting point liquid metal as a new class of phase change material: An emerging frontier in energy area. *Renewable and Sustainable Energy Reviews*, 21, pp.331–346.

Han, S., Kim, C. and Kwon, D., 1997. Thermal/oxidative degradation and stabilization of polyethylene glycol. *Polymer*, 38(2), pp.317–323.

Hastings, R. and Wall, M., 2007. *Sustainable Solar Housing: Exemplary buildings and technologies*, Earthscan.

He, B., Martin, V. and Setterwall, F., 2004. Phase transition temperature ranges and storage density of paraffin wax phase change materials. *Energy*, 29(11), pp.1785–1804.

Hu, H. et al., 2010. Preparation and properties of graphene nanosheets–polystyrene nanocomposites via in situ emulsion polymerization. *Chemical Physics Letters*, 484(4–6), pp.247–253.

Huang, J., Lu, S., Kong, X., Liu, S. and Li, Y., 2013. Form-Stable Phase Change Materials Based on Eutectic Mixture of Tetradecanol and Fatty Acids for Building Energy Storage: Preparation and Performance Analysis. *Materials*, 6(10), pp.4758–4775.

Huang, X., Alva, G., Liu, L. and Fang, G., 2017. Preparation, characterization and thermal properties of fatty acid eutectics/bentonite/expanded graphite composites as novel form–stable thermal energy storage materials. *Solar Energy Materials and Solar Cells*, 166, pp.157–166.

Hummel, R.E., 2013. *Understanding Materials Science: History · Properties · Applications*, Springer Science & Business Media.

Hummers, W.S. and Offeman, R.E., 1958. Preparation of Graphitic Oxide. *Journal of the American Chemical Society*, 80(6), pp.1339–1339.

Imperiyka, M., Ahmad, A., Hanifah, S.A. and Rahman, M.Y.A., 2013. Potential of UV-curable poly (glycidyl methacrylate-co-ethyl methacrylate)-based solid polymer electrolyte for lithium ion battery application. *International Journal of Electrochemical Science*, 8(9), pp.10932–10945.

İnce, Ş., Seki, Y., Akif Ezan, M., Turgut, A. and Erek, A., 2015. Thermal properties of myristic acid/graphite nanoplates composite phase change materials. *Renewable Energy*, 75, pp.243–248.

Irwan, Y.M. et al., 2013. A New Technique of Photovoltaic/Wind Hybrid System in Perlis. *Energy Procedia*, 36, pp.492–501.

Iten, M., Liu, S. and Shukla, A., 2016. A review on the air-PCM-TES application for free cooling and heating in the buildings. *Renewable and Sustainable Energy Reviews*, 61, pp.175–186.

Jamekhorshid, A., Sadrameli, S.M. and Farid, M., 2014. A review of microencapsulation methods of phase change materials (PCMs) as a thermal energy storage (TES) medium. *Renewable and Sustainable Energy Reviews*, 31, pp.531–542.

Jeong, H.-K. et al., 2008. Evidence of Graphitic AB Stacking Order of Graphite Oxides. *Journal of the American Chemical Society*, 130(4), pp.1362–1366.

Karaman, S., Karaipekli, A., Sarı, A. and Biçer, A., 2011. Polyethylene glycol (PEG)/diatomite composite as a novel form-stable phase change material for thermal energy storage. *Solar Energy Materials and Solar Cells*, 95(7), pp.1647–1653.

Kaygusuz, K., Alkan, C., Sari, A. and Uzun, O., 2008. Encapsulated Fatty Acids in an Acrylic Resin as Shape-stabilized Phase Change Materials for Latent Heat Thermal Energy Storage. *Energy Sources, Part A: Recovery, Utilization, and Environmental Effects*, 30(11), pp.1050–1059.

Kee, S.Y., Munusamy, Y. and Ong, K.S., 2018. Review of solar water heaters incorporating solid-liquid organic phase change materials as thermal storage. *Applied Thermal Engineering*, 131, pp.455–471.

Kenisarin, M. and Mahkamov, K., 2007. Solar energy storage using phase change materials. *Renewable and Sustainable Energy Reviews*, 11(9), pp.1913–1965.

Kenisarin, M.M. and Kenisarina, K.M., 2012. Form-stable phase change materials for thermal energy storage. *Renewable and Sustainable Energy Reviews*, 16(4), pp.1999–2040.

Khadiran, T., Hussein, M.Z., Zainal, Z. and Rusli, R., 2015. Encapsulation techniques for organic phase change materials as thermal energy storage medium: A review. *Solar Energy Materials and Solar Cells*, 143, pp.78–98.

Kheradmand, M. et al., 2015. Assessing the feasibility of impregnating phase change materials in lightweight aggregate for development of thermal energy storage systems. *Construction and Building Materials*, 89, pp.48–59.

Kong, X., Zhong, Y., Rong, X., Min, C. and Qi, C., 2016. Building Energy Storage Panel Based on Paraffin/Expanded Perlite: Preparation and Thermal Performance Study. *Materials*, 9(2), p.70.

Konios, D., Stylianakis, M.M., Stratakis, E. and Kymakis, E., 2014. Dispersion behaviour of graphene oxide and reduced graphene oxide. *Journal of Colloid and Interface Science*, 430, pp.108–112.

Konuklu, Y., Unal, M. and Paksoy, H.O., 2014. Microencapsulation of caprylic acid with different wall materials as phase change material for thermal energy storage. *Solar Energy Materials and Solar Cells*, 120, Part B, pp.536–542.

Koschenz, M. and Lehmann, B., 2004. Development of a thermally activated ceiling panel with PCM for application in lightweight and retrofitted buildings. *Energy and Buildings*, 36(6), pp.567–578.

Lawindy, A.M.Y.E., El- Kade, K.M.A., Mahmoud, W.E. and Hassan, H.H., 2002. Physical studies of foamed reinforced rubber composites Part I. Mechanical properties of foamed ethylene–propylene–diene terpolymer and nitrile–butadiene rubber composites. *Polymer International*, 51(7), pp.601–606.

Lerf, A., He, H., Forster, M. and Klinowski, J., 1998. Structure of Graphite Oxide Revisited. *The Journal of Physical Chemistry B*, 102(23), pp.4477–4482.

Li, B., Liu, T., Hu, L., Wang, Y. and Nie, S., 2013. Facile preparation and adjustable thermal property of stearic acid–graphene oxide composite as shape-stabilized phase change material. *Chemical Engineering Journal*, 215–216, pp.819–826.

Li, H., Chen, H., Li, X. and Sanjayan, J.G., 2014. Development of thermal energy storage composites and prevention of PCM leakage. *Applied Energy*, 135, pp.225–233.

Li, M., Wu, Z. and Kao, H., 2011. Study on preparation, structure and thermal energy storage property of capric–palmitic acid/attapulgite composite phase change materials. *Applied Energy*, 88(9), pp.3125–3132.

Liang, J. et al., 2009. Molecular-Level Dispersion of Graphene into Poly(vinyl alcohol) and Effective Reinforcement of their Nanocomposites. *Advanced Functional Materials*, 19(14), pp.2297–2302.

Liu, J., Li, X., Xu, L. and Zhang, P., 2016. Investigation of aging behavior and mechanism of nitrile-butadiene rubber (NBR) in the accelerated thermal aging environment. *Polymer Testing*, 54, pp.59–66.

Liu, T., Ping Lim, K., Chauhari Tjiu, W., Pramoda, K.P. and Chen, Z.-K., 2003. Preparation and characterization of nylon 11/organoclay nanocomposites. *Polymer*, 44(12), pp.3529–3535.

Luo, Z. et al., 2017. Fabrication and characterization of form-stable capric-palmitic-stearic acid ternary eutectic mixture/nano-SiO2 composite phase change material. *Energy and Buildings*, 147, pp.41–46.

Ma, B. et al., 2013. Preparation of composite shape-stabilized phase change materials for highway pavements. *Construction and Building Materials*, 42, pp.114–121.

Maaraoui, S., Clodic, D. and Dalicieux, P., 2012. Heat Pump With a Condenser Including Solid-Liquid Phase Change Material. Available at: http://docs.lib.purdue.edu/iracc/1194/ [Accessed: 9 September 2015].

Mahfuz, M.H., Anisur, M.R., Kibria, M.A., Saidur, R. and Metselaar, I.H.S.C., 2014. Performance investigation of thermal energy storage system with Phase Change Material (PCM) for solar water heating application. *International Communications in Heat and Mass Transfer*, 57, pp.132–139.

Mak, K.F., Ju, L., Wang, F. and Heinz, T.F., 2012. Optical spectroscopy of graphene: From the far infrared to the ultraviolet. *Solid State Communications*, 152(15), pp.1341–1349.

Markos, F.M. and Sentian, J., 2016. Potential of Solar Energy in Kota Kinabalu, Sabah: An Estimate Using a Photovoltaic System Model. *Journal of Physics: Conference Series*, 710(1), p.012032.

Mehrali, M., Latibari, S.T., Mehrali, M., Metselaar, H.S.C. and Silakhori, M., 2013. Shape-stabilized phase change materials with high thermal conductivity based on paraffin/graphene oxide composite. *Energy Conversion and Management*, 67, pp.275–282.

Mei, D., Zhang, B., Liu, R., Zhang, Y. and Liu, J., 2011. Preparation of capric acid/halloysite nanotube composite as form-stable phase change material for thermal energy storage. *Solar Energy Materials and Solar Cells*, 95(10), pp.2772–2777.

Memon, S.A., Liao, W., Yang, S., Cui, H. and Shah, S.F.A., 2015. Development of Composite PCMs by Incorporation of Paraffin into Various Building. *Materials*, 8(2), pp.499–518.

Meng, X. et al., 2013. Preparation and thermal properties of fatty acids/CNTs composite as shape-stabilized phase change materials. *Journal of Thermal Analysis and Calorimetry*, 111(1), pp.377–384.

Moghbelli, E., Banyay, R. and Sue, H.-J., 2014. Effect of moisture exposure on scratch resistance of PMMA. *Tribology International*, 69, pp.46–51.

Molefi, J.A., Luyt, A.S. and Krupa, I., 2010. Comparison of LDPE, LLDPE and HDPE as matrices for phase change materials based on a soft Fischer–Tropsch paraffin wax. *Thermochimica Acta*, 500(1), pp.88–92.

Montemayor, C. and Midland, M., 2012. Effect of Silicone Conformal Coating on Surface Insulation Resistance (SIR) For Printed Circuit Board Assemblies.

Mukhopadhyay, P. and Gupta, R.K., 2012. *Graphite, Graphene, and Their Polymer Nanocomposites*, CRC Press.

Okhay, O. et al., 2016. Thin film versus paper-like reduced graphene oxide: Comparative study of structural, electrical, and thermoelectrical properties. *Journal of Applied Physics*, 120(5), p.051706.

Park, C.-H. et al., 2012. Preparation and characterization of (polyurethane/nylon-6) nanofiber/ (silicone) film composites <Emphasis Type="Italic">via</Emphasis> electrospinning and dip-coating. *Fibers and Polymers*, 13(3), pp.339–345.

Pei, S. and Cheng, H.-M., 2012. The reduction of graphene oxide. *Carbon*, 50(9), pp.3210–3228.

Peng, S., Fan, X., Li, S. and Zhang, J., 2013. Green synthesis and characterization of graphite oxide by orthogonal experiment. *Journal of the Chilean Chemical Society*, 58(4), pp.2213–2217.

Pham, V.H. et al., 2010. One-step synthesis of superior dispersion of chemically converted graphene in organic solvents. *Chemical Communications*, 46(24), pp.4375–4377.

Pielichowska, K. et al., 2008. PEO/fatty acid blends for thermal energy storage materials. Structural/morphological features and hydrogen interactions. *European Polymer Journal*, 44(10), pp.3344–3360.

Pielichowska, K. and Pielichowski, K., 2014. Phase change materials for thermal energy storage. *Progress in Materials Science*, 65, pp.67–123.

Qian, T. et al., 2015. Polyethylene glycol/mesoporous calcium silicate shape-stabilized composite phase change material: Preparation, characterization, and adjustable thermal property. *Energy*. Available at: http://www.sciencedirect.com/science/article/pii/S0360544215000675 [Accessed: 27 February 2015].

Ramakrishnan, S., Sanjayan, J., Wang, X., Alam, M. and Wilson, J., 2015. A novel paraffin/expanded perlite composite phase change material for prevention of PCM leakage in cementitious composites. *Applied Energy*, 157, pp.85–94.

Ren, P.-G., Yan, D.-X., Ji, X., Chen, T. and Li, Z.-M., 2011. Temperature dependence of graphene oxide reduced by hydrazine hydrate. *Nanotechnology*, 22(5), p.055705.

Sadasivuni, K.K., Ponnamma, D., Kim, J. and Thomas, S., 2015. *Graphene-Based Polymer Nanocomposites in Electronics*, Springer.

Sarbu, I. and Sebarchievici, C., 2018. A Comprehensive Review of Thermal Energy Storage. *Sustainability*, 10(1), p.191.

Sarbu, I. and Sebarchievici, C., 2016. *Solar heating and cooling systems: Fundamentals, experiments and applications*, Academic Press.

Sari, A., Karapekl, A., Akaay, M., Onal, A. and Kavak, F., 2006. Polymer/palmitic acid blends as shape-stabilized phase change material for latent heat thermal energy storage. *Asian Journal of Chemistry*, 18(1), p.439.

Sari, A. and Kaygusuz, K., 2007. Poly(vinyl alcohol)/Fatty Acid Blends for Thermal Energy Storage. *Energy Sources, Part A: Recovery, Utilization, and Environmental Effects*, 29(10), pp.873–883.

Sari, A. and Kaygusuz, K., 2006. Studies on poly (vinyl chloride)/fatty acid blends as shape-stabilized phase change material for latent heat thermal energy storage. *Indian Journal of Engineering and Materials Sciences*, 13(3), p.253.

Sarı, A., 2004. Form-stable paraffin/high density polyethylene composites as solid–liquid phase change material for thermal energy storage: preparation and thermal properties. *Energy Conversion and Management*, 45(13), pp.2033–2042.

Sarı, A., Alkan, C. and Bilgin, C., 2014. Micro/nano encapsulation of some paraffin eutectic mixtures with poly(methyl methacrylate) shell: Preparation, characterization and latent heat thermal energy storage properties. *Applied Energy*, 136, pp.217–227.

Sarı, A., Alkan, C., Karaipekli, A. and Önal, A., 2008a. Preparation, characterization and thermal properties of styrene maleic anhydride copolymer (SMA)/fatty acid composites as form stable phase change materials. *Energy Conversion and Management*, 49(2), pp.373–380.

Sarı, A., Alkan, C., Karaipekli, A. and Önal, A., 2008b. Preparation, characterization and thermal properties of styrene maleic anhydride copolymer (SMA)/fatty acid composites as form stable phase change materials. *Energy Conversion and Management*, 49(2), pp.373–380.

Sarı, A., Alkan, C. and Özcan, A.N., 2015. Synthesis and characterization of micro/nano capsules of PMMA/capric–stearic acid eutectic mixture for low temperature-thermal energy storage in buildings. *Energy and Buildings*, 90, pp.106–113.

Sarı, A. and Karaipekli, A., 2007. Thermal conductivity and latent heat thermal energy storage characteristics of paraffin/expanded graphite composite as phase change material. *Applied Thermal Engineering*, 27(8), pp.1271–1277.

Sarı, A., Karaipekli, A. and Alkan, C., 2009. Preparation, characterization and thermal properties of lauric acid/expanded perlite as novel form-stable composite phase change material. *Chemical Engineering Journal*, 155(3), pp.899–904.

Şentürk, S.B., Kahraman, D., Alkan, C. and Gökçe, İ., 2011. Biodegradable PEG/cellulose, PEG/agarose and PEG/chitosan blends as shape stabilized phase

change materials for latent heat energy storage. *Carbohydrate Polymers*, 84(1), pp.141–144.

Shanti, R. et al., 2017. Degradation of ultra-high molecular weight poly(methyl methacrylate- co -butyl acrylate- co -acrylic acid) under ultra violet irradiation. *RSC Advances*, 7(1), pp.112–120.

Shanti, R. et al., 2016. Poly(methyl methacrylate-co-butyl acrylate-co-acrylic acid): Physico-chemical characterization and targeted dye sensitized solar cell application. *Materials & Design*, 108, pp.560–569.

Sharma, A., Sharma, S.D. and Buddhi, D., 2002. Accelerated thermal cycle test of acetamide, stearic acid and paraffin wax for solar thermal latent heat storage applications. *Energy Conversion and Management*, 43(14), pp.1923–1930.

Sharma, A., Tyagi, V.V., Chen, C.R. and Buddhi, D., 2009. Review on thermal energy storage with phase change materials and applications. *Renewable and Sustainable Energy Reviews*, 13(2), pp.318–345.

Sharma, R.K., Ganesan, P., Tyagi, V.V., Metselaar, H.S.C. and Sandaran, S.C., 2015. Developments in organic solid–liquid phase change materials and their applications in thermal energy storage. *Energy Conversion and Management*, 95, pp.193–228.

Sharma, S.D., Kitano, H. and Sagara, K., 2004. Phase change materials for low temperature solar thermal applications. *Res. Rep. Fac. Eng. Mie Univ*, 29, pp.31–64.

Shen, X.-J., Pei, X.-Q., Fu, S.-Y. and Friedrich, K., 2013. Significantly modified tribological performance of epoxy nanocomposites at very low graphene oxide content. *Polymer*, 54(3), pp.1234–1242.

Shin, H.-J. et al., 2009. Efficient Reduction of Graphite Oxide by Sodium Borohydride and Its Effect on Electrical Conductance. *Advanced Functional Materials*, 19(12), pp.1987–1992.

Siddiqui, M.O.R. and Sun, D., 2015. Computational analysis of effective thermal conductivity of microencapsulated phase change material coated composite fabrics. *Journal of Composite Materials*, 49(19), pp.2337–2348.

Silakhori, M. et al., 2013. Accelerated Thermal Cycling Test of Microencapsulated Paraffin Wax/Polyaniline Made by Simple Preparation Method for Solar Thermal Energy Storage. *Materials*, 6(5), pp.1608–1620.

Singh, V.K. et al., 2012. Microwave absorbing properties of a thermally reduced graphene oxide/nitrile butadiene rubber composite. *Carbon*, 50(6), pp.2202–2208.

Socaciu, L., PLEŞA, A., UNGUREŞAN, P. and Giurgiu, O., 2014. Review on phase change materials for building applications. *Leonardo Electronic Journal of Practices and Technologies*, 13(25), pp.179–194.

Song, S., Dong, L., Chen, S., Xie, H. and Xiong, C., 2014a. Stearic–capric acid eutectic/activated-attapulgiate composite as form-stable phase change material for thermal energy storage. *Energy Conversion and Management*, 81, pp.306–311.

Song, S., Dong, L., Qu, Z., Ren, J. and Xiong, C., 2014b. Microencapsulated capric–stearic acid with silica shell as a novel phase change material for thermal energy storage. *Applied Thermal Engineering*, 70(1), pp.546–551.

Souayfane, F., Fardoun, F. and Biwole, P.-H., 2016. Phase change materials (PCM) for cooling applications in buildings: A review. *Energy and Buildings*, 129, pp.396–431.

Spyrou, K. and Rudolf, P., 2014. An Introduction to Graphene. In: Georgakilas, V., (ed.) *Functionalization of Graphene*. Wiley-VCH Verlag GmbH & Co. KGaA, pp. 1–20.

Stankovich, S. et al., 2007. Synthesis of graphene-based nanosheets via chemical reduction of exfoliated graphite oxide. *Carbon*, 45(7), pp.1558–1565.

Staudenmaier, L., 1898. Verfahren zur darstellung der graphitsäure. *European Journal of Inorganic Chemistry*, 31(2), pp.1481–1487.

Su, W., Darkwa, J. and Kokogiannakis, G., 2015. Review of solid–liquid phase change materials and their encapsulation technologies. *Renewable and Sustainable Energy Reviews*, 48, pp.373–391.

Sun, Z., Zhang, Y., Zheng, S., Park, Y. and Frost, R.L., 2013. Preparation and thermal energy storage properties of paraffin/calcined diatomite composites as form-stable phase change materials. *Thermochimica Acta*, 558, pp.16–21.

Swallowe, G.M., 2013. *Mechanical Properties and Testing of Polymers: an A–Z reference*, Springer Science & Business Media.

Synthomer, 2018, *Product detail- SYNTHOMER X6311* [Online]. Available at: https://www.synthomer.com/index.php?id=52&tx_productdatabase_pi1[view]=1&tx_productdatabase_pi1[mat]=7003&L=&tx_productdatabase_pi1[rev]=48191&template_id= [Accessed: 7 June 2018].

Szabó, T. et al., 2006. Evolution of surface functional groups in a series of progressively oxidized graphite oxides. *Chemistry of materials*, 18(11), pp.2740–2749.

Tang, B., Wang, L., Xu, Y., Xiu, J. and Zhang, S., 2016. Hexadecanol/phase change polyurethane composite as form-stable phase change material for thermal energy storage. *Solar Energy Materials and Solar Cells*, 144, pp.1–6.

Tang, B., Wei, H., Zhao, D. and Zhang, S., 2017a. Light-heat conversion and thermal conductivity enhancement of PEG/SiO2 composite PCM by in situ Ti4O7 doping. *Solar Energy Materials and Solar Cells*, 161, pp.183–189.

Tang, L.-S. et al., 2017b. Polyethylene glycol/graphene oxide aerogel shape-stabilized phase change materials for photo-to-thermal energy conversion and storage via tuning the oxidation degree of graphene oxide. *Energy Conversion and Management*, 146, pp.253–264.

Tatsidjodoung, P., Le Pierrès, N. and Luo, L., 2013. A review of potential materials for thermal energy storage in building applications. *Renewable and Sustainable Energy Reviews*, 18, pp.327–349.

Thema, F. et al., 2012. Synthesis and characterization of graphene thin films by chemical reduction of exfoliated and intercalated graphite oxide. *Journal of chemistry*, 2013.

Tian, Y. and Zhao, C.Y., 2013. A review of solar collectors and thermal energy storage in solar thermal applications. *Applied Energy*, 104, pp.538–553.

Tien, H.N. et al., 2012. Enhanced solvothermal reduction of graphene oxide in a mixed solution of sulfuric acid and organic solvent. *Chemical engineering journal*, 211, pp.97–103.

Tomar, A.K., Mahendia, S. and Kumar, S., 2011. Structural characterization of PMMA blended with chemically synthesized PAni. *Adv. Appl. Sci. Res*, 2(3), pp.327–333.

Torikai, A., Ohno, M. and Fueki, K., 1990. Photodegradation of poly(methyl methacrylate) by monochromatic light: Quantum yield, effect of wavelengths, and light intensity. *Journal of Applied Polymer Science*, 41(5–6), pp.1023–1032.

Tripathi, S.N., Saini, P., Gupta, D. and Choudhary, V., 2013. Electrical and mechanical properties of PMMA/reduced graphene oxide nanocomposites prepared via in situ polymerization. *Journal of Materials Science*, 48(18), pp.6223–6232.

Tyagi, V.V. and Buddhi, D., 2007. PCM thermal storage in buildings: A state of art. *Renewable and Sustainable Energy Reviews*, 11(6), pp.1146–1166.

Verdejo, R., Bernal, M.M., Romasanta, L.J. and Lopez-Manchado, M.A., 2011. Graphene filled polymer nanocomposites. *Journal of Materials Chemistry*, 21(10), pp.3301–3310.

Wang, C. et al., 2012a. Shape-stabilized phase change materials based on polyethylene glycol/porous carbon composite: The influence of the pore structure of the carbon materials. *Solar Energy Materials and Solar Cells*, 105, pp.21–26.

Wang, G. et al., 2008a. Facile synthesis and characterization of graphene nanosheets. *The Journal of Physical Chemistry C*, 112(22), pp.8192–8195.

Wang, H. and Hu, Y.H., 2011. Effect of Oxygen Content on Structures of Graphite Oxides. *Industrial & Engineering Chemistry Research*, 50(10), pp.6132–6137.

Wang, L. and Meng, D., 2010a. Fatty acid eutectic/polymethyl methacrylate composite as form-stable phase change material for thermal energy storage. *Applied Energy*, 87(8), pp.2660–2665.

Wang, L. and Meng, D., 2010b. Fatty acid eutectic/polymethyl methacrylate composite as form-stable phase change material for thermal energy storage. *Applied Energy*, 87(8), pp.2660–2665.

Wang, X. et al., 2008b. Transparent Carbon Films as Electrodes in Organic Solar Cells. *Angewandte Chemie International Edition*, 47(16), pp.2990–2992.

Wang, Y., Tang, B. and Zhang, S., 2012b. Light–thermal conversion organic shape-stabilized phase-change materials with broadband harvesting for visible light of solar radiation. *RSC Advances*, 2(30), pp.11372–11378.

Wang, Y., Tang, B. and Zhang, S., 2012c. Novel organic solar thermal energy storage materials: efficient visible light-driven reversible solid–liquid phase transition. *Journal of Materials Chemistry*, 22(35), p.18145.

Wang, Y., Tang, B. and Zhang, S., 2012d. Visible light-driven organic form-stable phase change materials for solar energy storage. *RSC Advances*, 2(14), pp.5964–5967.

Wang, Y., Xia, T.D., Feng, H.X. and Zhang, H., 2011a. Stearic acid/polymethylmethacrylate composite as form-stable phase change materials for latent heat thermal energy storage. *Renewable Energy*, 36(6), pp.1814–1820.

Wang, Y., Xia, T.D., Zheng, H. and Feng, H.X., 2011b. Stearic acid/silica fume composite as form-stable phase change material for thermal energy storage. *Energy and Buildings*, 43(9), pp.2365–2370.

Wang, Z. et al., 2014. Rapid Charging of Thermal Energy Storage Materials through Plasmonic Heating. *Scientific Reports*, 4. Available at: http://www.nature.com.www.ezplib.ukm.my/srep/2014/140901/srep06246/full/srep06246.html?WT.ec_id=SREP-639-20140902 [Accessed: 20 November 2014].

Xiao, M., Feng, B. and Gong, K., 2002. Preparation and performance of shape stabilized phase change thermal storage materials with high thermal conductivity. *Energy Conversion and Management*, 43(1), pp.103–108.

Xu, B., Li, P. and Chan, C., 2015. Application of phase change materials for thermal energy storage in concentrated solar thermal power plants: A review to recent developments. *Applied Energy*, 160, pp.286–307.

Xu, B., Wang, B., Zhang, C. and Zhou, J., 2017. Synthesis and light-heat conversion performance of hybrid particles decorated MWCNTs/paraffin phase change materials. *Thermochimica Acta*, 652, pp.77–84.

Yang, D. et al., 2009. Chemical analysis of graphene oxide films after heat and chemical treatments by X-ray photoelectron and Micro-Raman spectroscopy. *Carbon*, 47(1), pp.145–152.

Yang, J. et al., 2017. Largely enhanced thermal conductivity of poly (ethylene glycol)/boron nitride composite phase change materials for solar-thermal-electric energy conversion and storage with very low content of graphene nanoplatelets. *Chemical Engineering Journal*, 315, pp.481–490.

Yang, X.F. et al., 2001. Weathering degradation of a polyurethane coating. *Polymer Degradation and Stability*, 74(2), pp.341–351.

Yuan, Y., Zhang, N., Tao, W., Cao, X. and He, Y., 2014. Fatty acids as phase change materials: A review. *Renewable and Sustainable Energy Reviews*, 29, pp.482–498.

Zhang, H., Zhou, L. and Yu, C., 2014. Highly crystallized Fe 2 O 3 nanocrystals on graphene: a lithium ion battery anode material with enhanced cycling. *RSC Advances*, 4(1), pp.495–499.

Zhang, J. et al., 2010. Reduction of graphene oxide viaL-ascorbic acid. *Chemical Communications*, 46(7), pp.1112–1114.

Zhang, Y., Ding, J., Wang, X., Yang, R. and Lin, K., 2006. Influence of additives on thermal conductivity of shape-stabilized phase change material. *Solar Energy Materials and Solar Cells*, 90(11), pp.1692–1702.

Zhao, X.-Y. et al., 2007. Nitrile butadiene rubber/hindered phenol nanocomposites with improved strength and high damping performance. *Polymer*, 48(20), pp.6056–6063.

Zhou, D., Zhao, C.Y. and Tian, Y., 2012. Review on thermal energy storage with phase change materials (PCMs) in building applications. *Applied Energy*, 92, pp.593–605.

Zhou, X. et al., 2011. Reducing Graphene Oxide via Hydroxylamine: A Simple and Efficient Route to Graphene. *The Journal of Physical Chemistry C*, 115(24), pp.11957–11961.

Zhu, C., Guo, S., Fang, Y. and Dong, S., 2010. Reducing Sugar: New Functional Molecules for the Green Synthesis of Graphene Nanosheets. *ACS Nano*, 4(4), pp.2429–2437.

APPENDIX A

polymers

MDPI

Article

Effect of Preparation Methods on the Tensile, Morphology and Solar Energy Conversion Efficiency of RGO/PMMA Nanocomposites

Shin Yiing Kee [1], Yamuna Munusamy [1,*], Kok Seng Ong [2] and Koon Chun Lai [1]

[1] Department of PetroChemical Engineering, Faculty of Engineering and Green Technology, Universiti Tunku Abdul Rahman, Jalan Universiti, Bandar Barat, Kampar, Perak 31900, Malaysia; nicolekee88@hotmail.com (S.Y.K.); laikc@utar.edu.my (K.C.L.)

[2] Department of Industrial Engineering, Faculty of Engineering and Green Technology, Universiti Tunku Abdul Rahman, Jalan Universiti, Bandar Barat, Kampar, Perak 31900, Malaysia; skong@utar.edu.my

* Correspondence: yamunam@utar.edu.my; Tel.: +60-54688888

Academic Editor: Wei Min Huang

Received: 1 May 2017; Accepted: 14 June 2017; Published: 18 June 2017

Abstract: In this study, reduced graphene oxide (RGO)/polymethyl methacrylate (PMMA) nanocomposites were prepared by employing in situ polymerization and solution blending methods. In terms of mechanical properties, RGO loading increased the Young's modulus but decreased the elongation at break for RGO/PMMA nanocomposites. Tensile strength for solution blended RGO/PMMA nanocomposites increased after adding 0.5 wt % RGO, which was attributed to the good dispersion of RGO in the nanocomposites as evidenced from SEM and TEM. Solar energy conversion efficiency measurement results showed that the optimum concentration of RGO in the RGO/PMMA nanocomposites was found to be 1.0 wt % in order to achieve the maximum solar energy conversion efficiency of 25%. In the present study, the solution blended nanocomposites exhibited better overall properties than in situ polymerized nanocomposites owing to the better dispersion of RGO in solution blending. These findings would contribute to future work in search of higher conversion efficiency using nanocomposites.

Keywords: RGO; PMMA; solar energy conversion efficiency; morphology; synthesis method

1. Introduction

Graphene is a monolayer hexagonal sp^2 hybridized carbon sheet. It has received much attention in recent years due to its high mechanical strength, large specific surface area, and excellent thermal and electrical conductivity [1,2]. Graphene can be synthesized through various methods, such as chemical vapor deposition (CVD), plasma enhanced CVD (PECVD), graphitization of a carbon-containing substrate, solvothermal, organic synthesis, and chemical reduction of graphene oxide [3–5]. Graphene obtained by the reduction of graphene oxide through thermal, chemical or electrical treatments is generally known as reduced graphene oxide (RGO). Research works involving graphene/polymer nanocomposites have been carried out widely with regard to many applications, such as electromagnetic shielding, corrosion-resistant coating, antistatic, lithium ion batteries, supercapacitors, fuel cells, photovoltaic devices, biosensing systems and photocatalysts [6–8]. Researchers have synthesized graphene/polymer nanocomposites with several polymer matrices such as polystyrene, poly(vinyl alcohol), low density polyethylene, polymethyl methacrylate, epoxy and natural rubber composite using different preparation methods like melt intercalation, solution blending, in situ polymerization, etc. [9–17]. Despite various materials having been proposed for heat dissipation [18,19], the highly thermally conductive graphene-based nanocomposites have recently

APPENDIX B

materials

MDPI

Article

Thermal Performance Study of Composite Phase Change Material with Polyacrylicand Conformal Coating

Shin Yiing Kee [1], Yamuna Munusamy [1,*], Kok Seng Ong [1], Hendrik Simon Cornelis Metselaar [2], Swee Yong Chee [3] and Koon Chun Lai [1]

[1] Faculty of Engineering and Green Technology, Universiti Tunku Abdul Rahman, Kampar 31900, Malaysia; nicolekee88@hotmail.com (S.Y.K.); skong@utar.edu.my (K.S.O.); laikc@utar.edu.my (K.C.L.)
[2] Department of Mechanical Engineering and Advanced Material Research Center, University of Malaya, Kuala Lumpur 50603, Malaysia; h.metselaar@um.edu.my
[3] Faculty of Science, Universiti Tunku Abdul Rahman, Kampar 31900, Malaysia; csy@utar.edu.my
* Correspondence: yamunam@utar.edu.my; Tel.: +60-5-468-8888

Received: 24 May 2017; Accepted: 17 June 2017; Published: 28 July 2017

Abstract: The composite PCM was prepared by blending polymethyl methacrylate (PMMA) and myristic acid (MA) in different weight percentages. The MA and PMMA were selected as PCM and supporting material, respectively. As liquid MA may leak out during the phase transition, this study proposes the use of two coatings, namely a polyacrylic coating and a conformal coating to overcome the leakage problem. Both coatings were studied in terms of the leakage test, chemical compatibility, thermal stability, morphology, and reliability. No leakage was found in the PCMs with coatings compared to those without under the same proportions of MA/PMMA, thus justifying the use of coatings in the present study. The chemically compatibility was confirmed by FTIR spectra: the functional groups of PCMs were in accordance with those of coatings. DSC showed that the coatings did not significantly change the melting and freezing temperatures, however, they improved the thermal stability of composite PCMs as seen in TGA analysis. Furthermore, the composite PCMs demonstrated good thermal reliability after 1000 times thermal cycling. The latent heat of melting reduced by only 0.16% and 1.02% for the PCMs coated with conformal coating and polyacrylic coating, respectively. Therefore, the proposed coatings can be considered in preparing fatty acid/PMMA blends attributed to the good stability, compatibility and leakage prevention.

Keywords: phase change material; PMMA; myristic acid; polyacrylic coating; conformal coating

1. Introduction

The greenhouse effect is the main driving force for switching from fossil fuel energy to various renewable energy sources such as solar, wind, and hydro energy. Solar energy is a popular renewable resources for electricity generation and thermal energy storage (TES). A comparative study on world energy consumption released by the International Energy Agency pointed out that solar array installations will supply about 45% of worldwide energy demand in 2050 [1]. TES is rapidly growing in mitigating energy crises and reducing environmental pollution [2]. In particular, the use of phase change material (PCM) for TES is one of the most prospective techniques [3–6]. PCM has high latent heat and capable of storing heat energy with a small temperature change during phase transition [7,8]. It stores five to 14 times more heat per unit volume than sensible storage materials such as water, masonry, and rock [9]. Moreover, a significant reduction in storage volume can be achieved using PCM compared to sensible heat storage [10].

APPENDIX C

Applied Thermal Engineering 131 (2018) 455–471

Contents lists available at ScienceDirect

Applied Thermal Engineering

journal homepage: www.elsevier.com/locate/apthermeng

Review of solar water heaters incorporating solid-liquid organic phase change materials as thermal storage

Shin Yiing Kee [a], Yamuna Munusamy [a,*], Kok Seng Ong [b]

[a] Department of PetroChemical Engineering, Faculty of Engineering and Green Technology, Universiti Tunku Abdul Rahman, Jalan Universiti, Bandar Barat, 31900 Kampar, Perak, Malaysia
[b] Department of Industrial Engineering, Faculty of Engineering and Green Technology, Universiti Tunku Abdul Rahman, Jalan Universiti, Bandar Barat, 31900 Kampar, Perak, Malaysia

HIGHLIGHTS

- Thermal and light absorption properties of composite PCMs are reviewed.
- Research gap that limits the practical application of PCMs in SWH is discussed.
- Types of PCM and their performance in SWH are reviewed.
- Recent development in the designs of SWHs incorporating PCMs as TES is reviewed.
- Recommendation on tank design is included to optimize performance of SWH.

ARTICLE INFO

Article history:
Received 19 July 2017
Revised 5 November 2017
Accepted 7 December 2017
Available online 7 December 2017

Keywords:
Phase change material
Solid-liquid PCM
Thermal energy storage
Solar water heater
Tank design

ABSTRACT

Solar water heater (SWH) incorporating solid-liquid organic phase change materials as thermal energy storage (TES) have attracted attention since 1970s. However, the development of these PCMs to practical application had been restricted by its low thermal stability and thermal conductivity. Recently many type of composite solid-liquid organic PCMs had been developed and studied to overcome these problems. The effect of polymer/porous materials composition, nanoparticles loading and photo-absorption properties of photothermal energy conversion material on the thermal stability, thermal conductivity and light absorption of composite PCMs are reviewed and analyzed. Besides, practical application of PCMs in SWHs are reviewed and compared as well. Research gaps for future development and application of composite PCMs had been identified and discussed as well.

Contents

1. Introduction 456
2. Recent development of solid-liquid organic PCM composite materials as TES 457
   2.1. Form stable composite PCM materials (FSCPCM) to improve thermal stability 457
   2.2. Composite PCM materials to increase the thermal conductivity 457
   2.3. PCM composite materials to enhance light absorption 459
3. Solid-liquid organic PCM in solar water heater 459
   3.1. Types of PCM 462
   3.2. Tank designs 462

Abbreviations: aEVC, modified expanded vermiculite/carbon composite treated with nitric acid; CA, capric acid; Cu, copper; Cu_2O, copper(I) oxide; FSCPCM, form stable composite PCM materials; GO, graphene oxide; HDPE, high density polyethylene; HPC, heat pipe condenser; HPSCs, evacuated tube heat pipe solar collector; LHS, latent heat storage; MA, myristic acid; MPEG, methoxy polyethylene glycol; MPSiO$_2$, mesoporous silica nanoparticles; MWCNT, multi walled carbon nanotubes; PCM, phase change material; PEG, polyethylene glycol; PMMA, polymethyl methacrylate; SA, stearic acid; SEM, scanning electron microscope; SiO_2, silicone dioxide; SWH, solar water heater; TCNTs, mechano-chemical treated carbon nanotubes; TES, thermal energy storage; TGA, thermogravimetric Analysis; Ti_4O_7, titanium black; TiO_2, titanium dioxide.

* Corresponding author.
E-mail addresses: nicolekee88@1utar.my (S.Y. Kee), yamunam@utar.edu.my (Y. Munusamy), skong@utar.edu.my (K.S. Ong).

https://doi.org/10.1016/j.applthermaleng.2017.12.032
1359-4311/

APPENDIX D

Thermal Performance Study of Form-Stable Composite Phase Change Material with Polyacrylic

Shin Yiing Kee [1], Yamuna Munusamy [1,a)], Kok Seng Ong [2], Swee Yong Chee[3] and Shimalaa Sanmuggam[1]

[1]*Department of PetroChemical Engineering, Faculty of Engineering and Green Technology, Universiti Tunku Abdul Rahman, Malaysia*
[2]*Department of Industrial Engineering, Faculty of Engineering and Green Technology, Universiti Tunku Abdul Rahman, Malaysia*
[3]*Department of Chemical Science, Faculty of Science, Universiti Tunku Abdul Rahman, Malaysia*

[a)]Corresponding author: yamunam@utar.edu.my

Abstract. Phase change material (PCM) is one of the most popular and widely used as thermal energy storage material because it is able to absorb and release a large amount of latent heat during a phase change process over a narrow temperature range. In this work, the form-stable composite PCM was prepared by blending of PMMA and myristic acid in different weight percentage. PMMA was used as a supporting material while myristic acid was used as PCM. Theoretically, PCM can be encapsulated in the support material after blending. However, a small amount of liquid PCMs can leak out from supporting material due to the volume change in phase change process. Therefore, a form-stable composite PCM with polyacrylic coating was studied. Leakage test was carried out to determine the leakage percentage of the form-stable composite PCM. Fourier transform infrared spectroscopy (FTIR) was used to characterize the chemical compatibility of the form-stable PCM composite while differential scanning calorimetry (DSC) was used to study the melting, freezing point and the latent heat of melting and freezing for the form-stable composite PCM.

INTRODUCTION

Thermal energy storage (TES) is an important energy storage to improve energy saving and efficiency by overcoming the inconsistency and mismatch between energy supply and demand. There are three main types of TES systems: sensible heat, latent heat and thermo-chemical. Latent heat storage using phase change material (PCM) is one of the most popular type because they have high latent heat and able to store a large amount of heat energy in a small volume with a small temperature change in the phase change process [1].

PCMs which are commonly used as TES are organic PCMs, inorganic PCMs and eutectic PCMs [2,3]. Among organic PCMs, fatty acid is popular because they have high latent heat, reproducible melting and freezing behaviour and freeze with no supercooling [4]. However, fatty acid is acidic and mildly corrosive. Therefore, many studied were done on form-stable composite PCMs which are prepared by blending of polymer and fatty acid. Generally, polymer is used as a supporting material to prevent the leaking of melted fatty acid during phase change process. Polymers such as poly(methyl methacrylate) (PMMA), styrene maleic anhydride copolymer (SMA) and poly(ethylene oxide) (PEO) have been used to blend with fatty acid to produce form-stable composite PCM [5–7].Previous research showed that the polymer has a good compatibility with fatty acid. Besides, the form-stable PCMs also have proper phase change temperature and good latent heat make it suitable to be used as TES materials in man application.

Green and Sustainable Technology
AIP Conf. Proc. 1878, 070008-1–070008-8; doi: 10.1063/1.4979379
Published by AIP Publishing. 978-0-7354-1496-9/$30.00

APPENDIX E

Proceeding – 3rd Putrajaya International Built Environment, Technology and Engineering Conference (PIBEC3), 9 – 10 October, 2017. Hotel Bangi-Putrajaya, Bangi, Malaysia. ISBN 978 – 967- 2072- 10- 2

DEVELOPMENT OF FORM STABLE COMPOSITE PHASE CHANGE MATERIAL WITH POLYMER COATING FOR THERMAL ENERGY STORAGE

Kee Shin Yiing
Faculty of Engineering and Green Technology,
Universiti Tunku Abdul Rahman, 31900 Kampar, Malaysia.
Email: nicolekee88@hotmail.com

Yamuna Munusamy
Faculty of Engineering and Green Technology,
Universiti Tunku Abdul Rahman, 31900 Kampar, Malaysia.
Email: yamunam@utar.edu.my

Ong Kok Seng
Faculty of Engineering and Green Technology,
Universiti Tunku Abdul Rahman, 31900 Kampar, Malaysia.
Email: skong@utar.edu.my

Chee Swee Yong
Faculty of Science, Universiti Tunku Abdul Rahman,
31900 Kampar, Malaysia;
Email: csy@utar.edu.my

Yu Gen Qian
Faculty of Engineering and Green Technology,
Universiti Tunku Abdul Rahman, 31900 Kampar, Malaysia.
Email: yugq268@hotmail.com

ABSTRACT

Phase change material (PCM) is one of the most widely used thermal energy storage material because it can store a large amount of latent heat during a phase change process over a narrow temperature range. This work is focused on the preparation of form stable composite PCM using polymer coating. Form stable PCM composite is developed to improve thermal stability of PCM over phase change temperature. It also can reduce volume change during phase change process. Polymer coating and myristic acid (MA) were used as shell and PCM, respectively. Polymer coating can prevent the reaction of myritic acid with the outside environment. Two types of polymer coating were used in this study: nitrile butadiene rubber and polyacrylic coating. MA was coated with different polymer coating combination to find out which polymer coating give the best thermal stability. Leakage test was carried out to determine the leakage percentage of the form-stable composite PCMs. Fourier transform infrared spectroscopy (FTIR) was used to determine chemical functional group of polymer coating, MA and form stable composite PCM. Results showed that sample 5 (MA pellet coated with 2 layers NBR) and sample 6 (MA pellet coated with 1 layer NBR and layer PA) were the most stable sample as no leaking was found after heating in oven at 65°C for 10 hours .

Keywords: polymer coating, phase change materia, thermal energy storage.

APPENDIX F

IConCEES 2017 IOP Publishing
IOP Conf. Series: Earth and Environmental Science **140** (2018) 012008 doi:10.1088/1755-1315/140/1/012008

Development of form stable Poly(methyl methacrylate) (PMMA) coated thermal phase change material for solar water heater applications

Y Munusamy[1], S Shanmugam[1] and Kee Shi-Ying[1]

[1] Faculty of Engineering and Green Technology, Universiti Tunku Abdul Rahman, Jalan Universiti, Bandar Barat, 31900 Kampar, Perak.

E-mail: yamunam@utar.edu.my

Abstract. Phase change material (PCM) is one of the most popular and widely used thermal energy storage material in solar water heater because it able to absorb and release a large amount of latent heat during a phase change process over a narrow temperature range. However the practical application of PCM is limited by two major issues; 1) leakage which leads to material loss and corrosion of tank and 2) large volume change during phase change process which cause pressure build up in the tank. In this work, form-stable PCM was prepared by coating myristic acid with Poly(methyl methacrylate) (PMMA) to prevent leakage of PCM. PMMA was mixed with different weight percentage (0.1, 0.2, 0.3, 0.4 and 0.5 wt%) of dicumyl peroxide (DCP). The purpose of adding DCP to PMMA is to crosslink the polymer and to increase the mechanical strength of PMMA to hold the myristic acid content inside the coating during the phase change process. Leakage test results showed that PMMA mixed with 0.1% DCP exhibit 0% leakage. This result is further supported by Field Emission Scanning Electron Microscopy (FESEM) images and Fourier transform infrared spectroscopy (FTIR) analysis results, where a compact and uniform coating without cracks were formed for PCM coated with PMMA with 0.1% DCP. Differential scanning calorimetry (DSC) results shows that the melting point of form-stable PCM is 55°C, freezing point is 50°C, the latent heat of melting and freezing is 67.59 J/g.

1. Introduction

Phase change material (PCM) is the most common and prospective technique being used to store latent heat energy. This is because of its storing and releasing capability of very large amount of energy for each unit mass at nearly a constant temperature [1]. In solar water heater (SWH), effective application of PCM could increase the reliability of the system during low solar gain hours without the need for back up electrical power. The size of the storage tank on the roof will reduce significantly because PCM able to store fourteen to fifteen times extra heat for each unit volume compared to sensible storage materials such as rock masonry or water [2-3].

However throughout the phase change process, PCM tends to melt and corrodes the wall of the SWH heat storage tank [4-5]. Moreover the PCM will also go through large volume change during the melting and freezing cycle which can cause pressure build up in the tank during melting and inefficient heat transfer due to air gap during freezing. Thus, PCM must be well contained to avoid them from leaking out and minimize the volume change during the phase change process. This measure must be taken into consideration in order to use them practically.